

UC Santa Cruz

UC Santa Cruz Electronic Theses and Dissertations

Title

The Lineage Progression of Neural Stem Cells

Permalink

<https://escholarship.org/uc/item/8v50d031>

Author

Liang, Xiaoyi Guo

Publication Date

2022

Peer reviewed|Thesis/dissertation

UNIVERSITY OF CALIFORNIA
SANTA CRUZ

THE LINEAGE PROGRESSION OF NEURAL STEM CELLS

A dissertation submitted in partial satisfaction
of the requirements for the degree of

DOCTOR OF PHILOSOPHY

in

MOLECULAR, CELL AND DEVELOPMENTAL BIOLOGY

by

Xiaoyi G Liang

September 2022

The Dissertation of Xiaoyi G Liang
is approved:

Professor Bin Chen, chair

Professor David Feldheim

Professor Euseok Kim

Peter Biehl

Vice Provost and Dean of Graduate Studies

Copyright © by
Xiaoyi G Liang
2022

Table of Contents

Abstract	vii
Acknowledgements	ix
Chapter 1: Introduction	1
Neural stem cells in the developing cerebral cortex	1
Sonic Hedgehog signaling pathway	6
Innovation and Significance	9
Chapter 2: Cortical neural stem cell lineage progression is regulated by extrinsic signaling molecule sonic hedgehog	12
Results	12
Gsx2 is expressed in a subpopulation of IPCs in the cortex.....	12
Cortical NSCs generate Gsx2 ⁺ IPCs at late embryonic stages.....	13
Lineage tracing reveals the tri-potency of Gsx2 ⁺ IPCs in the cortex.....	15
The Shh signaling pathway is required for the cortical RGCs to generate OB-INs .	16
Increased exposure to Shh signaling during neurogenesis of deep-layer pyramidal neurons causes a premature fate switch to generate OB-INs and oligodendrocytes	18
Shh signaling promotes OB-IN and cortical oligodendrocyte fates through reducing Gli3R.....	20
scRNA-Seq analysis supports the existence of Gsx2 ⁺ tri-IPCs in the developing cortex.....	21
In vivo validation of markers of tri-IPCs and their lineage progression in the cortical SVZ.....	25
Chapter 3: Sonic hedgehog signaling is critical for cortical RGCs to generate oligodendrocytes and astrocytes	27
Results	27
Shh signaling promotes the generation and proliferation of MIPCs.....	27
Shh activate the transcription of Egfr and Fgfr3 in IPCs	29
Anti-correlation of Gli3 and Olig2 in VZ/SVZ.....	31
Gli3 binds to both confirmed and potential enhancers of Olig1/2	32

Defects in Olig2 ^{-/-} mouse brain	34
These Gli3 binding sites are required for Olig1/2 expression in RGCs and SVZ MIPCs	35
4C-Seq reveals physical interactions between Gli3 binding sites and Olig1/2 promoters	38
Chapter 4: Pax6 represses OB lineage in the cortical RGCs during development	41
Results:	41
Pax6 is required for cortical RGCs to repress OB lineage and oligodendrocyte lineage during development	41
Pax6 & Gli3 regulate the lineage switch synergistically	43
Chapter 5: Discussion and Future directions	44
Cortical NSCs, PyN-IPCs, tri-IPCs, OPCs, OB-IPCs, Glia-IPCs, and their lineage progression	44
Shh signaling promotes the generation of OB-INs and cortical oligodendrocytes by reducing Gli3R	46
Shh signaling is essential for cortical RGCs to generate astrocyte lineage and reduced Fgf and Egfr signaling in the IPCs in Smo cko contributes to the gliogenesis defects.	49
Gli3 binds to multiple enhancers to regulate the transcription of Olig2 and Olig1 which not only affect Cortical OPCs, AS-IPCs but also OB-IPCs	50
A core gene regulatory network governing a common developmental trajectory for forebrain NSCs to generate OB-INs	51
Pax6 & Gli3 regulate cortical RGC lineage switch synergistically	52
Figures	55
Figure 1. Cortical NSCs generate Gsx2 ⁺ tri- IPCs that give rise not only to OB Interneurons but also to cortical oligodendrocytes and astrocytes	55
Figure 2. Cells of the OB interneuron lineage are not generated in the cortical SVZ of Smo cko mice at P2	57
Figure 3. Overexpression of ShhN in the cortex by IUE induces OB interneuron and oligodendrocyte lineages in the cortical SVZ	58
Figure 4. Shh signaling regulates the production of OB interneurons and oligodendrocytes in the cortical VZ-SVZ predominately by reducing Gli3	60
Figure 5. scRNA-Seq analysis of cells in the E16.5 wild-type cortices and in the ShhN-IUE cortices	61
Figure 6. scRNA-Seq analysis of the progenitor cells in the ShhN-IUE sample	62

Figure 7. In vivo validation of markers of tri-IPCs and OB-IPCs	64
Figure 8. Gsx2 is expressed in the cortex. Related to Figure 1.	66
Figure 9. Cortical NSCs give rise to Gsx2 ⁺ cells in the cortex. Related to Figure 1.	68
Figure 10. Cortical Emx1 ⁺ NSCs generate Gsx2 ⁺ tri-IPCs. Related to Figure 1.	70
Figure 11. Eomes ⁺ IPCs continue to be generated from NSCs in the Smo cko mice. Related to Figure 2.	72
Figure 12. Less MIPCs were generated at late embryonic stage in Smo cko mouse brain.	74
Figure 13. Less MIPCs were proliferating at late embryonic stage in Smo cko mouse brain.	76
Figure 14. Shh signaling is both necessary and sufficient for the expression of Egfr which activate the mitogen activated protein kinase (MAPK) pathway and generate cortical glia.	78
Figure 15. Establishing CHIP-seq, CUT&RUN, and ATAC-seq methods.	80
Figure 16. Gli3 CHIP-seq revealed peaks at Fgfr3 and Gsx2 genes.	81
Figure 17. Less proliferation in hGFAPcre; Fgfr1 ^{F/F} ; Fgfr2 ^{F/F} ; Fgfr3 ^{F/F} (Fgfr Tcko) mouse brain at E18.5.	82
Figure 18. Most of the remaining Phospho-MAPK ⁺ cells in hGFAPcre; Fgfr1 ^{F/F} ; Fgfr2 ^{F/F} ; Fgfr3 ^{F/F} (Fgfr Tcko) are Egfr ⁺ cells.	83
Figure 19. Anti-correlation between Gli3 and Olig2 in VZ/SVZ.	84
Figure 20. Less oligodendrocytes, astrocytes and OB interneurons were found in Olig2 knockout mouse brain.	86
Figure 21. Gli3 binds to the predicted enhancers of Olig1/2 loci.	87
Figure 22. Enhancer e14414 and E2 regulates Olig2 and Olig1 expression in cortical VZ/SVZ.	88
Figure 23. Olig2 and Olig1 expression in cortical VZ/SVZ requires enhancer e14414, E3 and E2 at P0.	89
Figure 24. Enhancer e14414 regulates Olig2 expression in lateral VZ/SVZ.	90
Figure 25. e14414 and E2 regulate gliogenesis in the dorsal cortex and E2 is involved in OB interneuron development.	92
Figure 26. Olig2 ⁺ and Id1 ⁺ cells are decreased in Enhancer e14414 knockout and E3 knockout.	94
Figure 27. 4C-Seq data revealed physical interactions between Olig2/Olig1 promoters and Gli3 binding sites.	96
Figure 28. Anti-correlation of Pax6 and Olig2 in VZ/SVZ.	98
Figure 29. Pax6 represses OB lineage.	100
Figure 30. Pax6 and Gli3 repress OB lineage synergistically.	101

Materials and Methods	103
Animals	103
Immunohistochemistry	103
In situ hybridization.....	104
EdU labeling	106
CUT&RUN-seq.....	106
ATAC-seq.....	106
RNA-seq	107
scRNA-Seq library preparation.....	108
scRNA-Seq analysis.....	108
Quantification and statistical analysis	110
Data and code availability	111
In utero electroporation	111
Image acquisition and analysis.....	111
ChIP-seq.....	113
4C-Seq	113
Bibliography	116

Abstract

THE LINEAGE PROGRESSION OF NEURAL STEM CELLS

Xiaoyi G Liang

Neural stem cells (NSCs) in the embryonic neocortex sequentially generate different subtypes of glutamatergic projection neurons. Following that, NSCs undergo a major switch in their progenitor properties and produce g-aminobutyric acid (GABAergic) interneurons for the olfactory bulb (OB), cortical oligodendrocytes, and astrocytes. Herein, I provide evidence for the molecular mechanism that underlies this switch in the neocortical NSCs.

At around E16.5, mouse neocortical NSCs start to generate Gsx2-expressing (Gsx2⁺) intermediate progenitor cells (IPCs). *In vivo* lineage tracing study revealed that Gsx2⁺ IPC population gives rise not only to OB interneurons (OB-INs) but also to cortical oligodendrocytes and astrocytes, suggesting that they are a multipotent population. I found that Sonic Hedgehog signaling is both necessary and sufficient for the generation of Gsx2⁺ IPCs by reducing Gli3R protein levels. Using single-cell RNA sequencing, I identified the transcriptional profile of Gsx2⁺ IPCs and the process of the lineage switch of cortical NSCs.

The Gli3 ChIP-seq revealed 4 binding sites in Olig2/Olig1 locus and two of them are also bound by Pax6 shown by the Pax6 ChIP-seq data. Chromatin at these 4 binding sites show increased accessibility in the ATAC-seq assay. CUT&RUN analysis using histone marks indicates that

they are potential enhancers. I generated the enhancer knock-out mice and found that these binding sites are essential for Olig2/Olig1 expression in NSCs and IPCs. The circularized chromosome conformation capture (4C) experiments revealed physical interactions between these binding sites and Olig2/Olig1 promoters. More importantly, I found that OB lineage cells and Olig2 positive cells are dramatically increased in the *hGFAP-Cre; Gli3^{F/F}; Pax6^{F/F} (Gli3 Pax6 dcko)* which indicates that Gli3 and Pax6 are involved in a common regulatory mechanism that regulate NSCs lineage switch.

Acknowledgements

First and foremost, I would like to express my sincere gratitude to my mentor, Dr. Bin Chen, for the continuous support of my Ph.D study, for her patience, motivation, and immense knowledge. I have benefited greatly from your wealth of knowledge and meticulous editing. I am extremely grateful that you took me on as a student and continued to have faith in me over the years. I would not be who I am today without all your encouragement, guidance, and support.

Importantly, I would like to thank all current and past members of the Chen lab, for their thoughtful input into my dissertation research. I would like to thank Dr. Yue Zhang in particular, for all your guidance and help with my project. I would not have completed my thesis research without your guidance at the beginning of my Ph.D program. You taught me nearly all the techniques and it would have never been possible without you. I can always reach to you for any questions about my thesis research even after you have left the lab. I would like to thank Kendy Hoang, my lab partner. We have been working on this project for 3 years. I genuinely admire what we have accomplished together. The following graduate students and undergrads in the Chen lab have all played particularly essential roles in the work presented here: Jeremiah Tsyporin, Thomas Fin, Zhaoxu Chen, Fangyuan Qu. This work would not have been possible without all your help.

Additionally, I would like to thank Dr. John Rubenstein, Dr. Zhengang Yang, Dr. Rohinton Kamakaka, Dr. Namrita Dhillon for their helpful

comments into the dissertation work herein. I would like to thank Guoping Liu, Teng Guo and all the co-authors on the “Cortical Neural Stem Cell Lineage Progression Is Regulated by Extrinsic Signaling Molecule Sonic Hedgehog” paper for their help with the sc-RNA-Seq experiments and immunostaining. I would like to thank Dr.Xin Shen who provided us with the human PLAC-seq data and Dr.Louis-Jan Pilaz who helped us generating the enhancer knock-out mice. I would like to thank Dr. Axel Visel and Kitt Paraiso who helped us generating the enhancer reporter mice.

I can't emphasize enough how thankful I am for the love and support my family has always shown. My husband and best friend Xiao Liang, my twin sister Xiaofei Guo, my parents and parents in law, I love you all so much, and I am so incredibly grateful for all your encouragement throughout this lengthy endeavor. I am blessed to have you all by my side.

This study was supported by National Institutes of Health (NIH) grant to Bin Chen (R01MH094589, R01NS0897772 and R01NS089777-06A1); grants to Z.Y. from National Key Research and Development Program of China (2018YFA0108000), the National Natural Science Foundation of China (NSFC 31630032 and 31820103006), the Shanghai Municipal Science and Technology Major Project (2018SHZDZX01), and ZJLab; a NIH grant to A.B. (K99 NS111731); a National Institute of Neurological Disorders and Stroke (NINDS) grant to A.R.K. (R35NS097305); and a National Institute of Mental Health (NIMH) grant to J.L.R. (MH049428).

The findings presented here represent a substantial collaborative effort, which would have otherwise been impossible to accomplish without

the fantastic group of friends, family, coworkers, collaborators, and advisors
I have just described.

Chapter 1: Introduction

Neural stem cells in the developing cerebral cortex

Neural stem cells (NSCs) are the ultimate source of all neurons, oligodendrocytes, and astrocytes. Prenatally, NSCs correspond to radial glial cells (RGCs) that are regionally and temporally specified and generate diverse neuronal and glial cell types appropriate for their location and time (Bayraktar et al., 2015; Kriegstein and Alvarez-Buylla, 2009; Kwan et al., 2012). Although much progress has been made toward understanding temporal cell-fate specification in the developing invertebrate ventral nerve cord and brain (Doe, 2017; Kohwi and Doe, 2013), the mechanisms responsible for temporal lineage specification of NSCs in the mammalian brain remain largely unknown.

The mouse cerebral cortex is a six-layered structure, consisting of both glutamatergic pyramidal projection neurons (PyNs) derived from cortical ventricular zone (VZ) and subventricular zone (SVZ), and g-aminobutyric acid (GABAergic) interneurons that arise from subcortical progenitor domains. During development, embryonic NSCs located in the cortical VZ sequentially generate distinct subtypes of PyNs in an inside-out pattern (Figure A): deep-layer PyNs are born first, followed by PyNs of superficial layers (Kriegstein and Alvarez-Buylla, 2009; Kwan et al., 2012; Leone et al., 2008). The local interneurons, however, derive from NSCs located in the medial and caudal ganglionic eminences (MGEs and CGEs,

respectively) in the ventral forebrain and migrate tangentially into the cerebral cortex (Hu et al., 2017; Lim et al., 2018).

As the production of PyNs ceases, cortical NSCs switch to generating cortical glia and GABAergic olfactory bulb (OB) interneurons (Figure B) (Kessar et al., 2006; Kohwi et al., 2007; Kriegstein and Alvarez-Buylla, 2009; Kwan et al., 2012; Merkle et al., 2007; Ventura and Goldman, 2007; Young et al., 2007). With timelapse imaging *in vitro*, it was previously demonstrated that individual embryonic day-11.5 (E11.5) mouse cortical RGCs generate TBR1-expressing (TBR1⁺) PyNs, followed by Gad1 and Sp8 double-positive (Gad1⁺Sp8⁺) OB interneurons (OB-INs) (Cai et al., 2013). A recent lineage analysis using barcoded virus libraries confirmed this result and revealed that individual early cortical RGCs generate both PyNs and OB-INs *in vivo* (Bayraktar et al., 2015). Lineage analysis of late embryonic cortical RGCs showed that, although they no longer produce PyNs, they generate cortical astrocytes and oligodendrocytes (Gao et al., 2014; Guo et al., 2013). Thus, cortical RGCs progress from generating PyNs to oligodendrocytes, astrocytes, and OB GABAergic interneurons at the end of cortical neurogenesis.

In chapter 2, I show that at the end of PyN production, cortical NSCs begin generating Gsx2⁺ intermediate progenitor cells (IPCs) in the SVZ. Importantly, we demonstrate that Gsx2⁺ cells are tri-potent IPCs (tri-IPCs) at the population level, giving rise to OB-INs, cortical oligodendrocytes, and astrocytes. We show that Sonic Hedgehog (Shh) signaling is both necessary and sufficient for cortical RGCs to switch from generating PyNs

to producing $Gsx2^+$ tri-IPCs and OB-INs; this switch requires blocking the formation of the Gli3 transcription repressor (Gli3R). Finally, single cell RNA sequencing (scRNA-Seq) analysis confirms these findings and identifies the molecular signatures of $Gsx2^+$ IPCs in the cortex.

In chapter 3, I show that that less MIPCs were generated in *Smo cko* mouse brain and less MIPCs were proliferating at late embryonic stage. More importantly, I found Shh signaling activates the transcription of *Egfr* and *Fgfr3* in IPCs, and directly activate the transcription of genes such as *Olig1/2* and *Gsx2*. Gli3 Chip-seq and CUT&RUN-seq revealed 4 binding sites with histone modification and these Gli3 binding sites are required for *Olig1/2* expression in RGCs and in the dorsal cortex. Finally, our 4C-Seq reveals physical interactions between Gli3 binding sites and *Olig1/2* promoters.

In chapter 4, I found 2 binding sites via Pax6 Chip-seq which overlap with Gli3 binding sites at *Olig2* locus. Anti-correlation of *Pax6* and *Olig2* was found in the dorsal VZ/SVZ. More OB-INs and $Olig2^+$ cells were generated by knocking out Gli3 and Pax6 which indicates that Pax6 and Gli3 repress OB-INs lineage and glial cell lineage synergistically.

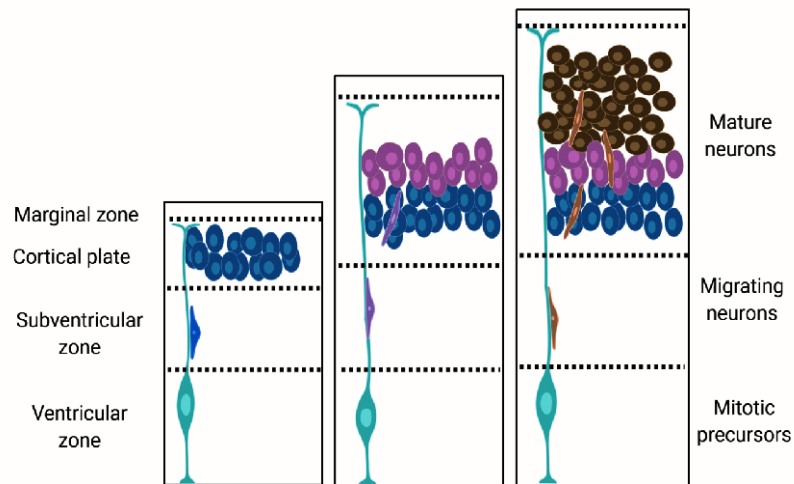


Figure A: The Inside out pattern of cortical neurogenesis.

During development, embryonic NSCs located in the cortical VZ sequentially generate distinct subtypes of PyNs in an inside-out pattern: deep-layer PyNs are born first, followed by PyNs of superficial layer. The local interneurons, however, derive from NSCs located in the medial and caudal ganglionic eminences (MGEs and CGEs, respectively) in the ventral forebrain and migrate tangentially into the cerebral cortex (Kriegstein and Alvarez-Buylla, 2009; Kwan et al., 2012; Leone et al., 2008).

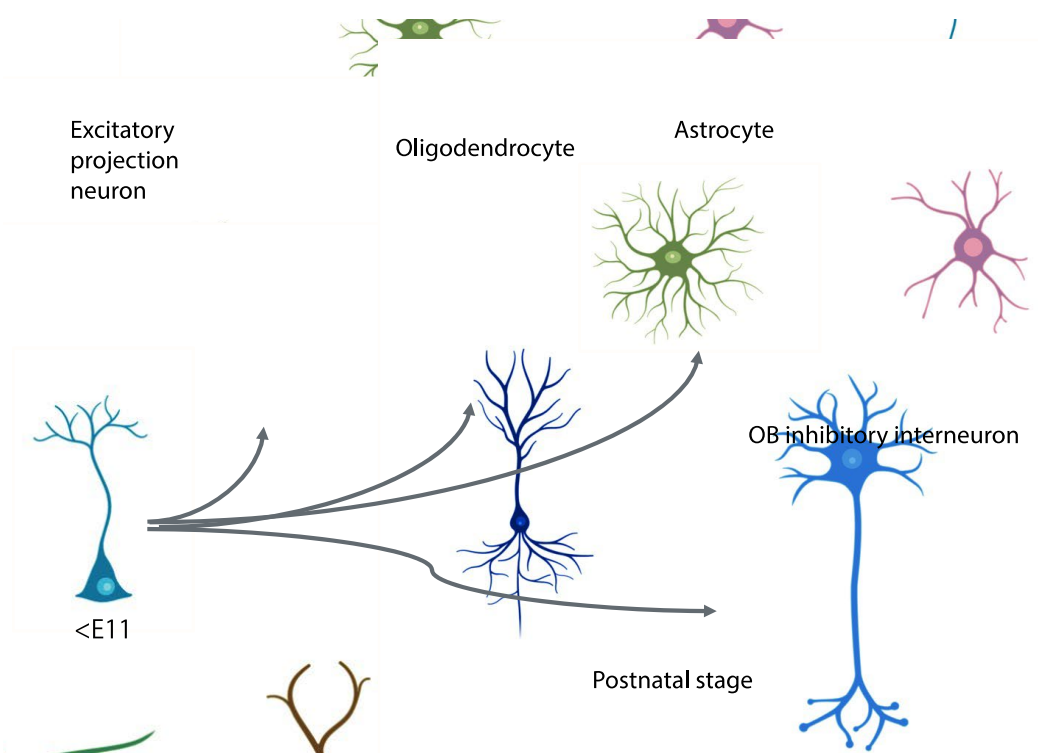


Figure B: Lineage progression of cortical neural stem cells.

At early embryonic stage, neural stem cells generate excitatory neurons and then switch its lineage to generate oligodendrocytes, astrocytes and OB inhibitory interneurons (Kessarlis et al., 2006; Kohwi et al., 2007; Kriegstein and Alvarez-Buylla, 2009; Kwan et al., 2012; Merkle et al., 2007; Ventura and Goldman, 2007; Young et al., 2007).

Sonic Hedgehog signaling pathway

Recently, it has been shown that Sonic Hedgehog (Shh) signaling is critical for cortical RGCs to generate oligodendrocytes (Winkler et al., 2018), but the mechanism regulating the switch for cortical RGCs to generate OB-INs is unknown.

Shh signaling shows a ventral-high and dorsal-low gradient in the VZ of developing forebrain because of the high expression of Shh from ventral cells and the high expression of Gli3R in the dorsal progenitors (Hébert and Fishell, 2008; Sousa and Fishell, 2010). Regulated Shh signaling and Gli activities are essential for the initial dorsal-ventral patterning of the forebrain and the development of cortical interneurons from the ventral forebrain. Ventral forebrain structures are missing in the *Shh*^{-/-} mice (Ohkubo et al., 2002). Loss of *Gli3* function in extra-toes mice (*Gli3* mutants) resulted in ventralization of the cerebral cortex: genes normally expressed in the cerebral cortex were lost; instead, genes associated with ventral and GABAergic neuronal identities were expressed in the dorsal telencephalon (Rallu et al., 2002; Theil et al., 1999; Tole et al., 2000).

There are 3 effectors in canonical Shh signaling pathway: Gli1, Gli2 and Gli3 (Fernandes-Silva et al., 2017). Shh signaling modifies Gli2 to form an activator and Gli3 to attenuate formation of a repressor (Fernandes-Silva et al., 2017; Vaillant and Monard, 2009). High level Shh signaling induces transcription of *Gli1* and both Gli2 and Gli3 have been shown to mediate the downstream signaling of Shh; Gli2 can both activate (Gli2A) and repress

(Gli2R) gene expression, whereas Gli3 acts mostly as a transcription repressor (Gli3R) (Hui and Angers, 2011). Gli2 and Gli3 are expressed in the cortical VZ/SVZ throughout embryonic development (Sousa and Fishell, 2010) and in the SVZ of the lateral ventricle postnatally (Petrova et al., 2013; Wang et al., 2014). Shh signaling does not occur in the absence of Shh ligand wherein Ptch1 inhibits Smo resulting in full length Gli1/Gli2 sequestration in the cytoplasm by Sufu, which promotes the formation of truncated Gli proteins which are repressors to repress the target gene expression (Figure C) (Fernandes-Silva et al., 2017; Vaillant and Monard, 2009). Upon ligand binding, Ptch1 no longer inhibits Smo, Smo becomes activated and induces dissociation of Sufu/Gli complexes and the full length Gli1/Gli2 will activate downstream target genes (Fernandes-Silva et al., 2017; Vaillant and Monard, 2009). *Smo* encodes a G-protein-coupled receptor that is an essential signal transducer for the Shh pathway. We could do loss of function experiment by knocking out *Smo* and do gain of function experiment using *SmoM2* allele which constitutively expresses activated Smo protein and activate Shh signaling pathway upon cre-mediated DNA recombination.

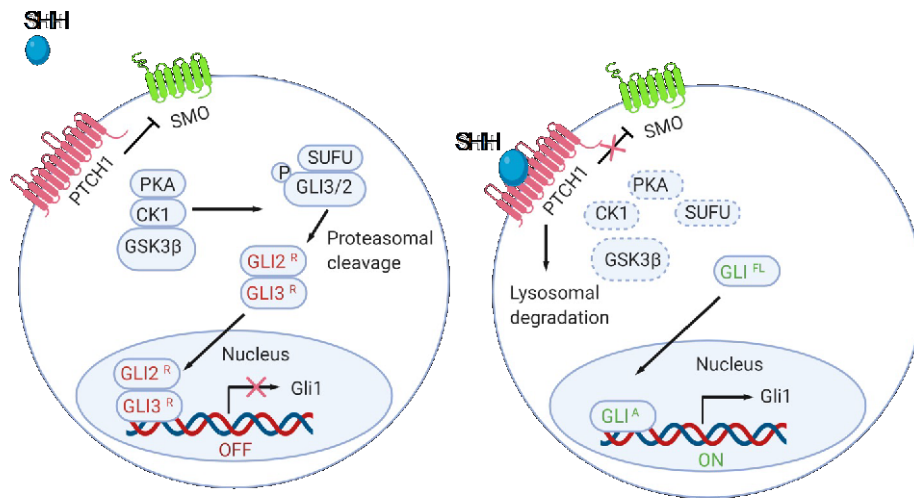


Figure C: Shh signaling pathway.

Shh signaling (left) does not occur in the absence of Shh ligand wherein Ptch1 inhibits Smo resulting in full-length Gli1/Gli2 sequestration in the cytoplasm by Sufu and promotes the formation of truncated Gli proteins which repress the target gene expression. Upon ligand binding (right), Ptch1 no longer inhibits Smo, Smo becomes activated and induces dissociation of Sufu/Gli complexes and the full-length Gli1/Gli2 activate downstream target gene expression (Fernandes-Silva, Correia-Pinto, and Moura 2017).

Innovation and Significance

In the developing mouse brain, proper control of neural stem cell lineage switch is of vital importance to ensure the production of diverse neuronal and glial cell types with exquisite spatiotemporal accuracy and is essential for neural circuit formation and brain function. Understanding the temporal lineage progression of neural stem cells may uncover the pathologies in many neurodevelopmental diseases including autism (Zeidán-Chuliá et al., 2016) and Alzheimer' disease (Nasrabad et al., 2018).

Mechanisms underlying the temporal lineage progression of NSCs have been under extensive investigation (Kohwi and Doe, 2013)(Miyares and Lee, 2019). It is now clear that both spatial and temporal mechanisms cooperate to generate diverse neuronal and glial cell types. Several signaling pathways, including Fgf, Wnt, and Shh pattern the neuroepithelium into distinct progenitor domains along Dorsal-Ventral (D-V) and Anterior-Posterior (A-P) axes. However, the molecular mechanisms that regulate temporal lineage progression of NSCs in the mammalian brain are largely unknown. The molecular mechanisms underlying cortical RGCs remain elusive.

The goal of my thesis research is to determine the molecular mechanisms that regulate the lineage switch of cortical RGCs. I found upon Shh signaling, cortical RGCs generate multipotent intermediate progenitors (MIPCs) that, at the population level, give rise to OB interneurons and both types of glia (Zhang et al., 2020). Cortical astrocyte precursors originate

from either translocating RGCs, or from IPCs in the subventricular zone (SVZ) (Kriegstein and Alvarez-Buylla, 2009). I found that Shh signaling promotes the generation of MIPCs in the SVZ, and it is required for generating translocating RGCs and in general for specifying the astrocyte lineage. I found that translocating RGCs are missing when Shh signaling is blocked. Furthermore, I found that Shh signaling is required for the expression of *Egfr* and *Fgfr3* in MIPCs, both of which activate the mitogen activated protein kinase (MAPK) pathway, which is necessary for lineage specification and generation of cortical glia (Li et al., 2012). Based on my data, I found that (1) The transiting MIPCs are multipotent or bipotent at single cell level; and (2) Shh signaling promotes cortical RGC lineage switch in multiple ways, including activating the transcription of *Egfr* and *Fgfr3* in IPCs, and directly activating the transcription of genes such as *Olig1/2* and *Gsx2*, which are essential for glia and OB-INs development. (3) Gli3 directly binds to *Olig1/2* enhancers which are crucial for the cortical glia and OB-INs development. I've demonstrated the physical interaction of between these enhancers and *Olig1/2* genes. (4) Pax6 directly binds to *Olig1/2* enhancers which overlap with Gli3 binding sites. I found that Pax6 and Gli3 repress OB-INs lineage and glial cell lineage synergistically.

The mechanisms for this lineage switch are fundamental for unraveling how the brain is constructed, yet the answer remains largely unknown. Determining how lineage progression of NSCs is regulated in the cortex will shed light on this process in other brain regions. Furthermore, mutations in Shh pathway genes lead to severe neurodevelopmental

defects in human (Carballo et al., 2018; Majd and Penas-Prado, 2019). Unraveling how the Shh pathway regulates lineage progression of RGCs will provide novel insights into these neurological diseases (Carballo et al., 2018; Majd and Penas-Prado, 2019). I've proved that increased Shh signaling is necessary and sufficient for the lineage switch of cortical RGCs through multiple ways which shed light on this longstanding question. In this thesis research, I utilized cutting-edge approaches to study brain development, integrating intersectional lineage analyses with genomic techniques. I used RNA-seq, sc-RNA-seq, 4C-Seq, CUT&RUN, ChIP-seq, ATAC-seq, and enhancer analysis, to aid in phenotypic analysis of mutant mice to determine the molecular mechanisms underlying the lineage switch.

The text of this dissertation will present, discuss, and include results from the published paper and a paper in preparation for submission:

- (1) Yue Zhang, Guoping Liu, Teng Guo, Xiaoyi G. Liang, Heng Du, Lin Yang, Aparna Bhaduri, Xiaosu Li, Zhejun Xu, Zhuangzhi Zhang, Zhenmeiyu Li, Miao He, Jeremiah Tsyporin, Arnold R. Kriegstein, John L. Rubenstein, Zhengang Yang, and Bin Chen. Cortical Neural Stem Cell Lineage Progression Is Regulated by Extrinsic Signaling Molecule Sonic Hedgehog. *Cell Reports* 30, 4490–4504, March 31, 2020. Reprinted with permission.
- (2) Xiaoyi G. Liang, Kendy Hoang, Yue Zhang, Zhaoxu Chen, Fangyuan Qu, Bin Chen et al., A conserved mechanism regulating neurogenesis to gliogenesis switch in the cerebral cortex.

Chapter 2: Cortical neural stem cell lineage progression is regulated by extrinsic signaling molecule sonic hedgehog

Results

Gsx2 is expressed in a subpopulation of IPCs in the cortex

It has been recently identified that the Gsx2/1–Dlx1/2–Sp8/Sp9–Tshz1–Prokr2 genetic pathway is crucial for generating virtually all OB-INs (Guo et al., 2019; Li et al., 2018). In this transcriptional cascade, Gsx2 is at the top of the hierarchy, and its expression and functions in NSCs and IPCs in the lateral ganglionic eminence (LGE) have been well documented (Guo et al., 2019; Toresson and Campbell; Waclaw et al., 2009; Wang et al., 2013a). It is known that a subpopulation of OB-INs is derived from cortical progenitors (Kriegstein and Alvarez-Buylla, 2009). However, it is unclear whether the above transcription factors are expressed by cortical progenitors. To answer that question, I examined the expression of Gsx2 in the cortex. At E16.5, the time when the production of PyNs ceases, only a few cells in the cortical SVZ weakly expressed Gsx2 (Figure 1A). From E17.5 to P21, Gsx2⁺ cells were observed in the cortical SVZ and intermediate zone (Figure 1A and Figure 8A). Guoping Liu and Teng Guo, my collaborator at Fudan University, analyzed co-expression of Gsx2 and Mki67 in the E18.5 cortex and found that 86.1% of Gsx2⁺ cells expressed Mki67 and 30.4% of Mki67⁺ cells in the SVZ expressed Gsx2 (Figures 8B and 8C). This suggests that Gsx2⁺ cells represent a subpopulation of the

cycling progenitors in the cortex. Although *Gsx2* is expressed in NSCs and IPCs in the VZ and SVZ of the LGE (Guo et al., 2019; Wang et al., 2013b), I did not observe *Gsx2*⁺ cells in the cortical VZ, indicating that they are IPCs, rather than the primary VZ RGCs.

I next asked how numerous *Gsx2*⁺ cells are in the cortex in prenatal and postnatal stages. To address this question, Guoping Liu and Teng Guo quantified the numbers of *Gsx2*⁺ cells in the cortex at E18.5, P1, P3, P5, and P7 in the rostro-caudal and medio-lateral axes (Figures 8D - 8F). In general, *GSX2*⁺ cells showed a lateral to medial spatial gradient with the numbers of *GSX2*⁺ cells highest in the intermediate cortex and fewer in the rostral and caudal cortices at all stages (Figures 8D - 8F). Interestingly, it appeared that there were more cortical *GSX2*⁺ cells at P0 and P5 than at other stages (Figure 8F). Taken together, these results suggest that a subset of IPCs in the cortex express *Gsx2* in the prenatal and postnatal mouse telencephalon. *Eomesodermin* (*Eomes*; *Tbr2*) is a transcription factor of the T-box family expressed by IPCs in the PyN lineage of the cortex (Bulfone et al., 1999; Hevner, 2019; Lv et al., 2019). I did not observe co-expression of *Gsx2* and *Eomes* in the cortex (Figures 8D and 8E). The ratios of *Gsx2*⁺ cells to *Eomes*⁺ cells increase with developmental stages from 0.25 at E18.5 to 2.7 at P7 (Figure 8G), as the numbers of *Eomes*⁺ cells drop sharply in the postnatal cortex (Kowalczyk et al., 2009).

Cortical NSCs generate *Gsx2*⁺ IPCs at late embryonic stages

To determine whether the $Gsx2^+$ IPCs in the cortex originated from the cortical VZ or migrated from the LGE, we performed intersectional (IS) analysis using *Cre* and *Flpo* recombinases in combination with an *IS* reporter mouse line (He et al., 2016) (Figure 1B). We generated the $Gsx2^{Flpo}$ allele by inserting a *P2A-Flpo-T2A-Flpo* cassette immediately before the stop codon of the endogenous *Gsx2* gene (Figure 9A). We confirmed the specificity of *Flpo* activity in the $Gsx2^+$ cells by breeding the $Gsx2^{Flpo/+}$ mice with *Rosa26-tdTomato-FRT* mice (He et al., 2016). TdTomato (tdT) expression was observed in the LGE and MGE at E13.5 and E14.5 (Figure 9B), consistent with the expression pattern of *Gsx2* protein. To perform intersectional lineage analysis, Guoping Liu and Teng Guo delivered *pCAG-Cre* plasmids specifically into the cortical VZ of $Gsx2^{Flpo/+}; IS$ embryos on E14.5 by in utero electroporation (IUE). In this experiment, cells generated from electroporated cortical RGCs that did not go through a $Gsx2^+$ stage expressed tdT. On the other hand, cells generated from the electroporated RGCs that did go through a $Gsx2^+$ stage expressed GFP (Figure 1B). We examined the brains at E18.5. The electroporation sites were confirmed by examining tdT expression (Figure 1C). We observed many tdT⁺ cells that extended from the IUE VZ/SVZ to the cortical plate. Fewer GFP⁺ cells were observed; most of them were in the cortical SVZ, intermediate zone and some in the cortical plate (Figure 1C). GFP⁺ cells were not observed in the cortical VZ. Moreover, the GFP⁺ cells in the cortical SVZ did not have a bipolar shape with elongated radial fibers that projected toward the pial surface (Figure 1C), providing evidence that they were not RGCs.

Lineage tracing reveals the tri-potency of Gsx2⁺ IPCs in the cortex

We next examined the lineages of the Gsx2⁺ cortical IPCs. We electroporated *pCAG-Cre* plasmids into the cortical VZ of *Gsx2^{Flpo/+}; IS* embryos on E14.5 and analyzed the brains and OBs at P21. We observed many tdT⁺ and/or GFP⁺ interneurons in the OB; 42.6% of lineage-traced cells were GFP⁺, 28.7% tdT⁺, and 28.7% of cells expressed both GFP and tdT (Figure 1D and 1E). The GFP⁺tdT⁺ interneurons in the OB were due to the perdurance of the tdT protein, and these neurons were possibly generated later than the GFP⁺-only cells. The total percentage of GFP⁺ and GFP⁺tdT⁺ cells among all the lineage-traced OB-INs were about 71.3%. Although we cannot exclude the possibility that a small number of cortical RGCs directly give rise to OB-INs without going through a Gsx2⁺ IPC stage, this number was likely an underestimate because of the lower recombination efficiency of the *Flp-FRT* system compared with the *Cre-Loxp* system (Buchholz et al., 1998). Thus, most, if not all, of the OB-INs originating from the cortical VZ were the progeny of Gsx2⁺ cortical IPCs.

We also observed a substantial number of GFP⁺ cells in the cortex; their morphology and expression of Olig2 and S100b indicated that these were oligodendrocytes and astrocytes (Figures 1F - 1H). The ratio of oligodendrocytes to astrocytes was 6:1 (Figure 1I). These results demonstrated that cortical Gsx2⁺ IPCs give rise not only to interneurons in the OB but also to cortical oligodendrocytes and astrocytes, suggesting that,

at the population level, the $Gsx2^+$ cells are tri-potent IPCs or tri-IPCs. However, it is unclear whether individual $Gsx2^+$ IPCs give rise to all three lineages or the $Gsx2^+$ IPCs consist of different uni-potent or bi-potent IPC populations that produce one or two cell lineages.

To confirm our IUE-based lineage-tracing results, I examined *Emx1^{Cre/+}; Gsx2^{Fipo/+}; IS* triple-transgenic mice in which Cre recombinase was activated in cortical RGCs at approximately E10.5 (Gorski et al., 2002) (Figure 10). At P21, we observed many GFP⁺ interneurons in the OB (Figure 10F) and GFP⁺Olig2⁺ oligodendrocytes and GFP⁺S100b⁺ astrocytes in the cortex (Figures 10A - 10C). About 10% of Olig2⁺ cells and 4% of S100b⁺ cells were labeled by GFP (Figure 10D), suggesting that $Gsx2^+$ IPCs contribute to small portions of cortical oligodendrocytes and astrocytes. The ratio of oligodendrocytes to astrocytes among the GFP⁺ glial cells was 6:1 (84.7% versus 15.3%) (Figure 10E), similar to those observed with the *pCAGIG-Cre* IUE approach (Figures 1F - 1I). Together, these results demonstrated that the cortical $Gsx2^+$ cell population at late embryonic and early postnatal stages generates OB-INs and both types of cortical glia.

The Shh signaling pathway is required for the cortical RGCs to generate OB-INs

Neurogenesis in the ventral telencephalon largely generates GABAergic neurons. Shh signaling promotes ventral identities during development throughout the neuroaxis (Hébert and Fishell, 2008). OB-INs

production from the dorsal cortex was observed concurrently with increased expression in the cortical VZ/SVZ at P0 and P7 of *Gli1*, which encodes a transcription factor that promotes Shh signaling (Tong et al., 2015). To explore the possibility that OB-IN production requires Shh signaling, we deleted the Smoothed (Smo) gene utilizing an *hGFAP-Cre* allele (Zhuo et al., 2001). *Smo* encodes a G-protein- coupled receptor that is an essential signal transducer for the Shh pathway. *hGFAP-Cre* is active in the cortical RGCs from E13.5 and in the LGE and CGE from E16.5.

Guoping Liu and Teng Guo compared the expression of OB-IN lineage markers in the *hGFAP-Cre; Smo^{F/F}* (*Smo cko*) mice with littermate control *hGFAP-Cre; Smo^{F/+}* mice at P2 using in situ RNA hybridization and immunohistochemistry (Figure 2). Reduced expression of *Gli1* mRNA confirmed decreased Shh signaling in the cortical VZ/SVZ of *Smo cko* mice (Figure 2A). Almost all *Gsx2⁺* cells were lost in the rostral and caudal cortical SVZ (Figures 2B - 2D), as were cells expressing OB-IN markers *Sp9*, *Tshz1*, and *Prokr2* and the pan-GABAergic neuron marker *Gad1* (Figure 2A). The number of *Sp8⁺* cells in the cortical SVZ was also significantly reduced (Figures 2B - 2D); the remaining *Sp8⁺* cells in the *Smo cko* cortical SVZ were probably CGE-derived cortical interneurons (Ma et al., 2012). The lack of OB-INs in the cortical VZ/SVZ of *Smo cko* mice could be due to a defect in fate specification or to reduced cell proliferation. To distinguish between these possibilities, I examined numbers of *Eomes⁺* cells and cell proliferation by administrating EdU to label S-phase cells 2 h before sacrificing the mice. At P0, the number of *EdU⁺* cells in the mutant VZ was

not significantly different from that in the control brains. However, in the *Smo* *cko* SVZ, there were fewer Eomes⁺ cells, and there was a significant reduction of the Eomes⁺EdU⁺ cells (Figures 11A and 11C). This observation was consistent with a previous report that Shh signaling is not required for cortical RGC proliferation, but rather, it promotes the proliferation of cortical IPCs (Komada et al., 2013). Unlike at P0, by P3, the number of Eomes⁺ cells was not significantly affected (Figures 11B and 11C). We postulate that the restored Eomes⁺ IPC cells at P3 likely originated from the cortical RGCs. The reduced OB lineage cells and normal Eomes⁺ cell number at P3 provide further evidence that Shh signaling drives cortical RGCs to switch from generating Eomes⁺ IPCs to Gsx2⁺ IPCs and OB-INs.

Increased exposure to Shh signaling during neurogenesis of deep-layer pyramidal neurons causes a premature fate switch to generate OB-INs and oligodendrocytes

Recently, it was reported that Shh signaling promotes cortical RGCs to generate oligodendrocytes (Winkler et al., 2018). Both Gsx2⁺ and Olig2⁺ cells appear in the cortical SVZ around E16.5 during normal development (Figure 1A) (Winkler et al., 2018). Is this because cortical RGCs are exposed to increased Shh signal at the end of cortical neurogenesis or because they become competent to respond to Shh signaling to generate these cell types only at that time? To address those questions, we ectopically expressed Shh in the cortical VZ by electroporating the *pCAG-*

ShhN-ires-GFP plasmid into wild-type (WT) mice at E13.5 (the peak time for generating layer-5 cortical projection neurons) and examined the brains at E18.5 (Figure 3A). Controls were electroporated with the *pCAG-GFP* plasmid. Brains electroporated with the *pCAG-ShhN-ires-GFP* had increased *Gli1* and *Ptch1* expression, consistent with increased activation of the Shh signaling pathway (Figure 3A) (Shikata et al., 2011). Furthermore, more cells expressed OB-IN lineage markers: *Gsx2*, *Ascl1*, *Dlx2*, *Sp8*, *Sp9*, *Tshz1*, *Prokr2*, and *Gad1* (Figures 3A and 3B). The number of *Olig2*⁺ cells also increased (Figure 3B), consistent with a previous report (Winkler et al., 2018). Bulk RNA-seq analysis confirmed the increased expression of genes associated with OB-INs (*Gsx2*, *Ascl1*, *Dlx1/2*, *Gad1*, *Sp8/9*, *Tshz1*, and *Prokr2*) and oligodendrocytes (*Olig1/2*, *Pdgfra*, and *Sox10*) in the cortices electroporated with *pCAG-ShhN-ires-GFP* at P0 (Figure 3C). Thus, cortical RGCs can respond to increased Shh signaling to generate OB-INs and oligodendrocytes even during the peak time of producing PyNs.

Yue Zhang and I investigated the effect of increased Shh pathway activation on OB-IN generation using the conditional *Rosa26^{SmoM2}* allele, which, upon CRE-mediated recombination, expresses a constitutively active Smo protein, independent of Shh signaling (Jeong et al., 2004). We examined the cortex of *hGFAP-Cre; Rosa26^{SmoM2/+}* and littermate control mice (*Rosa26^{SmoM2/+}*) at E17.5. Similar to Shh overexpression, in *hGFAP-Cre; Rosa26^{SmoM2/+}* mice we observed increased numbers of cells expressing OB-IN and oligodendrocyte lineage markers (data not shown). Most PyNs are generated between E11.5 and E16.5 in the neocortex. Our

RNA-seq data from the P0 cortex of *hGFAP-Cre; Rosa26^{SmoM2/+}* mice showed mis-regulation of many genes associated with PyNs (data not shown). Consistently, misregulated PyN gene expression in the Shh-IUE cortex was also observed at P0 (data not shown). These results indicate that cortical PyN development is compromised after overexpression of *ShhN* or *SmoM2* at E13.5 (Yabut et al., 2015).

Shh signaling promotes OB-IN and cortical oligodendrocyte fates through reducing Gli3R

Both Gli2 and Gli3 have been shown to mediate the downstream signaling of Shh; Gli2 can both activate (Gli2A) and repress (Gli2R) gene expression, whereas Gli3 acts mostly as a transcription repressor (Gli3R)(Hui and Angers, 2011). Gli2 and Gli3 are expressed in the cortical VZ/SVZ throughout embryonic development (Sousa and Fishell, 2010) and in the SVZ of the lateral ventricle postnatally (Petrova et al., 2013; Wang et al., 2014). To determine whether the Shh pathway promotes cortical RGCs to generate Gsx2⁺ IPCs through activating Gli2A or through reducing Gli3R, Yue and I examined the brains of *hGFAP-Cre; Gli2^{F/F} (Gli2 cko)* (Corrales et al., 2006), *hGFAPCre; Gli3^{F/F} (Gli3 cko)* (Blaess et al., 2008), and *hGFAP-Cre; Gli2^{F/F}; Gli3^{F/F} (Gli2 Gli3 dcko)* mice at P0 (Figures 4A–4D). Compared with the WT mice, the numbers of Gsx2⁺, Sp8⁺, and Olig2⁺ cells were not significantly affected in the *Gli2 cko* mice (Figure 4E), but their numbers were significantly increased in cortical VZ/SVZ of the *Gli3 cko* mice (Figures

4C and 4E). These results suggested that Gli2 is not required for the lineage switch, whereas Gli3 inhibits the cortical RGCs from generating OB-INs and oligodendrocytes. Consistent with that, significantly more Gsx2⁺, Sp8⁺, and Olig2⁺ cells were present in the cortical VZ/SVZ of the *Gli2 Gli3 dcko* than in the WT brains (Figure 4E).

Yue and I next examined the brains of *hGFAP-Cre; Smo^{F/F}; Gli3^{F/F}* (*Smo Gli3 dcko*) mice. Although the numbers of Gsx2⁺, Sp8⁺, and Olig2⁺ cells were reduced in the *Smo cko* mice (Figures 2B–2D, 4B, and 4E), they were restored in the *Smo Gli3 dcko* mice. Compared with the WT, more Gsx2⁺, Sp8⁺, and Olig2⁺ cells were observed in the cortical VZ/SVZ of *Smo Gli3 dcko* mice at P0 (Figures 4D and 4E). These results indicate that Gli3 inhibits cortical RGCs from generating OB-INs and oligodendrocytes, and that Shh pathway activation blocks this inhibition to enable the production of those cell lineages.

We analyzed neurogenesis in the adult SVZ (P90). Whole mount of the lateral wall of lateral ventricle stained with antibody against DCX showed a marked decrease in neuroblast chains in *Smo cko* mice (Figure 11D), but this defect was largely rescued in *Smo Gli3 dcko* mice (Figure 11D). Thus, Gli3 also inhibits neurogenesis of OB-INs in the adult SVZ.

scRNA-Seq analysis supports the existence of Gsx2⁺ tri-IPCs in the developing cortex

Guoping Liu and Teng Guo performed scRNA-Seq to analyze the cortical progenitors undergoing the lineage switch. Neocortices from E16.5 WT mice (wt sample) and from E16.5 cortices that were electroporated with *pCAG-ShhN-ires-GFP* plasmids on E13.5 (ShhN-IUE sample) were dissected, dissociated into single-cell suspensions, and sequenced using the 10X genomics platform. After removing outlier cells that had a high percentage of ribosomal or mitochondrial genes, 7,494 cells in the wt sample and 8,311 cells in the ShhN-IUE sample were used for analysis, with an average of 2,450 genes detected per cell (Figures 5A and 5B).

After confirming no batch effect between the two samples, dimensionality reduction followed by unsupervised clustering using Louvian community detection (Blondel et al., 2008) and visualization with t-Distributed Stochastic Neighbor Embedding (t-SNE) (Macosko et al., 2015) revealed 31 clusters in the wt sample and 36 clusters in the ShhN-IUE sample (data not shown). Gene ontology analysis classified those clusters into discrete populations, including RGCs, IPCs, PyNs, cortical interneurons (CINs), endothelial cells (ECs) and microglia, and Cajal-Retzius cells (CRs) (Figure 5A). In the ShhN-IUE sample, we identified additional clusters with molecular signatures of tri-IPCs, oligodendrocyte progenitor cells (OPCs), and OB-IN IPCs (OB-IPCs) that were not identified in the wt sample (Figures 5A, 5B, S6, and S7). This was likely due to the small numbers of tri-IPCs, OPCs, and OB-IPCs present in the WT cortical SVZ at E16.5. Indeed, we observed only 8 *Gsx2*⁺ (0.10% of the population) and 27 *Olig2*⁺ (0.36%) progenitor cells in the wt sample, whereas there were 214 *Gsx2*⁺ (2.57%)

and 222 Olig2⁺ (2.67%) progenitor cells after ShhN-IUE (Figures 5C and 5D). Five days after ShhN-IUE, we observed Tshz1⁺ and Prokr2⁺ OB immature interneurons in the E18.5 cortices by in situ RNA hybridization (Figure 3A), but we did not find Tshz1⁺ and Prokr2⁺ cells 3 days after ShhN-IUE in the E16.5 cortices in our scRNA-Seq results. This is likely due to the OB-IPCs not having enough time to differentiate into postmitotic OB-INs at E16.5. An astrocyte cluster was not identified at this time; astrocytes are generated mainly after PyN neurogenesis.

The gene regulatory network Gsx2/1–Dlx1/2–Sp8/Sp9–Tshz1–Prokr2 is crucial for the generation and differentiation of virtually all OB-INs, and the homeobox transcription factor genes, Dlx1/2, are central and essential components in this transcriptional code (Guo et al., 2019; Li et al., 2018). Previous fate mapping studies demonstrated that Dlx1/2-Cre and Dlx5/6-Cre only label neurons, but not oligodendrocytes or astrocytes (Potter et al., 2009; Stenman et al., 2003), strongly suggesting that once IPCs express Dlx family genes, their neuronal fate has been determined. It is also known that Gsx2 and Dlx2 repress OPC specification (Chapman et al., 2013, 2018; Kohwi et al., 2007). Therefore, the IPCs that expressed Gsx2 and Dlx2/1 were most likely OB-IPCs, even though some of them also expressed Olig2. In contrast, those IPCs that expressed Gsx2 and Olig2/1, but not Dlx2/1, were likely tri-IPCs, with the potential to give rise to either OB-INs or cortical glia or both. Indeed, among the eight Gsx2⁺ cells in the wt sample, four cells expressed Dlx2/1 and Dcx (two of them also expressed Olig2/1) and were OB-IPCs (Figure 5E). The other four Gsx2⁺ cells

expressed *Olig2/1*, but not *Dlx2/1*, and were likely tri-IPCs (Figure 5E); they may have the potential to generate oligodendrocytes, astrocytes, and/or OB-INs (Figure 1).

Trajectory analysis using Monocle 2 (Qiu et al., 2017a, 2017b) on all the cells in the wt or the *Shh*-IUE sample was unsuccessful, likely because too many clusters were included. Thus, we focused our analysis on the progenitor cells. Louvian analysis of all the progenitor cells in the *Shh*N-IUE sample revealed seven clusters (Figures 6A and 6 B). Based on gene expression patterns, we identified them as RGCs (*Dbi*⁺*Aldoc*⁺*Slc1a3*⁺*Gli3*⁺), OB-IPCs (*Ascl1*⁺*Dlx1*⁺*Dlx2*⁺*Sp9*⁺), neuroblasts for OB-Ins (*Dcx*⁺*Dlx5*⁺*Gad1*⁺*Sp8*⁺), OPCs (*Olig1*⁺*Pdgfra*⁺*Sox8*⁺*Sox10*⁺), differentiating PyNs (PyNs) (*Sox11*⁺*Neurod6*⁺*Pou3f1*⁺*Satb2*⁺), and tri-IPCs (*Hes6*⁺*Btg2*⁺*Gsx2*⁺*Olig2*⁺) (Figures 6A–6C). t-SNE visualization (Figures 6A and 6C) showed that cells of the OB-IN lineage and the oligodendrocyte lineage were clearly segregated, exhibiting distinct molecular signatures. Monocle analysis predicted a developmental trajectory and pseudo-timeline progression of the progenitor clusters in the *Shh*N-IUE sample (Figures 6D and 6E). The lineage progression was predicted to start from RGCs passing through tri-IPCs; after which, two distinct trajectories were identified that led to either OPCs or OB-IPCs (Figure 6E). The tri-IPC population was located between RGCs and the OPCs and OB-IPCs, suggesting that tri-IPCs were a transitional cell type that generated OPCs and OB-IPCs, consistent with the lineage-tracing results (Figures 1C–1G).

***In vivo* validation of markers of tri-IPCs and their lineage progression in the cortical SVZ**

To further validate the molecular signatures of IPCs identified from the scRNA-Seq analysis, Guoping Liu and Teng Guo performed triple-immunostaining to examine expressions of Gsx2, Olig2, Dlx2, Sp9, and Sp8 in the E17.0 WT and ShhN-IUE cortices. Few Gsx2⁺ cells were observed in the WT cortex (Figure 7A). Compared with the Gsx2⁺ cells, more Olig2⁺ cells were observed (Figure 7A), with some of them derived from the LGE and MGE (Kessaris et al., 2006). There were many Dlx2⁺, Sp9⁺, and Sp8⁺ cells in the cortical SVZ; they were MGE- and/or CGE-derived cortical interneurons (Figures 7A and 7B) (Anderson et al., 1997; Liu et al., 2019; Ma et al., 2012). Although very rare in the E17.0 wt cortex, Gsx2⁺Olig2⁺Dlx2⁻ tri-IPCs (arrows in Figure 7A) and some Gsx2⁺Dlx2⁺ OB-IPCs (arrowheads in Figure 7A) were observed. In the E17.0 ShhN-IUE cortex. There were significant increases in the numbers of Gsx2⁺, Olig2⁺, Dlx2⁺, Sp9⁺, and Sp8⁺ cells in the VZ and/or SVZ compared with WT mice (Figures 7B–7E). Consistent with the scRNA-Seq results, significantly more Gsx2⁺ Dlx2⁺ OB-IPCs and Gsx2⁺ Olig2⁺ Dlx2⁻ tri-IPCs were present (Figure 7F). Very few IPCs expressed Gsx2 alone (Figure 7F). Almost all Gsx2⁺ cells segregated into either tri-IPCs or OB-IPCs, based on the expression of Dlx2.

A careful examination of the ShhN-IUE cortices revealed that, based on the position of Gsx2⁺ cells closer to the cortical VZ, Gsx2 expression began before Dlx2, and Dlx2 expression began before Sp8/9 (Figure 7G),

indicating a developmental progression along the OB-IN lineage: $Gsx2^+$ tri-IPCs generate $Dlx2^+$ OB-IPCs, which, in turn, generate $Sp9^+$ and $Sp8^+$ OB neuroblasts in the cortical SVZ. This observation supports our unsupervised trajectory analysis results (Figures 6D and 6E) and is consistent with the process of OB-IN development in the dorsal LGE (Guo et al., 2019).

Chapter 3: Sonic hedgehog signaling is critical for cortical RGCs to generate oligodendrocytes and astrocytes

Results

Shh signaling promotes the generation and proliferation of MIPCs

A recent paper showed that cortical neural stem cells start to generate $Ascl1^{+}Egfr^{+}$ apical multipotent intermediate progenitors (MIPCs), which then differentiate into basal MIPCs that express $Ascl1$, $Egfr$, $Olig2$, and $Mki67$ which give rise to most of the cortical oligodendrocytes and astrocytes and a subpopulation of OB-INs (Li et al., 2021). I confirmed the subtype specific marker expression in vivo via double or triple immunofluorescence analysis and confocal microscopy in our lab. I examined $Ascl1$, $Egfr$, and $Olig2$ expression at E16.5 and E17.5 (Figure 13, Figure 14). $Ascl1$ and $Egfr$ were expressed in a lateral high to medial low gradient in the cortical VZ/SVZ (Figure 13, Figure 14) which is consistent with the recent paper (Li et al., 2021). By E17.5, some RGCs were translocating to the cortical plate (CP), likely transforming into AS-IPCs and OPCs. The scRNA-Seq analyses in the recent paper showed that astrocyte lineage cells strongly expressed $Id1$, $Id3$ and $Egfr$ and OPCs expressed $Olig2$, $Sox10$, $Pdgfra$, $Olig1$ (Li et al., 2021). These markers were validated via immunofluorescence staining at E17.5, E18.5 and P0 (Figure 12, Figure 13).

Upon Shh signaling, cortical RGCs generate multipotent intermediate progenitors (MIPCs) that, at a population level, give rise to and both types of glia (Zhang et al., 2020). However, it is not known if Shh promotes the generation of MIPCs or Shh promotes the proliferation of MIPCs. To answer this question, Kendy and I performed birth dating experiment. The EdU was given at E16.5 and the brains were collected at P0. I examined EdU⁺ cells in VZ/SVZ, IZ and cortical plate in wildtype control and *Smo cko*. Less EdU⁺ positive cells were found in VZ/SVZ, IZ and CP in *Smo cko* (Figure 12C). In general, less cells were generated at E16.5 in *Smo cko* mouse brain. I then examined general glial cell marker Olig2. Less Olig2⁺EdU⁺ positive cells were found in *Smo cko* (Figures 12A and 12D). Our data suggested that less glial progenitors were generated in *Smo cko* mouse brain. Although it's been reported that multiple sources of Shh signaling promotes the generation of oligodendrocytes (Winkler et al., 2018), it remains unclear whether the generation of cortical astrocytes require Shh signaling. Cortical astrocyte precursors originate from either translocating RGCs, or from IPCs in the SVZ (Kriegstein and Alvarez-Buylla, 2009). Our RNA-seq showed increased expression of *Slc1a3*, *Aldh1l1*, *Fabp7*, and *ApoE* in *Gli3 cko* mice, and reduced expression of these genes in *Smo cko* cortices (data not shown). All of these genes are expressed in both RGCs and astrocytes (Dulken et al., 2017; Weng et al., 2019), implicating Shh signaling in promoting astrocyte development. I examined the astrocytes marker *Id1* and translocating RGC marker *Egfr*. Less *Id1*⁺EdU⁺ positive cells were found in *Smo cko* mouse brain (Figure 12). The *Egfr*⁺ translocating

RGCs which in general specify the astrocyte lineage are missing when Shh signaling is blocked (Figure 12B, Figure 13P and 13V). Our data suggested that the generation of cortical astrocytes requires Shh signaling. MIPC marker *Ascl1* was also examined and less *Ascl1*⁺*EdU*⁺ positive cells were found in *Smo cko* mouse brain implicating that Shh is required for cortical RGCs to generate MIPCs at late embryonic stage.

To examine if the proliferation of MIPCs when Shh signaling is blocked. Kendy and I collected E17.5 litter mate control and *Smo cko* mouse brain after 2h *EdU* injection. Less *EdU* and *Ki67* positive cells were found in *Smo cko* mouse brain (Figures 13M, 13S, 13R, 13X, 13Y). MIPC markers were examined, and we found Less *Olig2*⁺*EdU*⁺, *Id1*⁺*EdU*⁺, *Ascl1*⁺*EdU*⁺, *Egfr*⁺*EdU*⁺ positive cells in *Smo cko* mouse brain (Figure 13). Our data suggested that Shh signaling is required for the proliferation of MIPCs.

Shh activate the transcription of *Egfr* and *Fgfr3* in IPCs

It's been reported the Raf-MEK-MAPK pathway is a key regulator of gliogenesis. RGCs deficient in both *Mek1* and *Mek2* failed to transit to gliogenesis, resulting in absence of cortical AS-IPCs and OPCs (Li et al., 2012). This suggested that MEK/ERK MAPK signaling mediates the lineage switch of RGCs (Li et al., 2012). Interestingly, *Fgf* and *Egf* signaling, both of which can activate the Raf-MEK-MAPK pathway, has been implicated in directing the cell fate switch from neurons to astrocytes in the developing cortex (Beattie et al., 2017; Dinh Duong et al., 2019). To determine whether

these pathways were affected in the *Smo cko* cortices, I examined MAPK activities and gene expression. At E16 and E18.5, 90% of the MAPK cells in the IZ and cortical plate express Olig2 (Figure 14, Figure 16, Figure 17). MAPK signal dramatically decreased in *Smo cko* at E15 while Satb2⁺ PyNs and Tbr2⁺ IPCs remain unchanged (Figure 14). MAPK and Egfr signal got rescued in *Gli3 cko* mouse brain (Figure 14). Cortical MAPK⁺Olig2⁺ glial progenitors and cortical Id1⁺Olig2⁺ AS-IPCs are dramatically increased in *Gli3 cko* mouse brain at E16.5 which indicate that Shh is both necessary and sufficient to activate MAPK in the IZ and cortical plate to generate cortical glia by degrading Gli3R (Figure 14). RNA-Seq analysis of the P0 *Smo cko* cortices revealed significantly increased Fgfr1 expression (2 folds increase), and significantly reduced Fgfr3 (23% of wt), Egfr (21% of wt), and Tgfa (35% of wt), the major Egfr ligand in the cortex at this stage. Our scRNA-Seq showed that Fgfr1 is highly expressed in RGCs, Fgfr3 is expressed in RGCs and IPCs, while Egfr is expressed in MIPCs, AS-IPCs and Pre-OPCs (data not shown). My immunostaining confirmed reduced Egfr expression in the E17.5 *Smo cko* cortices (Figure 13). Consistent with increased Fgfr1 expression, I observed increased phospho-MAPK in the VZ of the *Smo cko* mice at P0 (Figure 14K). However, in the SVZ and cortical plate, the numbers of phospho-MAPK⁺ cells were reduced (Figure 14K), likely due to decreased Fgfr3, Egfr and Tgfa expression. I have observed decreased phospho-MAPK in IZ and cortical plate in *Emx1-cre Egfr^{F/F}* mouse brain, however, the phosphor-MAPK remain unchanged in the VZ (Figure 14J). Fgf signaling pathway is of vital importance for cell proliferation

and differentiation (Brewer et al., 2016; Diez del Corral and Morales, 2017; Korsensky and Ron, 2016). I examined diverse lineage markers in *hGFAPcre; Fgfr1^{F/F};Fgfr2^{F/F};Fgfr3^{F/F}(Fgfr Tcko)* mouse brain. The *Tcko* mouse die at birth. I have observed decreased Ki67⁺ cells in *Tcko* mouse brain at E18.5 which indicate less cell proliferation (Figure 17). The phospho-MAPK⁺ cells was dramatically decreased in VZ/SVZ, IZ and cortical plate, and the remaining phosphor-MAPK⁺ cells in *Tcko* mouse brain express *Egfr* which indicate that fgf signaling is the key to maintain phosphor-MAPK in RGCs (Figure 17, Figure 18). I also observed decreased Olig2⁺ Olig1⁺ Ascl1⁺ OPCs, Id1⁺ Sox9⁺ Egfr⁺ AS-IPCs, and Sp8⁺ OB- IPCs as well as Tbr2⁺ PyN-IPCs in *Tcko* mouse brain which indicate that fgf signaling regulate the proliferation of cortical RGCs and IPCs (Figure 17). Our data suggested that Shh signaling activates the transcription of *Egfr* and *Fgfr3* in IPCs to promote the lineage progression toward gliogenesis.

Anti-correlation of Gli3 and Olig2 in VZ/SVZ

We found that Olig1/2 is expressed in cortical SVZ upon RGC lineage switch, and they showed reduced expression in the cortical SVZ in *Smo cko* mice, and increased expression when Shh signaling was increased (Zhang et al., 2020). We have reported that Shh regulate cortical RGCs lineage switch by degrading Gli3R (Zhang et al., 2020). Olig2 is dramatically decreased in *Smo cko* (Figure 4) and increased in *Gli3 cko* mouse brain (Figure 4, Figure 14). I sectioned the P0 wildtype mouse brain and *Smo cko*

mouse brain at 12um and performed Gli3/Olig2 double immunofluorescence staining to examine the Olig2 and Gli3 expression at VZ/SVZ. 40X image was taken by 880 confocal microscope. I carefully quantified the fluorescence signal by using ImageJ. 90% of the Gli3 positive cells in the VZ/SVZ in the wildtype mouse brain showed cytoplasm staining, however, 90% of the Gli3 positive cells showed strong nucleus staining in the *Smo cko* mouse brain (Figure 19). Cells with high Gli3 signal showed low Olig2 signal in wildtype mouse brain based on the fluorescence signal quantification (Figure 19A). *Smo cko* mouse brain showed even stronger anti-correlation of Gli3 and Olig2 (Figure 19B). By knocking out *Smo*, Gli3 protein moves from the cytoplasm into the nucleus and represses target gene expression (Rimkus et al., 2016). Our data indicated that Gli3 directly repress Olig2 expression in cortical RGCs and IPCs.

Gli3 binds to both confirmed and potential enhancers of Olig1/2

To determine how Shh signaling regulate the lineage switch, Yue Zhang and I performed ChIP-seq and CUT&RUN using a Gli3 antibody and dissected cortices (n = 3 for each experiment). ChIP-seq and CUT&RUN revealed Gli3 binding sites (GBS) genome-wide. The results were highly consistent both within and between the ChIP-seq and CUT&RUN experiments, indicated by the specific binding to promoters and enhancers of Shh target genes such as *Gli1*. We identified 4414 Gli3 binding sites (GBS) using IDR (<https://www.encodeproject.org/software/idr/>), and the motifs

enriched in the GBS. The most significantly enriched motif is identical to the published Gli binding sequence (Figure 21, Figure 27).

The CUT&RUN data revealed histone modification changes upon Shh signaling (Figure 21). Yue and I performed CUT&RUN to study if Shh signaling affects histone modification in cortical cells. We utilized E16.5 wild-type and *SmoM2* cortices, and antibodies for H3K4Me3 and H3K27Me3, which are associated with active and inactive promoters/enhancers, respectively. Consistent with increased Gli1 expression in *SmoM2* cortices, we observed increased H3K4Me3 at the promoter, and decreased H3K27Me3 at the promoter and gene body (Figure 15).

Olig1/2 and *Gsx2* are essential for the development of cortical glia and OB interneurons, respectively (Liu et al., 2015; Marshall, 2005; Ono et al., 2008; Waclaw et al., 2009). Ectopic expression of *Gsx2* is sufficient for late cortical progenitor cells to generate OB interneurons (Waclaw et al., 2009). How transcription of these genes is regulated is not known. RNA-seq revealed that in both E16.5 *Gli3 cko* and *SmoM2* cortices, *Olig2*, *Gsx2* and *Olig1* were the 3 most significantly increased genes. Our ChIP-seq, CUT&RUN, and ATAC-seq analyses revealed that Gli3 binds to predicted enhancers of *Olig2* (Figure 21), *Gsx2* gene and *Fgfr3* gene (Figure 16) which indicate direct transcriptional repression.

Olig1 and *Olig2* genes are located 36 kb apart on chromosome 16. ChIP-seq revealed 4 GBS sites in their vicinity, located in highly conserved regions (Figure 21). None of the GBS overlapped with *Olig1* or *Olig2* promoter. GBS2 and GBS3 showed H3K27Me3 and H3K4Me3

modifications. In cortices electroporated with the *pCAG-Shh-N* (Shh-IUE) plasmids, ATAC-seq revealed increased chromatin accessibility at GBS2 and GBS3 (Figure 21), indicating possible enhancer activities. I determined if GBS1-3 and E2 are associated with known enhancers by mining the ENCODE data. GBS1 is located within the predicted enhancer e14414 (Figure 21), activity of which has been confirmed (Figure 27G). E2 overlaps with the predicted enhancer e14415 (Figure 21). GBS3 overlaps with enhancer e14416. Encode project predicted these enhancers to interact with the *Olig2* promoter (Figure 21) (<https://doi.org/10.1101/166652>). GBS2 does not overlap with any predicted or known enhancer (Figure 21).

Defects in *Olig2*^{-/-} mouse brain

Previous studies have shown that ectopic expression of *Olig2* led to over-production of cortical astrocytes and oligodendrocytes (Liu et al., 2015; Marshall, 2005), and that there was a severe reduction in cortical oligodendrocytes and white matter astrocytes in the *Olig2*^{-/-} and *Olig2 cko* mice (Cai et al., 2007; Ono et al., 2008, 2009; Takebayashi et al., 2002a). We generated *Olig2*^{-/-} mouse by using *Olig2*^{cre/+} mouse line. *Olig2*^{cre/+} mice have a Cre recombinase inserted into the only exon of the oligodendrocyte transcription factor 2 *Olig2* gene. The presence of cre abolishes expression of *Olig2*. *Olig2*^{cre/cre} has no function *Olig2* allele. I observed that *Olig2*^{cre/cre} mouse die shortly after birth which is consistent with previous paper (Takebayashi et al., 2002b). No *Olig2* expression in the *Olig2*^{cre/cre} and

decreased Olig1⁺ cells were found in mouse brain (Figures 20A, 20B, 20F, 20G). It's been reported that Olig2 regulates Sox10 expression in OPCs through regulating a conserved enhancer (Kuspert et al., 2011). The mature oligodendrocyte marker Sox10 (Elbaz and Popko, 2019; Traiffort et al., 2016) is absent in *Olig2^{cre/cre}* mouse brain (Figures 20K, 20P). As expected, I have also observed decreased Sox9⁺, Id1⁺ AS-IPCs and Aldh1l1⁺ astrocytes in the dorsal cortex (Figures 20D, 20I, 20K, 20P). Phospho-MAPK⁺ and Egrf⁺ cells were still present in the VZ/SVZ, IZ and cortical plate in the *Olig2^{cre/cre}* suggested that MAPK and Egrf signaling pathway functions upstream of Olig2. Ascl1⁺ MIPCs showed no change in *Olig2^{cre/cre}* (Figures 20N, 20S). I analyzed some E18.5 *Ascl1^{-/-}* mouse brain and found decreased Olig2 expression which indicate that Ascl1 functions upstream of Olig2 (data not shown). Olig2 expressed in MIPCs which can give rise to Oligodendrocytes, astrocytes and OB interneurons (Li et al., 2021). I carefully analyzed the OB interneuron marker Sp8 in the VZ/SVZ and found fewer Sp8⁺ cells in *Olig2^{cre/cre}* (Figures 20M, 20R) which indicated that in addition to severely glial cell deduction, deletion of Olig2 also impair OB interneuron production from cortical RGCs.

These Gli3 binding sites are required for Olig1/2 expression in RGCs and SVZ MIPCs

The *hGFAP* promoter is active in the mouse cortical RGCs during the lineage transition (Zhuo et al., 2001). Using the *hGFAP-GFP* transgenic

mice (Zhuo et al., 1997), a group recently enriched the late cortical RGCs and their proximal progeny cells at P1, and performed a single-cell ATAC-seq experiment (Li et al., 2021). Kendy analyzed this data and identified RGC, MIPC, AS-IPC, OL-IPC, and OB-IN IPC clusters and the ATAC-seq peaks enriched in each cluster. He found that the most enriched sc-ATAC-seq peaks in the MIPCs compared to the RGCs were located in the GBS2 and GBS3, while the GBS1 was equally accessible in the RGC and IPC clusters (data not shown).

There are two ways to test if an enhancer is required for the expression of a specific gene. To generate a compound heterozygous animal harboring one disruptive enhancer with a wild-type gene in one allele and a null gene but wild-type enhancers in the other allele or generate the straight enhancer knock-out mice (Osterwalder et al., 2018). We generated 4 knock-out mouse line via CRISPR/as9 technology: GBS1/e14414, E3, GBS2/E2 and GBS3/E1 knock-out mouse line (Figure 21) which harbor the loss-of-function alleles and they were all maintained as heterozygous (*Olig2* ^{Δ e14414/+}, *Olig2* ^{Δ E3/+}, *Olig2* ^{Δ E2/+}, *Olig2* ^{Δ E1/+}). These heterozygous and *Olig2*^{cre/+} are all viable and fertile.

To determine if these enhancers regulate *Olig2* expression, we generated compound heterozygous which has a null *Olig2* gene but wild-type enhancers on one allele and a wild-type *Olig2* gene with a disruptive enhancer allele by cross the enhancer heterozygous to *Olig2*^{cre/+}. I analyzed the *Olig2* and *Olig1* expression in the dorsal VZ/SVZ in these compound heterozygous by immunofluorescence staining (Figure 22). The Pax6

staining was used to show the VZ/SVZ where a dense band Pax6⁺ cells defined ventricular zone (VZ) and a diffuse band of Pax6⁺ cells defined subventricular zone (SVZ) (Martínez-Cerdeño et al., 2012). I compared the number of Olig2⁺ and Olig1⁺ cells of the compound heterozygous with *Olig2^{cre/+}* (Figure 22). Olig2⁺ and Olig1⁺ cells in VZ/SVZ were significantly reduced in *Olig2^{cre/Δe14414}*, *Olig2^{cre/ΔE2}* and *Olig2^{cre/cre}* which indicate that e14414 and E2 are required for the expression of Olig2 and Olig1 in dorsal RGCs and IPCs in VZ/SVZ (Figures 22Y and 22Z). GBS1 and e14414 overlap with confirmed hs1188 and mm817 enhancers, which drive strong LacZ expression in cortical progenitors (Figure 27G). This suggests that a physical proximity between e14414/hs1188/mm817 and a promoter is a likely mechanism how this enhancer activates gene expression in the cortex.

I examined the different lineage markers in the dorsal cortex in different compound heterozygous. I observed decreased Olig2⁺ cells in *Olig2^{cre/Δe14414}*, *Olig2^{cre/ΔE2}* but the Olig1⁺ cells showed no change (Figure 25U, 25V) which indicated that e14414 and E2 are required for the Olig2 expression in dorsal Olig2⁺ OPCs and oligodendrocytes. To our surprise, 80% of the *Olig2^{cre/ΔE2}* compound heterozygous die shortly after birth. The phenotype of *Olig2^{cre/ΔE2}* (Figure 25) is similar to *Olig2^{cre/cre}* (Figure 20) although not as severe. I not only observed decreased Id1⁺, Sox9⁺ AS-IPCs and Sox10⁺ oligodendrocytes in the dorsal cortex in *Olig2^{cre/ΔE2}* compound heterozygous but also decreased Sp8⁺ OB interneurons in the VZ/SVZ (Figure 25) which indicated that E2 is required for the development of dorsal IPCs.

To further test if these enhancers are required for Olig2/Olig1 expression, we generated straight enhancer knock-out mice by crossing the heterozygous together. The enhancer knock-out mice *Olig2^{Δe14414/Δe14414}*, *Olig2^{ΔE3/ΔE3}*, *Olig2^{ΔE2/ΔE2}*, *Olig2^{ΔE1/ΔE1}* are viable at P0 before collection. I observed decreased Olig2⁺ and Olig1⁺ cells in *Olig2^{Δe14414/Δe14414}*, *Olig2^{ΔE3/ΔE3}*, *Olig2^{ΔE2/ΔE2}* mice in VZ and SVZ (Figure 23) and decreased Olig2⁺ OPCs and Id1⁺ AS-IPCs in *Olig2^{Δe14414/Δe14414}*, *Olig2^{ΔE3/ΔE3}* mouse brain (Figure 26). I did not observe decreased OPCs, AS-IPCs in the cortex or OB interneurons in VZ/SVZ in *Olig2^{ΔE2/ΔE2}* mouse brain although the phenotype of *Olig2^{cre/ΔE2}* was much severe (Figure 25, Figure 26). Interestingly, I observed decreased Olig2⁺ and Olig1⁺ cells in VZ/SVZ in *Olig2^{ΔE3/ΔE3}* (Figures 23I - 23L) but not in *Olig2^{cre/ΔE3}* (Figures 22I - 22L). These data indicated that these different enhancers might function redundantly and could compensate for each other in multiple ways.

I also analyzed Olig2 expression in ventral brain and in lateral VZ/SVZ as well as medial VZ/SVZ and found decreased Olig2⁺ cells in *Olig2^{Δe14414/Δe14414}* and *Olig2^{cre/Δe14414}* which indicate that e14414 is not only required by dorsal RGCs and SVZ MPCs but also required for lateral RGCs and SVZ MIPCs (Figure 24).

4C-Seq reveals physical interactions between Gli3 binding sites and Olig1/2 promoters

Vista Enhancer browser (Visel et al., 2007) shows two overlapping enhancers, hs1188 in human and mm817 in mouse, direct robust LacZ expression in E11.5 mouse cerebral cortex (Figure 27G). This suggests that, if brought to close proximity with a promoter, hs1188 and mm817 direct gene expression in the cortex. Interestingly, the Gli3 binding site GBS1 lies within these enhancers, as well as in the predicted enhancer e14414 (Figure 27). Thus, e14414 and GBS1 are active in cortical progenitors. However, whether other predicted enhancers, GBS2, and GBS3 (Figure 27) regulate Olig1/2 cortical expression is unknown. I hypothesized that these predicted enhancers form long-range regulatory loops with the Olig1/2 promoter, and Gli3 prevents their activation and recruitment. Whether these interactions occur in vivo has not been tested.

To test this hypothesis, Kendy and I performed 4C-Seq experiments (Krijger et al., 2020) to test if there are physical interactions between these enhancers and Olig2/Olig1 promoter by using Olig2 and Olig1 promoter as viewpoints. We performed 4C-Seq by using E16/P0 cortical cells and cells from MGE/LGE in wildtype and *Smo cko* mouse brain to identify sequences that interact with Olig1/2 promoters (Figure 27). Two sets of primers (1844-2059 and 1731-2059) were designed by using Olig1 promoter as the viewpoint (methods). Another Two sets of primers (1840-2440 and 1171-1840) were designed by using Olig2 promoter as a viewpoint (methods).

The 4C peaks overlap with the 4 GBSs and predicted enhancers in wildtype samples, indicating their recruitment to the Olig1/2 promoters (Figure 27C). We observed some enhancers interact with both promoters,

suggesting common regulatory mechanisms for these 2 genes, and frequent chromatin interactions in the region (Figure 27C). Although we did not detect interactions between Olig2 and Olig1 promoter, the Hi-C data from our collaborator showed physical interactions between these two promoters (Data not shown). These are consistent with their co-expression in the same cortical cells. We observe reduced recruitment of GBS2/E2 in *Smo cko* cortices which indicates that Gli3R inhibits recruitment of these enhancers to the Olig1/2 promoters. The other 3 GBSs GBS1/e14414, E3 and GBS3/E1 were recruited to Olig2/Olig1 promoters in *Smo cko* samples. There are two possible explanations, firstly, increased Gli3R in *Smo cko* lead to less physical interactions in *Smo cko* but not inhibiting all physical interactions. Secondly, Gli3R may cause histone modifications which further inhibits the recruitment of polymerase or other transcription factors that facilitate the Olig2/Olig1 gene transcription.

Chapter 4: Pax6 represses OB lineage in the cortical RGCs during development

Results:

Pax6 is required for cortical RGCs to repress OB lineage and oligodendrocyte lineage during development

Gli3 and Pax6 are expressed in cortical neural stem cells and are known as important transcription factors that regulates dorsal ventral patterning (Hébert and Fishell, 2008). It's been reported that loss of Gli3 could rescue the dorsoventral patterning defects seen in *Shh*^{-/-} mutants and loss of Pax6 can partially rescues the loss of ventral structures in *Shh*^{-/-} mice (Fuccillo et al., 2006; Rallu et al., 2002). Pax6 was also known to be sufficient to induce a neurogenic fate in neural stem cells and showed a mutual exclusive expression with Olig2 in the postnatal SVZ (Jang and Goldman, 2011). I sectioned the P0 wildtype mouse brain at 12um and performed Pax6/Olig2 double immunofluorescence staining to examine the Pax6 and Olig2 expression in dorsal RGCs and MIPCs at VZ/SVZ. 40X image was taken by 880 confocal microscope. I quantified the florescence signal by using ImageJ. Cells with high Pax6 signal showed low Olig2 signal based on the florescence signal quantification (Figure 28A). During development, pax6 is expressed in the dorsal telencephalon and is downregulated in the ventral telencephalon, and the intersection of Pax6 and Gsx2 defined the pallial subpallial boundary (Hébert and Fishell, 2008).

Pax6 and Gsx2 showed mutual exclusive expression at the pallial subpallial boundary with minor overlap (Hébert and Fishell, 2008). We have previously reported that Shh signaling promotes the lineage progression of cortical RGCs to generate Gsx2 expressing MIPCs which can give rise to oligodendrocytes, astrocytes and OB interneurons (Zhang et al., 2020). To test if Pax6 repress gliogenesis and OB interneuron production in dorsal RGCs, I examined the lineage marker Olig2, Gsx2, Sp8, Tbr2, Ctip2 and Satb2 in E16 wildtype, *hGFAPcre Pax6^{F/F}* and *Emx1-cre Pax6^{F/F}* mouse brain (Figure 29). I found dramatically increased Olig2⁺, Gsx2⁺ and Sp8⁺ cells in the mutant brain with a dramatically decreased Tbr2⁺ cells (Figure 29) which suggested that removal of Pax6 in dorsal RGCs lead to overproduction of glial and OB lineage cells at the expenses of neural lineage cells. In addition to Gsx2⁺ and Sp8⁺ cells, I also observed increased Ctip2⁺ OB interneuron in the SVZ/IZ in the *Emx1-cre Pax6^{F/F}* mouse brain (Figures 29P, 29T, 29V). Cortical Satb2⁺ PyNs is dramatically decreased in *Emx1-cre Pax6^{F/F}* mouse brain (Figures 29 Q - U, 29V). To determine how Pax6 repress glial and OB lineage in dorsal RGCs, Yue and I performed Pax6 ChIP-seq by using E15 cortices (Figure 28H). We found that Pax6 not only binds to e14414 (GBS1) and e14416 (GBS3/E1) but also predicted enhancer e14412 (Figure 28H) which indicate a direct transcription repression. Our data indicates that Pax6 represses gliogenesis and OB interneuron generation in dorsal RGCs during development.

Pax6 & Gli3 regulate the lineage switch synergistically

Gli3 and Pax6 are both expressed in dorsal RGCs and regulate the lineage progression based on our data. We were wondering whether they work in the same protein complex. To test this, Yue Zhang, Tommy Finn and I performed co-IP experiment by using P0 wildtype cortices and *Smo cko* cortices. We did not pull down Pax6 by using Gli3 antibody and vice versa (Data not shown). To test if Gli3 and Pax6 work synergistically in repressing lineage progression, I examined P0 *hGFAPcre; Gli3^{F/+}; Pax6^{F/+} (dhet)* and *hGFAPcre; Gli3^{F/F}; Pax6^{F/F} (dcko)* mouse brain. I observed a gradually increased trend of Sp8 from wildtype, *hGFAPcre Pax6^{F/F}*, *dhet* and *dcko* (Figure 30). The Gsx2⁺ and Olig2⁺ cells were also increased in *dhet* and *dcko* mouse brain and the Tbr2⁺ cells were decreased in *dcko* (Figure 30). If Gli3 and Pax6 work in the same protein complex and function dependant to each other, I should have observed similar phenotype when compare *dcko* with Gli3 *cko*. However, I observed more severe phenotype in *dcko* mouse brain which suggest that Pax6 and Gli3 function in parallel.

Chapter 5: Discussion and Future directions

In this study, we show that the genetic program *Gsx1/2–Dlx1/2Sp8/9–Tshz1–Prokr2* is activated in the cortical SVZ at the end of cortical neurogenesis, and we uncover an extrinsic signaling pathway that regulates the lineage switch of cortical NSCs to generate OB-INs. Using loss-of-function and gain-of-function analyses, we show that activation of the Shh pathway is both necessary and sufficient for OB-IN generation in the cortical VZ/SVZ through reducing Gli3R. Blocking Shh signaling by deleting *Smo* leads to reduced production of OB-IN lineage, whereas ectopic activation of the Shh pathway by over-expressing *ShhN* or expressing the *SmoM2* allele leads to an early and over-production of OB-INs and cortical oligodendrocytes. Furthermore, lineage-tracing and scRNA-Seq analysis reveal that *Gsx2*⁺ cells derived from the cortical NSCs are tri-IPCs at the population level; they produce not only interneurons in the OB but also oligodendrocytes and astrocytes in the cortex. These findings reveal the mechanism by which RGC switch their lineage from production of cortical excitatory neurons to the generation of cortical oligodendrocytes, astrocytes, and inhibitory OB-INs.

Cortical NSCs, PyN-IPCs, tri-IPCs, OPCs, OB-IPCs, Glia-IPCs, and their lineage progression

Generating the diverse neuronal and glial cell types in the mammalian brain is a complex and highly regulated process. Shortly after neural tube closure, NSCs are spatially patterned into discrete progenitor domains. The spatially patterned NSCs undergo sequential neurogenesis and gliogenesis to generate the diverse neuronal and glial cell types (Kriegstein and Alvarez-Buylla, 2009; Kwan et al., 2012). NSCs change their lineage and generate different types of neurons and glial cells based on the developmental stages. In the cerebral cortex, early multipotent cortical RGCs first generate deep-layer PyNs, followed by upper-layer PyNs. At the end of cortical neurogenesis around E16.5, RGCs switch lineages and produce cortical oligodendrocytes, astrocytes, and OB-Ins (Fuentelba et al., 2015; Kriegstein and Alvarez-Buylla, 2009).

Although some PyNs are directly derived from RGCs and some RGCs can directly transform into astrocytes, it is worth noting that most neurons, oligodendrocytes, and astrocytes are not the direct progeny of NSCs but, instead, originate from IPCs (Kriegstein and Alvarez-Buylla, 2009). During the period of cortical neurogenesis around E11.5–E16.5, RGCs undergo asymmetric cell division to self-renew and to produce Eomes⁺ PyN - IPCs (Englund, 2005; Noctor et al., 2004), which exclusively generate PyNs (Lv et al., 2019; Mihalas et al., 2016; Vasistha et al., 2015). During late embryonic and postnatal stages in the mouse cortex, NSC lineage progression becomes complicated, and several distinct IPC populations emerge and coexist in the mouse cortex. OPCs are committed to the oligodendrocyte lineage, whereas OB-IPCs are committed to the OB-

IN lineage. Although in vitro studies have shown the existence of bi-potent glia-IPCs (O-2A cells) that give rise to both oligodendrocytes and astrocytes (Raff et al., 1983), this has not been confirmed in vivo during development.

In the present study, we used intersectional lineage tracing and scRNA-Seq analysis to provide evidence for the existence of Gsx2⁺ tri-IPCs and glia-IPCs in the cortex at the population level during development. These tri-IPCs give rise to OB-IPCs, which generate interneurons that migrate into OB through the rostral migratory stream. In addition, they produce a subset of glia-IPCs, which, in turn, generate OPCs and astrocytes in the cortex (Figures 6D and 6E). We emphasize that it remains to be determined whether single Gsx2⁺ cells proliferate and differentiate into more than one cell type or whether the Gsx2⁺ cells represent a heterogeneous population consisting of uni-potential and/or bi-potent neuronal and glial IPCs. Thus, careful analyses of complete lineages of cortical RGCs and IPCs that include their OB-IN progenies need to be performed. Potential methods that can be used include lineage analysis of individual Gsx2⁺ progenitors using MADM (Gao et al., 2014), barcoded virus (Bayraktar et al., 2015) or methods using genome editing (Bowling et al., 2020).

Shh signaling promotes the generation of OB-INs and cortical oligodendrocytes by reducing Gli3R

Shh activity shows a ventral-high and dorsal-low gradient in the VZ of developing forebrain because of the high expression of Shh from ventral

cells and the high expression of Gli3R in the dorsal progenitors (Hébert and Fishell, 2008; Sousa and Fishell, 2010). Regulated Shh signaling and Gli activities are essential for the initial dorsal-ventral patterning of the forebrain and the development of cortical interneurons from the ventral forebrain. Ventral forebrain structures are missing in the *Shh*^{-/-} mice (Ohkubo et al., 2002). Loss of Gli3 function in extra-toes mice (Gli3 mutants) resulted in ventralization of the cerebral cortex: genes normally expressed in the cerebral cortex were lost; instead, genes associated with ventral and GABAergic neuronal identities were expressed in the dorsal telencephalon (Rallu et al., 2002; Theil et al., 1999; Tole et al., 2000).

Here, we show that the lineage progression of cortical RGCs at late gestational stages is regulated by Shh signaling. During early cortical neurogenesis, RGCs with high GLI3R activity generate Eomes⁺ PyN - IPCs. Interneurons tangentially migrating from the MGE and CGE, start to arrive the cortex around E13.5, and their numbers continue to increase (Lim et al., 2018). As cortical neurogenesis proceeds, Shh secreted from migrating cortical interneurons and cells in the choroid plexus (Winkler et al., 2018) promotes the lineage switch of cortical RGCs to generate OB-INs and oligodendrocytes. Indeed, increased numbers of OB-IN and oligodendrocyte lineage cells were observed in the cortical VZ/SVZ of the *ShhN-IUE* and the *hGFAP-Cre; SmoM2* mice (Figures 3). In contrast, generation of both OB-IN and oligodendrocyte lineage cells from the cortical NSCs was reduced in the *Smo cko* mice (Figure 2) (Winkler and Franco, 2019; Winkler et al., 2018). Long-term blocking of Shh signaling also

resulted in a severe loss of NSCs and migrating neuroblasts in the adult SVZ and RMS (Balordi and Fishell, 2007). Significantly, removing Gli3 in *hGFAP-Cre; Smo cko* mice largely rescued OB-IN genesis and Olig2⁺ cell production in the cortex (Figure 4). Hence, Shh promotes the lineage switch of cortical RGCs to generate OB-INs and cortical oligodendrocytes by reducing Gli3R, rather than by directly promoting the Gli activator function, similar to their functions in neurogenesis in the postnatal SVZ and OB (Petrova et al., 2013; Wang et al., 2014).

Upon increased Shh signaling, Gli3R protein levels in some cortical RGCs decrease, allowing those RGCs to generate Gsx2⁺ and Olig2⁺ IPCs. How does Gli3R repress Gsx2 expression in the cortical VZ/SVZ? Previous studies have shown that expression of Dmrta2 (Dmrt5), Dmrt3, Emx1, and Emx2 in the cortical VZ was severely downregulated in *Gli3* mutant mice (Hasenpusch-Theil and Theil, 2021; Hasenpusch-Theil et al., 2018; Theil et al., 1999). A recent study demonstrated that transcription factors Dmrta2, Dmrt3, and Emx2 cooperatively repress Gsx2 expression to maintain cortical identity of the RGCs (Desmaris et al., 2018). Our Gli3 ChIP-seq showed that Gli3 binds to *Gsx2* gene (Figure 16). Furthermore, Dmrta2, Dmrt3 and Emx2 have been shown to bind to a ventral telencephalon-specific enhancer in the *Gsx2* locus (Desmaris et al., 2018). Thus, Gli3R could be key to maintaining the expression of Dmrta2, Dmrt3, and Emx2 in the cortical VZ during early neurogenesis and to preventing expression of Gsx2.

Shh signaling is essential for cortical RGCs to generate astrocyte lineage and reduced Fgf and Egfr signaling in the IPCs in *Smo cko* contributes to the gliogenesis defects.

In this study, we show that the Shh signaling pathway promotes the generation and proliferation of MIPCs to generate cortical oligodendrocytes and astrocytes as well as OB-INs. Our sc-RNA-seq showed that *Fgfr1* is highly expressed in RGCs, *Fgfr3* is expressed in RGCs and IPCs, while *Egfr* is expressed in MIPCs, AS-IPCs and Pre-OPCs (data not shown). Previous paper show that *Fgf3*, 15, 17, and 18 expression were lost in *Shh*^{-/-} mouse brain and mutating one or both functional *Gli3* alleles in *Shh* or *Smo* mutants partially rescued the loss of *fgf* gene phenotype which indicate that Shh promote the fgf signaling by reducing Gli3R (Hébert and Fishell, 2008; Rash and Grove, 2007). Direct repression evidence was shown by the Gli3 ChIP-seq where Gli3 binds to *Fgfr3* gene (Figure 16). And through loss-of-function analyses, we show that fgf signaling pathway is necessary to maintain MAPK signaling in RGCs and MIPCs (Figure 17). A gain of function experiment was done by other researchers suggested that Fgf signaling promotes astrocyte lineage (Dinh Duong et al., 2019). *Egfr* can also activate MAPK signaling pathway and its expression is blocked in *Smo cko* mutant brains and upregulated in *Gli3 cko* mouse brain(Figure 14) which indicate that Shh signaling is both necessary and sufficient for cortical RGCs and MIPCs to activate *Egfr* signaling. The phenotypic analysis of *Egfr cko* showed decreased MAPK in MIPCs (Figure 14). These findings reveal the mechanism by which Shh activate fgf signaling and *Egfr* signaling to

promote the proliferation and differentiation of RGCs switch their lineage from production of cortical excitatory neurons to the generation of cortical oligodendrocytes, astrocytes, and inhibitory OB-INs.

Gli3 binds to multiple enhancers to regulate the transcription of *Olig2* and *Olig1* which not only affect Cortical OPCs, AS-IPCs but also OB-IPCs

Shh signaling is both necessary and sufficient to induce *Olig2*⁺ cells (Traiffort et al., 2016; Wang and Almazan, 2016; Zhang et al., 2020). However, the molecular mechanisms of the regulation of *Olig2* gene were not well studied. We have shown that Shh is both necessary and sufficient to induce *Olig2* expression by reducing Gli3R (Zhang et al., 2020). And the loss of function analysis of *Olig2* gene revealed defects in both glial genesis and OB-INs generation. Our Gli3 ChIP-seq, CUT&RUN, and ATAC-seq analyses revealed that Gli3 binds to predicted enhancers of *Olig2* (Figure 21). Regulatory DNA elements such as enhancers can work over long distance and recruit transcription factors, polymerase to the gene promoter to switch genes on and off in a time and space specific manner (Levine, 2010). Previous studies focusing on limb development found that the enhancers work synergistically and redundantly where deletions of individual limb enhancers did not cause noticeable changes but removal of pairs of enhancers resulted in discernible phenotypes in limb morphology (Osterwalder et al., 2018). Strikingly, the loss of function analysis of the individual *Olig2* enhancers in this study showed dramatically decreased

Olig2 and Olig1 expression in RGCs and MIPCs in VZ/SVZ (Figure 22, Figure 18, Figure 23). And the phenotypic analysis of the straight knockouts and the compound heterozygous showed decreased OPCs, AS-IPCs or OB-INs which indicate their different function in different lineages (Figure 25, Figure 26). These enhancers may also function in different time points during development and could compensate for each other since the phenotype of the straight knockouts and their corresponding compound heterozygous were different (Figure 22, Figure 23, Figure 25, Figure 26). The e14414 enhancer is conserved from mouse to human and the e14414 enhancer and its human homologous sequence hs817 showed positive enhancer activity from the vista enhancer browser data base (Figure 27). The other enhancers in this study are being tested now.

A core gene regulatory network governing a common developmental trajectory for forebrain NSCs to generate OB-INs

The OB is the most anterior structure of the forebrain. Studies of neurogenesis in the OB have focused on the generation of the OB-INs, in particular, the postnatal and adult neurogenesis occurring in the mouse SVZ of the lateral walls of the lateral ventricle (Obernier and Alvarez-Buylla, 2019). Although NSCs in different domains along the lateral ventricle generate distinct types of neurons and glial cells during embryonic stages, a common trajectory of forebrain NSCs is to switch lineages to generate OB-INs at late embryonic and early postnatal stages (Kriegstein and Alvarez-Buylla, 2009; Obernier and Alvarez-Buylla, 2019).

We recently identified a gene regulatory network *Gsx1/2–Dlx1/2–Sp8/Sp9–Tshz1–Prokr2* that governs OB-IN development; mutations in *Gsx2/1*, *Dlx1/2*, *Sp8/Sp9*, or *Prokr2* genes result in an almost complete loss of mature OB-INs (Guo et al., 2019; Long et al., 2007; Wen et al., 2019). Furthermore, a recent study demonstrated that DLX1 and DLX2 can directly bind to the enhancers and promoters of *Sp8* and *Sp9* (Lindtner et al., 2019). Consistent with the essential regulatory function by this genetic pathway in OB-IN development, in the present study, we found that this genetic program is activated in cortical progenitors and their progenies when OB-INs are generated. Thus, in addition to functioning in the dorsal LGE during development, this core genetic program regulates the generation of OB-INs from all postnatal NSCs in the ventricular wall of the lateral ventricle.

***Pax6* & *Gli3* regulate cortical RGC lineage switch synergistically**

Pax6 and *Gli3* are both expressed in dorsal RGCs and are key transcription factors that controls dorsal-ventral patterning (Hébert and Fishell, 2008). Researchers have observed that loss of *Pax6* partially rescued the morphological defects in *Shh*^{-/-} mice (Fuccillo et al., 2006). During development, *pax6* is expressed in the dorsal telencephalon and is downregulated in the region that is set to be ventral telencephalon, and the intersection of *Pax6* and *Gsx2* defined the pallial subpallial boundary (Hébert and Fishell, 2008). *Pax6* and *Gsx2* showed mutual exclusive expression at the pallial subpallial boundary with minor overlap (Hébert and

Fishell, 2008). It's been reported that dorsal VZ progenitors in Pax6 mutants are progressively ventralized and produce GABA INs at the expenses of generating glutamatergic PyN (Kroll and O'Leary, 2005). We found dramatically increased Olig2⁺, Gsx2⁺ and Sp8⁺ cells in the Pax6 mutant brain with a dramatically decreased Tbr2⁺ and Satb2⁺ cells (Figure 29) which suggested that removal of Pax6 in dorsal RGCs lead to overproduction of glial and OB and glial lineage cells at the expenses of neural lineage cells. We also observed a gradually increased trend of Sp8 from wildtype, *hGFAPcre Pax6^{F/F}*, *hGFAPcre; Gli3^{F/+}; Pax6^{F/+}* and *hGFAPcre; Gli3^{F/F}; Pax6^{F/F}* (Figure 30) which indicate that the repression of OB lineage cells by Gli3 and Pax6 are dosage dependent. We did not pull down Pax6 by using Gli3 antibody and vice versa in our Co-IP experiment (data not shown). If Gli3 and Pax6 work in the same protein complex and function dependent to each other, we should have observed similar phenotype when compare the phenotype in *dcko* to *Gli3 cko* or *Pax6 cko*. However, we observed more severe phenotype in *dcko* mouse brain which suggest that Pax6 and Gli3 function in parallel. Our Pax6 ChIP-seq revealed 2 binding sites at Olig2 locus that overlap with Gli3 binding sites e14414 (GBS1) and e14416 (GBS3/E1) (Figure 28H) indicating Pax6 and Gli3 contribute to a common pathway that regulate the lineage progression of dorsal RGCs.

Through this thesis research, I demonstrated how Gli3R and Pax6 regulate cortical RGCs lineage progression and identified Olig1/2 enhancers. In the future, by generating the enhancer-reporter mice and

analyzing the enhancer activity at different point, we may elucidate how these enhancers function in specifying oligodendrocytes, astrocytes and OB-INs. We have found that these enhancers are relatively conserved through mice and human. It's been reported that Shh promotes the generation of human forebrain olig2 progenitors (Ortega et al., 2013) and this regulatory mechanism of *Olig2* is highly likely to be conserved in human. Future analysis on human PLAC-seq data or 4C-Seq experiments by using human cells will elucidate the regulatory mechanism of human *OLIG2* gene.

Figures

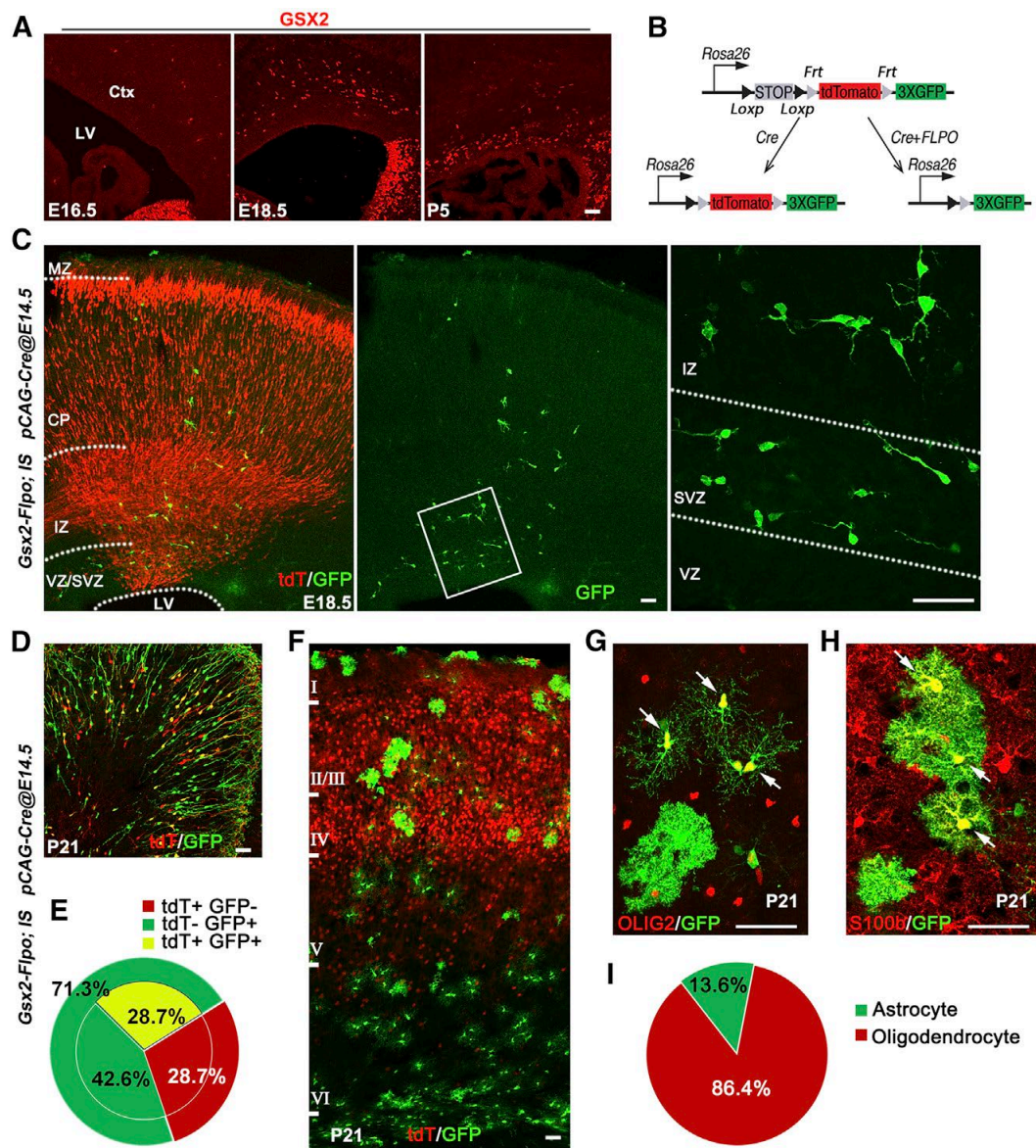


Figure 1. Cortical NSCs generate Gsx2⁺ tri-IPC that give rise not only to OB Interneurons but also to cortical oligodendrocytes and astrocytes

(A) Gsx2⁺ IPCs in the mouse cortical SVZ at E16.5, E18.5, and P5. Ctx, cortex; LV, lateral ventricle.

(B) The strategy of the intersectional lineage analysis.

(C) Plasmids *pCAG-Cre* were electroporated to the cortical VZ of *Gsx2^{Flo/+}; IS* mice at E14.5. GFP⁺ cells were observed in the SVZ and cortical plate at E18.5. CP, cortical plate; IZ, intermediate zone; MZ, marginal zone.

(D) GFP⁺ and/or tdT⁺ interneurons in the OB at P21.

(E) Quantification of the percentages of GFP⁺ and tdT⁺ cells among all the lineage-traced cells in the OB.

(F - H) Cortical GFP⁺ oligodendrocytes (Olig2⁺, arrows in G) and astrocytes (S100b⁺, arrows in H) with higher magnification images at P21. Note tdT⁺ PyNs located in cortical layers II–V (F).

(I) Percentages of oligodendrocytes and astrocytes among all GFP⁺ cells in the cortex. Data in (E) and (I) were from three mice each. Scale bars, 50 μm in (A), (C), (D), and (F - H).

Reprinted from “Cortical Neural Stem Cell Lineage Progression Is Regulated by Extrinsic Signaling Molecule Sonic Hedgehog” *Cell Reports* 30, 4490–4504, March 31, 2020. Reprinted with permission.

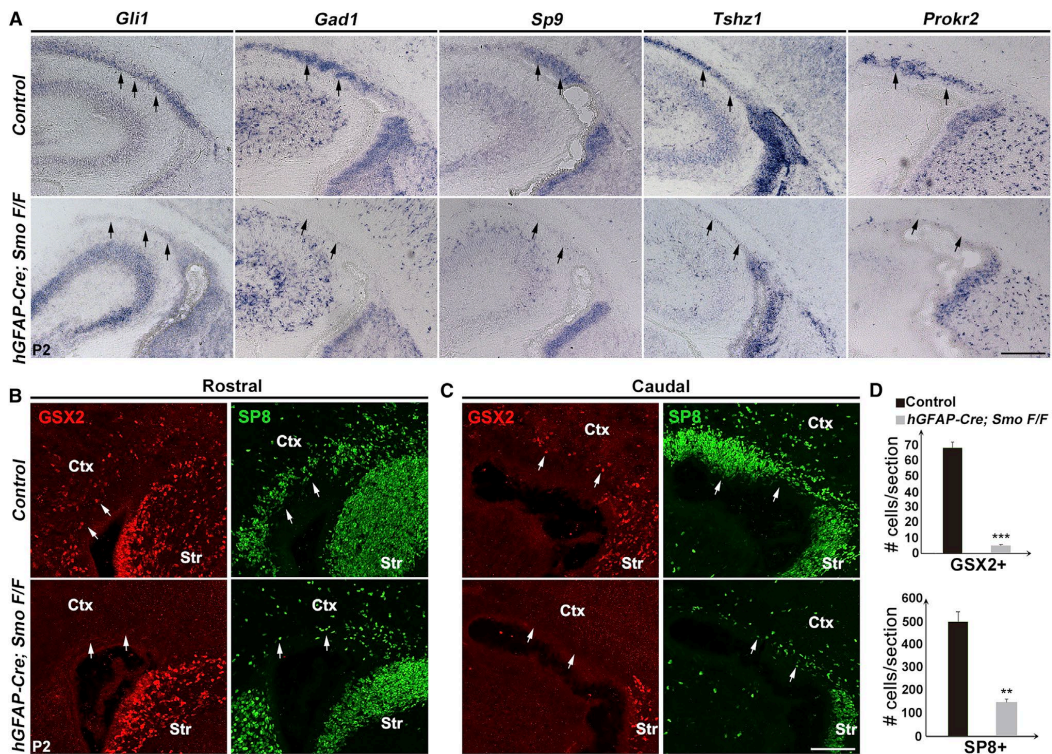


Figure 2. Cells of the OB interneuron lineage are not generated in the cortical SVZ of *Smo cko* mice at P2

(A) In situ RNA hybridization showing expressions of *Gli1*, *Gad1*, *Sp9*, *Tshz1*, and *Prokr2* in the caudal cortical SVZ (arrows) in the control and *hGFAP-Cre; Smo^{F/F}* (*Smo cko*) mice.

(B and C) *Gsx2* and *Sp8* (arrows) immunostainings of the rostral (B) and caudal (C) cortical sections from control and *Smo cko* mice at P2. Ctx, cortex; Str, striatum.

(D) Numbers of *Gsx2*⁺ and *Sp8*⁺ cells in the cortical SVZ per section. Data are presented as means ± SEM; n = 3. ***p < 0.001, **p < 0.01; Student's t test. Scale bars, 200 μm in (B) and (D).

Reprinted from “Cortical Neural Stem Cell Lineage Progression Is Regulated by Extrinsic Signaling Molecule Sonic Hedgehog” *Cell Reports* 30, 4490–4504, March 31, 2020. Reprinted with permission.

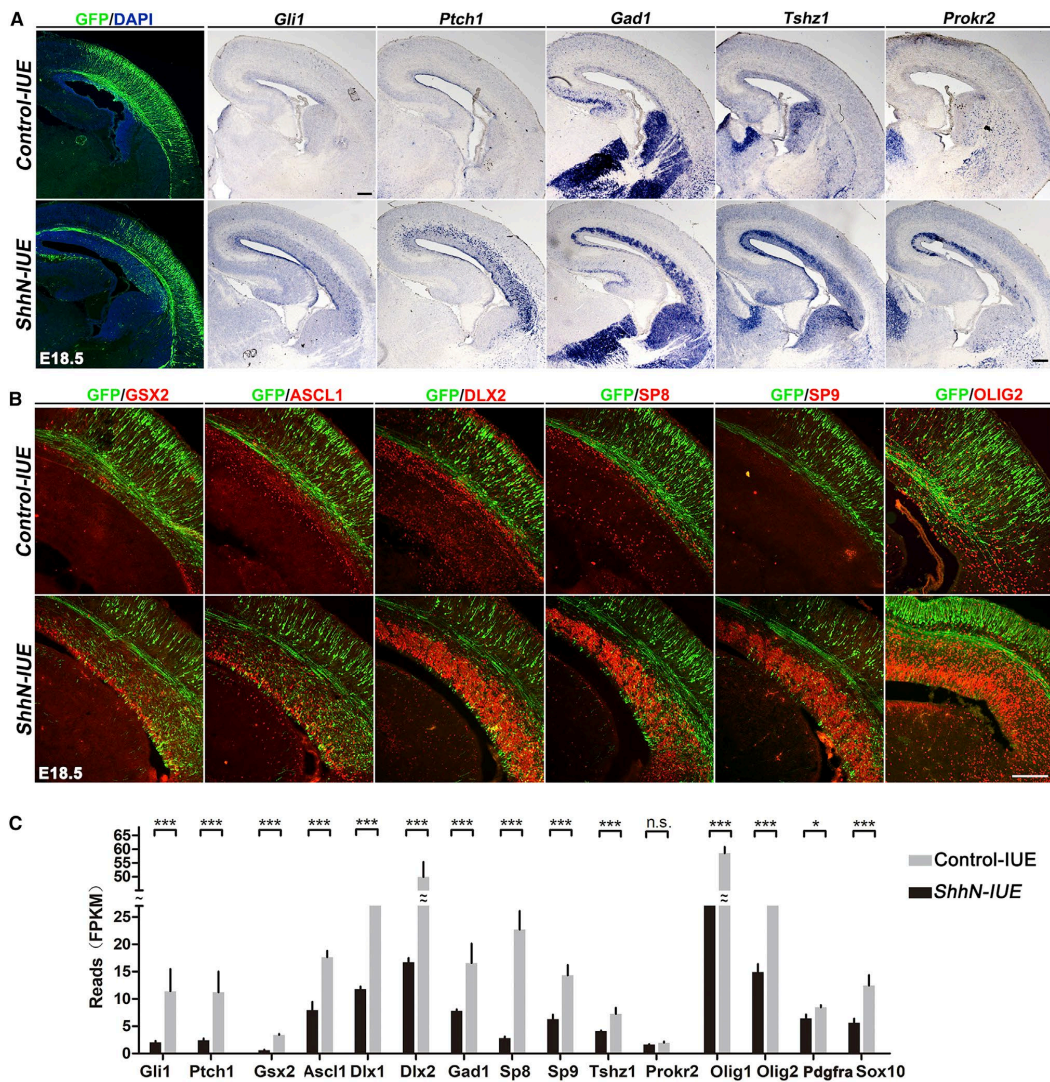


Figure 3. Overexpression of *ShhN* in the cortex by IUE induces OB interneuron and oligodendrocyte lineages in the cortical SVZ

(A) Control *pCAG-GFP* plasmids (control-IUE) or *pCAG-ShhN-ires-GFP* plasmids (ShhN-IUE) were electroporated into the cortical VZ on E13.5. The E18.5 brains were analyzed. The distribution patterns of electroporated cells (GFP⁺) in the cortex are shown. Note that the mRNA levels of *Gli1*, *Ptch1*, *Gad1*, *Tshz1*, and *Prokr2* were dramatically increased in the ShhN-IUE cortex.

(B) The expressions of *Gsx2*, *Ascl1*, *Dlx2*, *Sp8*, *Sp9*, and *Olig2* were greatly increased in the ShhN-IUE cortex.

(C) RNA-seq analysis revealed increased expression levels for Shh pathway target genes, OB interneuron lineage and oligodendrocyte lineage genes in the ShhN-IUE cortices at P0. Data are presented as means \pm SEM; n = 3. ***p < 0.001, *p < 0.05; n.s., non-significant; Student's t test in (C). Scale bars, 200 μ m in (A) and (B).

Reprinted from "Cortical Neural Stem Cell Lineage Progression Is Regulated by Extrinsic Signaling Molecule Sonic Hedgehog" *Cell Reports* 30, 4490–4504, March 31, 2020. Reprinted with permission.

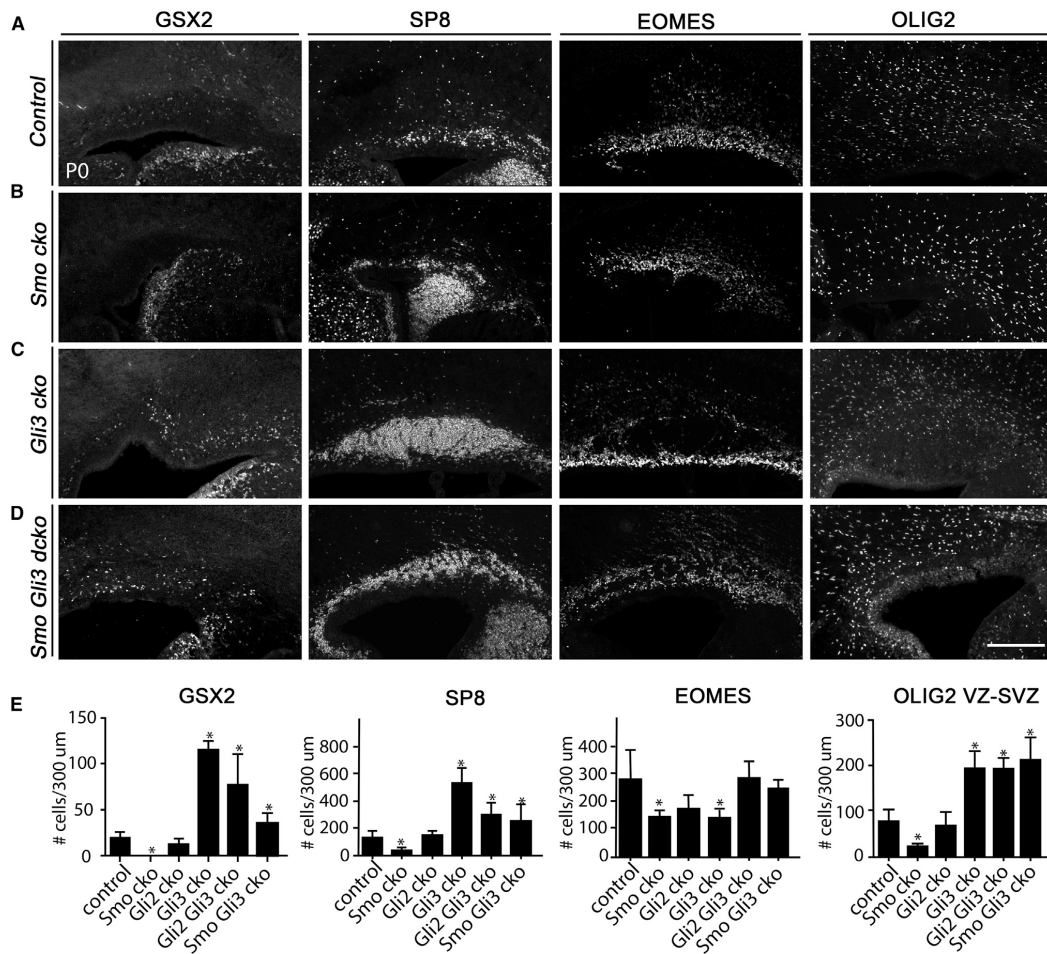


Figure 4. Shh signaling regulates the production of OB interneurons and oligodendrocytes in the cortical VZ-SVZ predominately by reducing Gli3

(A–D) Immunostainings for Gsx2, Sp8, Eomes, and Olig2 in wild-type (control) (A), *Smo cko* (B), *Gli3 cko* (C), and *Smo Gli3 dcko* (D) mice at P0.

(E) Quantification for the numbers of Gsx2⁺, Sp8⁺, Eomes⁺, and Olig2⁺ cells per 300 mm width in the cortical VZ-SVZ of control and mutant mice at P0.

Data are presented as means ± SEM; n = 3 mice per genotype. *p < 0.05; unpaired Student's t test in (E). Scale bars, 200 mm in (D).

Reprinted from “Cortical Neural Stem Cell Lineage Progression Is Regulated by Extrinsic Signaling Molecule Sonic Hedgehog” *Cell Reports* 30, 4490–4504, March 31, 2020. Reprinted with permission.

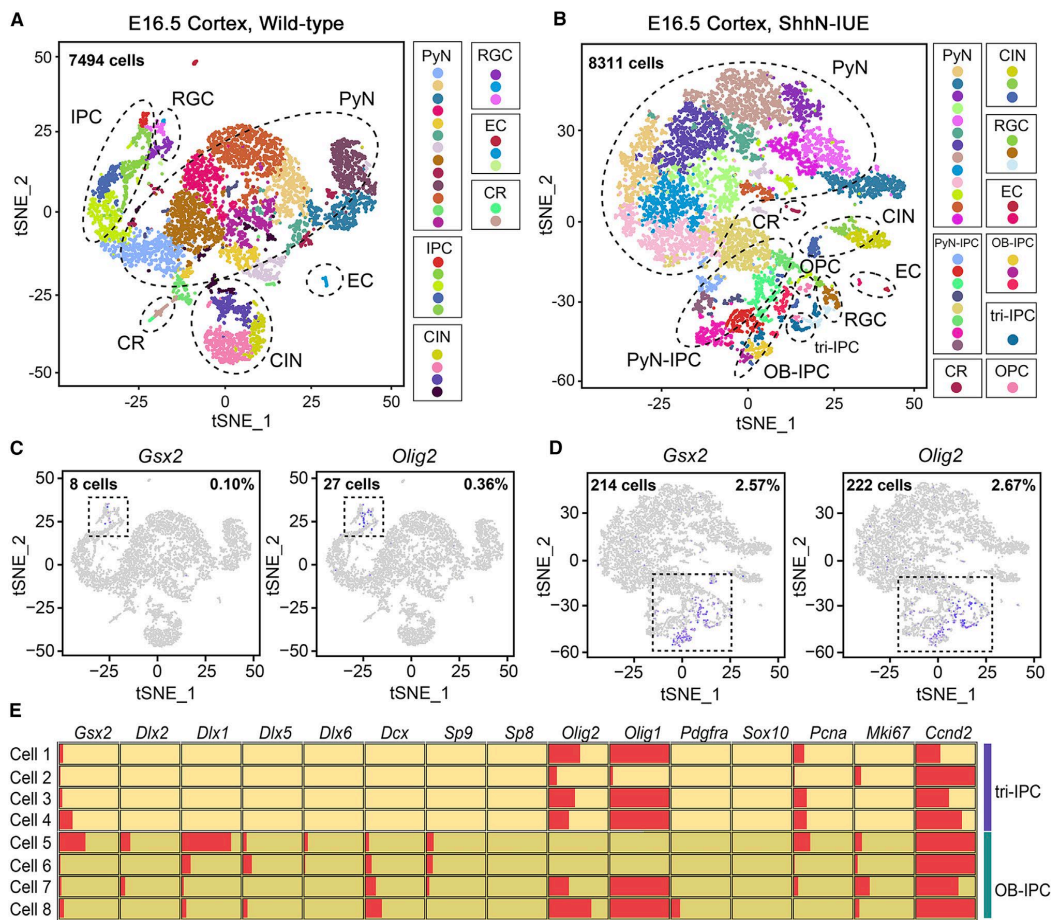


Figure 5. scRNA-Seq analysis of cells in the E16.5 wild-type cortices and in the ShhN-IUE cortices

(A and B) Scatterplot of cells after principal-component analysis and t-SNE visualization, colored according to Seurat clustering and annotated by major cell types for all the cells in the wild-type sample (A) and the ShhN-IUE sample (B).

(C and D) t-SNE of cells colored by mean expression of Gsx2 and Olig2 in wild-type (C) and ShhN-IUE (D) samples.

(E) The eight Gsx2⁺ cells in the E16.5 wild-type sample consisted of four tri-IPCs and four OB-IPCs, based on the expressions of specific genes.

Reprinted from “Cortical Neural Stem Cell Lineage Progression Is Regulated by Extrinsic Signaling Molecule Sonic Hedgehog” *Cell Reports* 30, 4490–4504, March 31, 2020. Reprinted with permission.

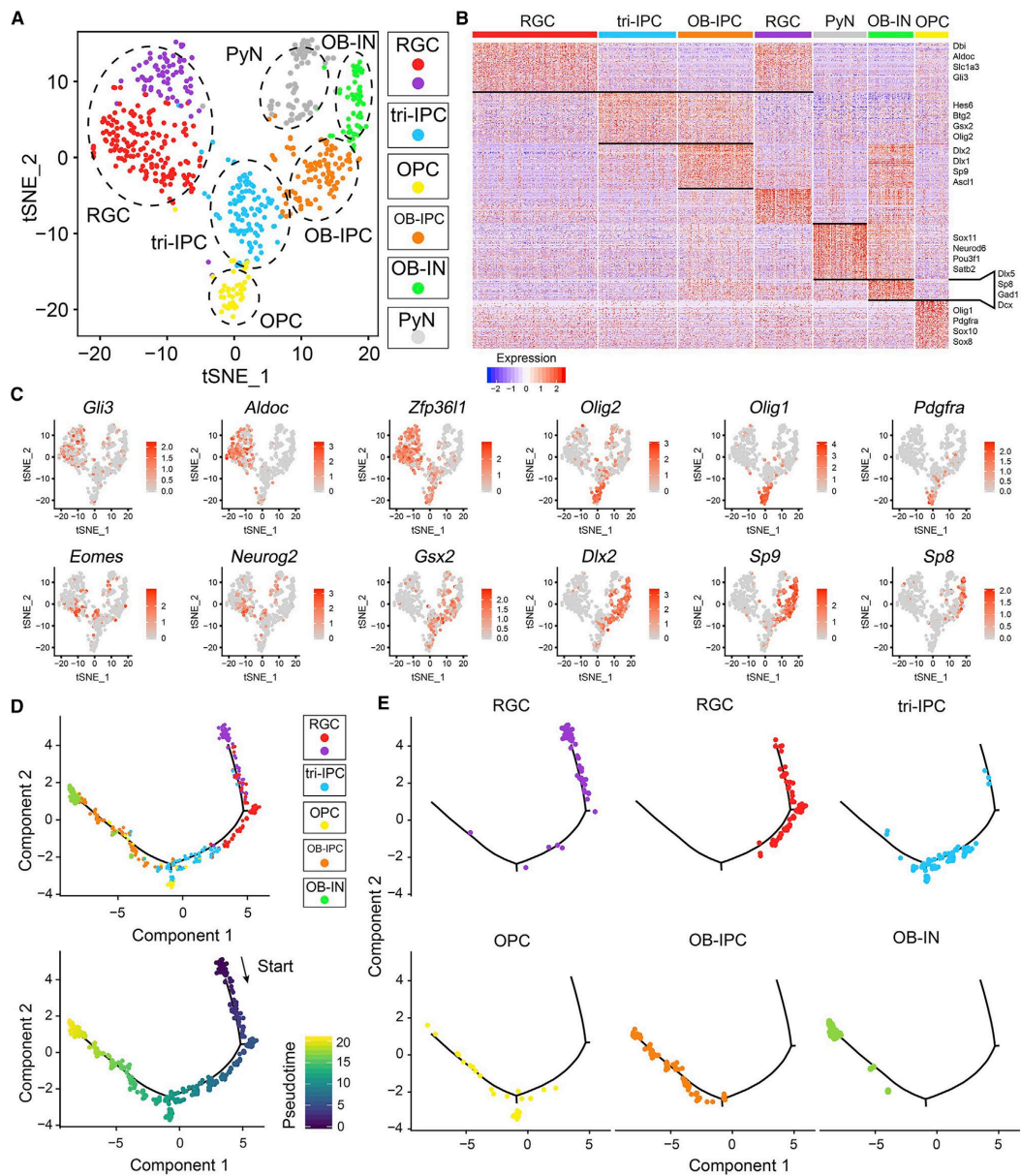


Figure 6. scRNA-Seq analysis of the progenitor cells in the ShhN-IUE sample

(A) Seurat clustering was performed on all the progenitor cells in the ShhN-IUE sample. Seven clusters were identified and annotated to six cell types based on gene expression features.

(B) Heatmap showing marker gene expressions in the seven cell clusters. Each column represents expressions in one cell, and each row represents expressions of one gene.

(C) The t-SNE plots of cells colored by mean expression of specific marker genes.

(D) Monocle analysis of all the progenitors in the ShhN-IUE samples revealed differentiation trajectories and pseudo-timelines along the cell differentiation axis. Each point represents a cell, colored by cluster identity (top) or pseudo-timeline (bottom).

(E) Seurat clusters shown along the predicted pseudo-timeline differentiation trajectory.

Reprinted from “Cortical Neural Stem Cell Lineage Progression Is Regulated by Extrinsic Signaling Molecule Sonic Hedgehog” *Cell Reports* 30, 4490–4504, March 31, 2020. Reprinted with permission.

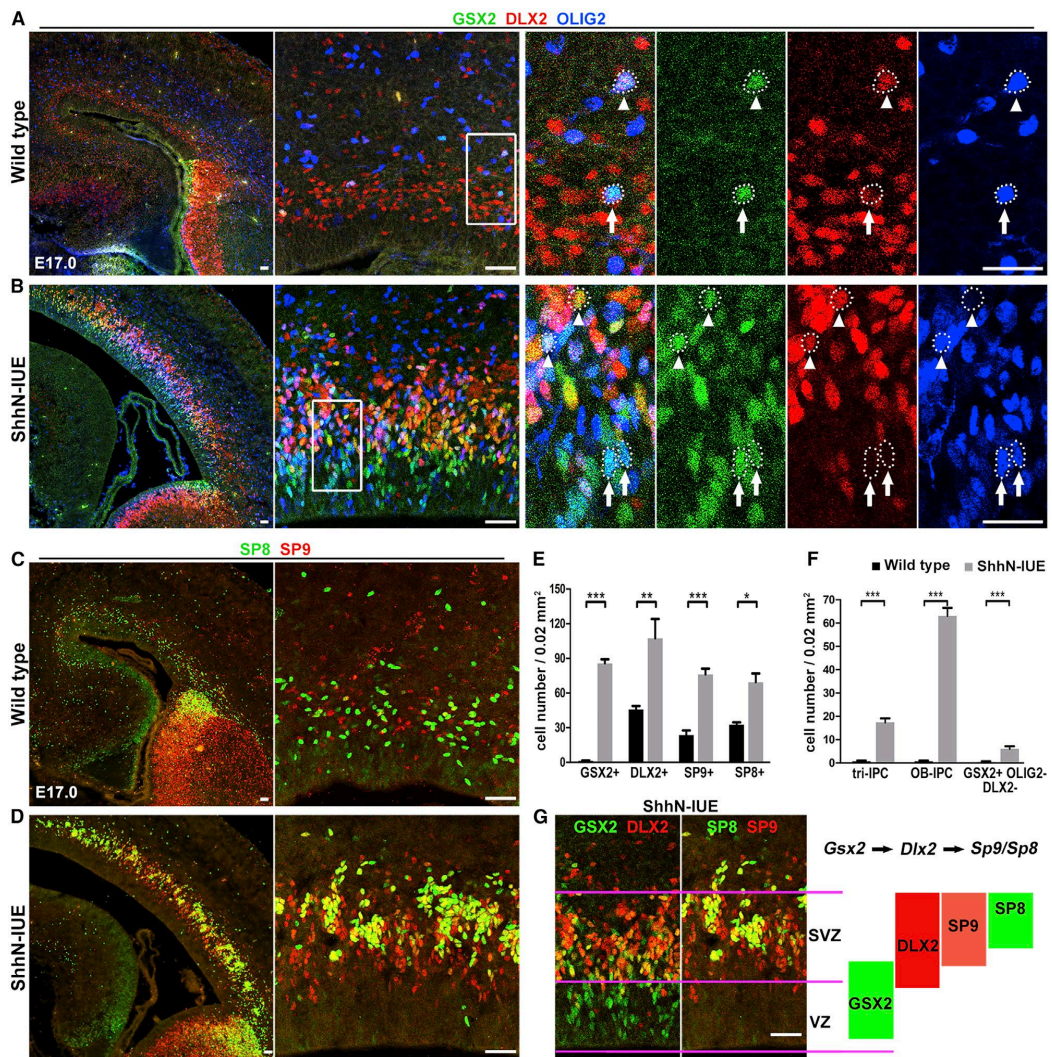


Figure 7. In vivo validation of markers of tri-IPCs and OB-IPCs

(A and B) The expression of Gsx2, Olig2, and Dlx2 in the cortical VZ/SVZ of wild-type (A) and ShhN-IUE (B) mice at E17. Note that very few GSX2⁺ cells (green) were present in the cortical SVZ. Arrows indicate Gsx2⁺Olig2⁺Dlx2⁻ tri-IPCs, and arrowheads indicate Gsx2⁺Dlx2⁺ OB-IPCs.

(C and D) The expression of Sp9 and Sp8 in the cortical VZ/SVZ of wild-type (C) and ShhN-IUE (D) mice at E17.

(E and F) More OB interneuron lineage cells (E) and more tri-IPCs and OB-IPCs (F) were observed in the ShhN-IUE cortices than in the controls.

(G) The sequential expression of Gsx2/Dlx2/Sp9/Sp8 is linked to lineage differentiation from tri-IPCs/OB-IPCs/OB neuroblasts, indicating the core transcriptional network for OB interneuron generation.

Data are presented as means \pm SEM; n = 3 mice for each condition. ***p < 0.001, **p < 0.01, *p < 0.05; Student's t test in (E) and (F). Scale bars, 50 μ m in (A)–(D) and (G).

Reprinted from “Cortical Neural Stem Cell Lineage Progression Is Regulated by Extrinsic Signaling Molecule Sonic Hedgehog” *Cell Reports* 30, 4490–4504, March 31, 2020. Reprinted with permission.

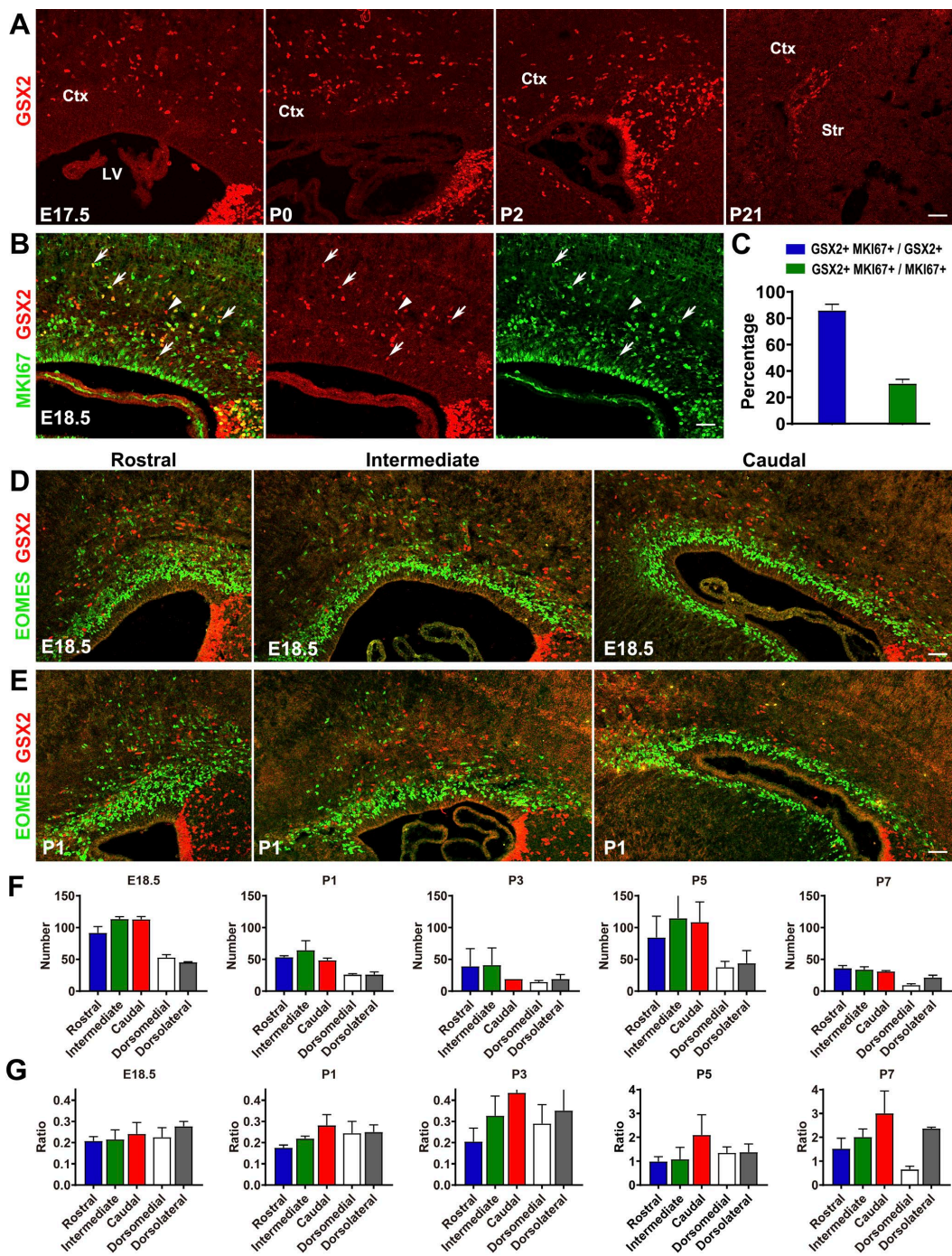


Figure 8. Gsx2 is expressed in the cortex. Related to Figure 1.

(A) Gsx2⁺ cells were observed in the mouse cortical SVZ and intermediate zone. Ctx, cortex; LV, lateral ventricle; Str, striatum.

(B) Co-localization analysis of Gsx2 and Mki67 expression in the E18.5 cortex. Note that most Gsx2⁺ cells expressed Mki67 (arrows); a few Gsx2⁺ cells did not express Mki67 (arrowhead).

(C) Quantification of the percentage of cortical Gsx2⁺ cells that expressed Mki67 and the percentage of Mki67⁺ cells in the cortical SVZ and intermediate zone that expressed Gsx2 at E18.5.

(D, E) Gsx2 and Eomes double - immunostained sections. Gsx2⁺ cells did not express Eomes.

(F) Quantification of numbers of Gsx2⁺ cells in the rostral, intermediate, caudal, dorsomedial and dorsolateral cortex within a 10- μ m-thick section.

(G) Quantification of ratios of Gsx2⁺ cells to Eomes⁺ cells in the cortex.

Scale bars, 50 μ m.

Reprinted from "Cortical Neural Stem Cell Lineage Progression Is Regulated by Extrinsic Signaling Molecule Sonic Hedgehog" *Cell Reports* 30, 4490–4504, March 31, 2020. Reprinted with permission.

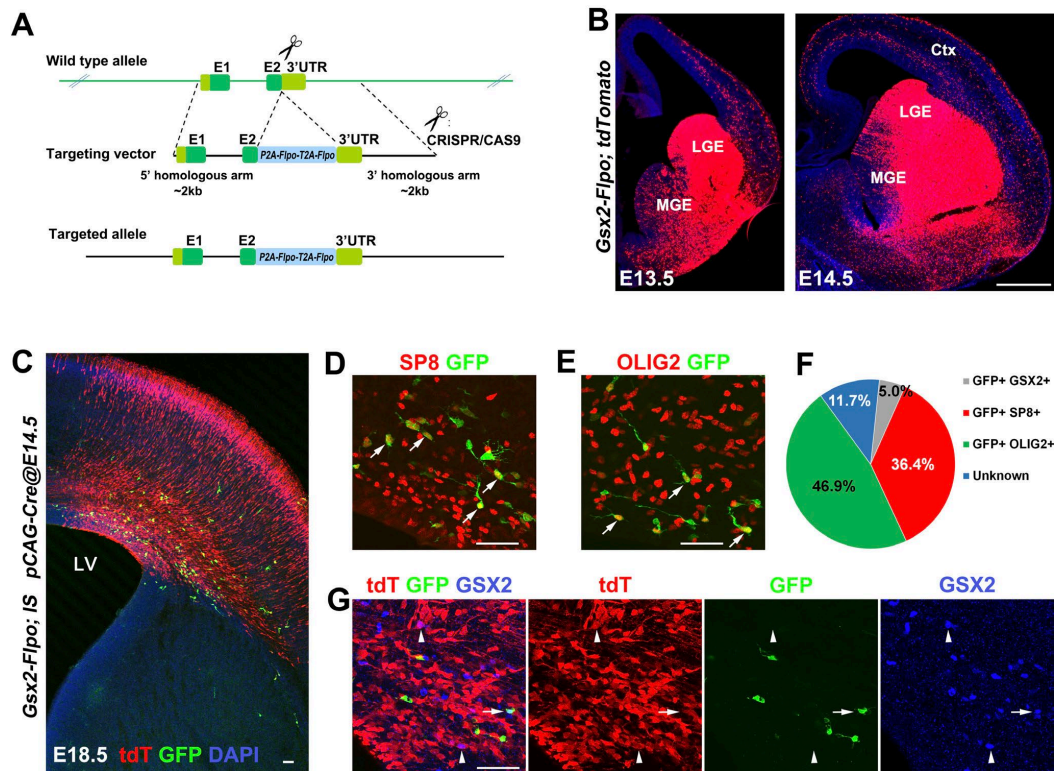


Figure 9. Cortical NSCs give rise to $Gsx2^+$ cells in the cortex. Related to Figure 1.

(A) The strategy for generating the $Gsx2^{Fipo}$ allele.

(B) The tdT^+ cells in the LGE, MGE and cortex of $Gsx2^{Fipo/+}; Rosa26-tdT-FRT$ mice at E13.5 and E14.5. Note strong expression of tdT in the VZ and SVZ in the LGE. Ctx, cortex.

(C) Plasmids $pCAG-Cre$ were electroporated to the cortical VZ of $Gsx2^{Fipo/+}; IS$ mice at E14.5. TdT^+ and GFP^+ cells were observed in the cortex at E18.5. LV, lateral ventricle.

(D, E) GFP^+Sp8^+ and GFP^+Olig2^+ cells (arrows) in the cortex.

(F) Quantification of the percentages of $Sp8^+$, $Olig2^+$ and $Gsx2^+$ cells among the GFP^+ cortical cells at E18.5.

(G) One $GFP^+tdT^+Gsx2^+$ cell (arrow) and two tdT^+Gsx2^+ cells (arrowheads) in the cortex. Note that these two cortical NSC-derived $Gsx2^+$ cells expressed tdT , but not GFP (arrowheads), suggesting the low recombination efficiency of the $Flp-FRT$ system.

Scale bars, 500 μm in (B); 50 μm in (C - E, G).

Reprinted from “Cortical Neural Stem Cell Lineage Progression Is Regulated by Extrinsic Signaling Molecule Sonic Hedgehog” *Cell Reports* 30, 4490–4504, March 31, 2020. Reprinted with permission.

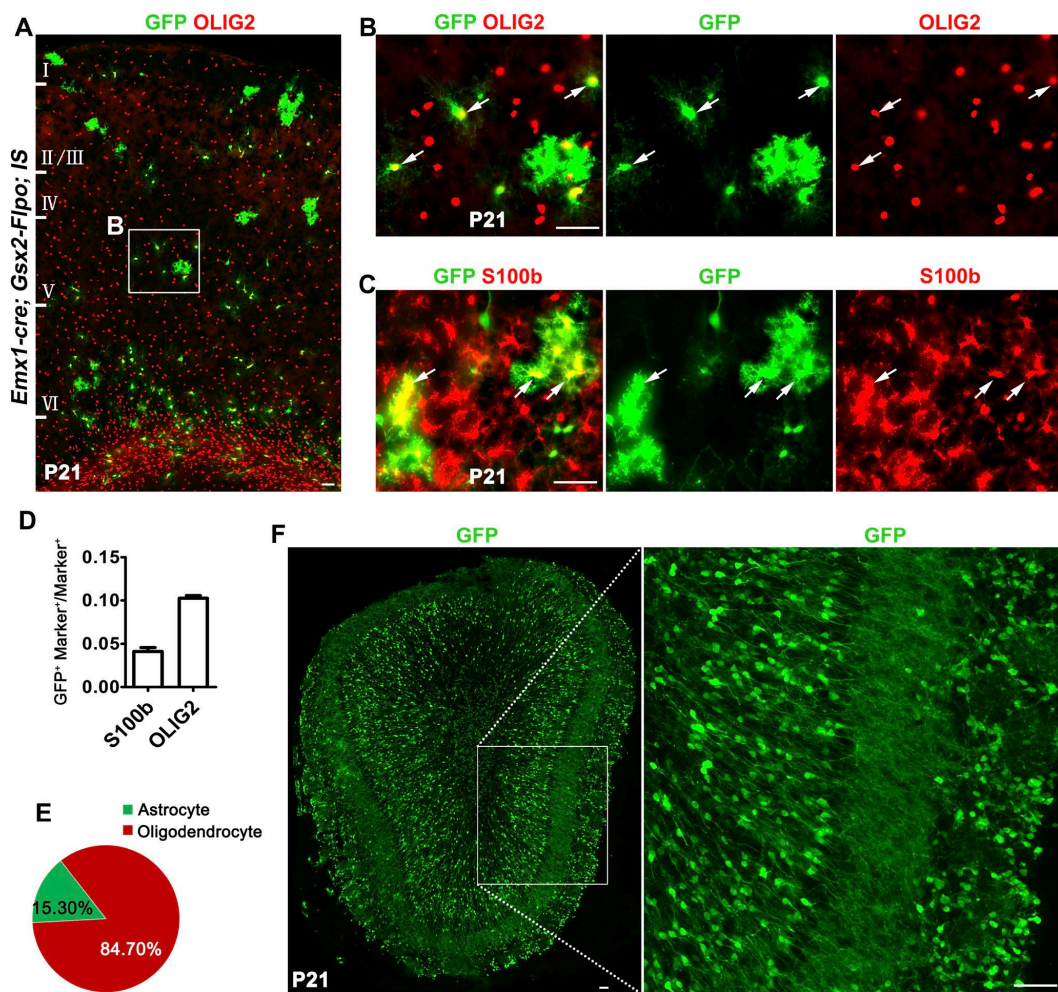


Figure 10. Cortical $Emx1^+$ NSCs generate $Gsx2^+$ tri-IPCs. Related to Figure 1.

(A-C) GFP^+Olig2^+ oligodendrocytes (A, B, arrows) and GFP^+S100b^+ astrocytes (C, arrows) in the cortices of $Emx1^{Cre/+}; Gsx2^{Flpo/+}; IS$ mice at P21.

(D) The percentage of $Olig2^+$ cells that was labeled with GFP and the percentage of $S100b^+$ cells that was labeled with GFP in the cortex of $Emx1^{Cre/+}; Gsx2^{Flpo/+}; IS$ mice at P21.

(E) Quantification of the percentages of oligodendrocytes and astrocytes among the GFP^+ cortical glial cells.

(F) GFP^+ OB interneurons at P21. Scale bars, 50 μm in (A - C, F).

Reprinted from "Cortical Neural Stem Cell Lineage Progression Is

Regulated by Extrinsic Signaling Molecule Sonic Hedgehog” *Cell Reports*
30, 4490–4504, March 31, 2020. Reprinted with permission.

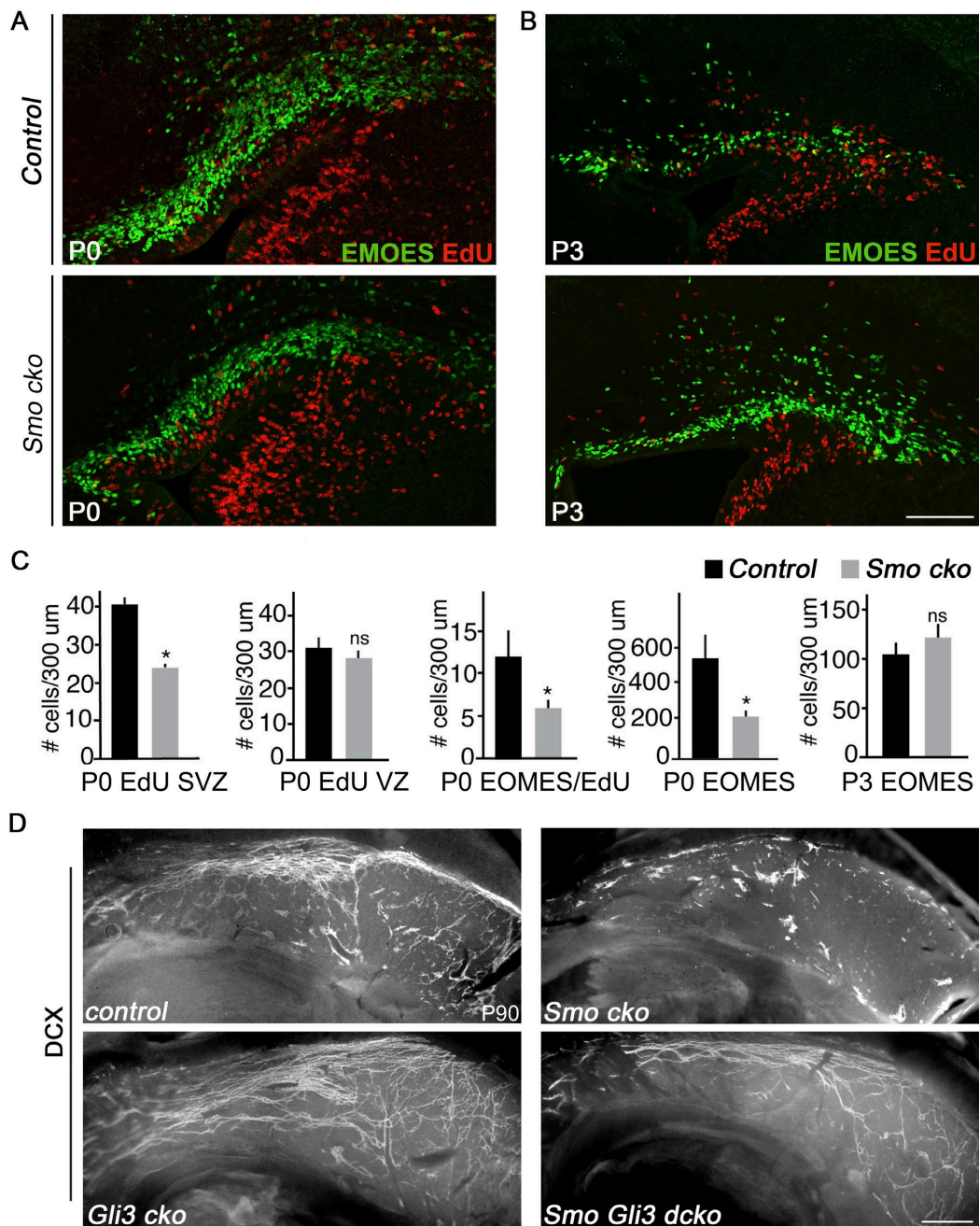


Figure 11. Eomes+ IPCs continue to be generated from NSCs in the *Smo cko* mice. Related to Figure 2.

(A and B) Eomes immunostaining and EdU labeling of S-phase cells in the P0 (A) and P3 (B) control (*Smo^{F/F}*) and *Smo cko* (*hGFAP-Cre; Smo^{F/F}*) cortices.

(C) Quantification of the EdU⁺, Eomes⁺, and EdU⁺Eomes⁺ cells per 300 μm width in the cortical VZ and SVZ at P0 and P3.

(D) Whole mount of the lateral wall of lateral ventricle stained with antibody against DCX showed a marked decrease in neuroblast chains in adult *Smo cko* mice (P90), while neurogenesis in the SVZ of adult *Smo Gli3 dcko* mice was largely rescued.

Data in (C) were represented as means + SEM (n = 3 per genotype per age). *, P < 0.05; unpaired Student's t test. Scale bars: 200 μ m in (A) and (B); 500 μ m in (D).

Reprinted from "Cortical Neural Stem Cell Lineage Progression Is Regulated by Extrinsic Signaling Molecule Sonic Hedgehog" *Cell Reports* 30, 4490–4504, March 31, 2020. Reprinted with permission.

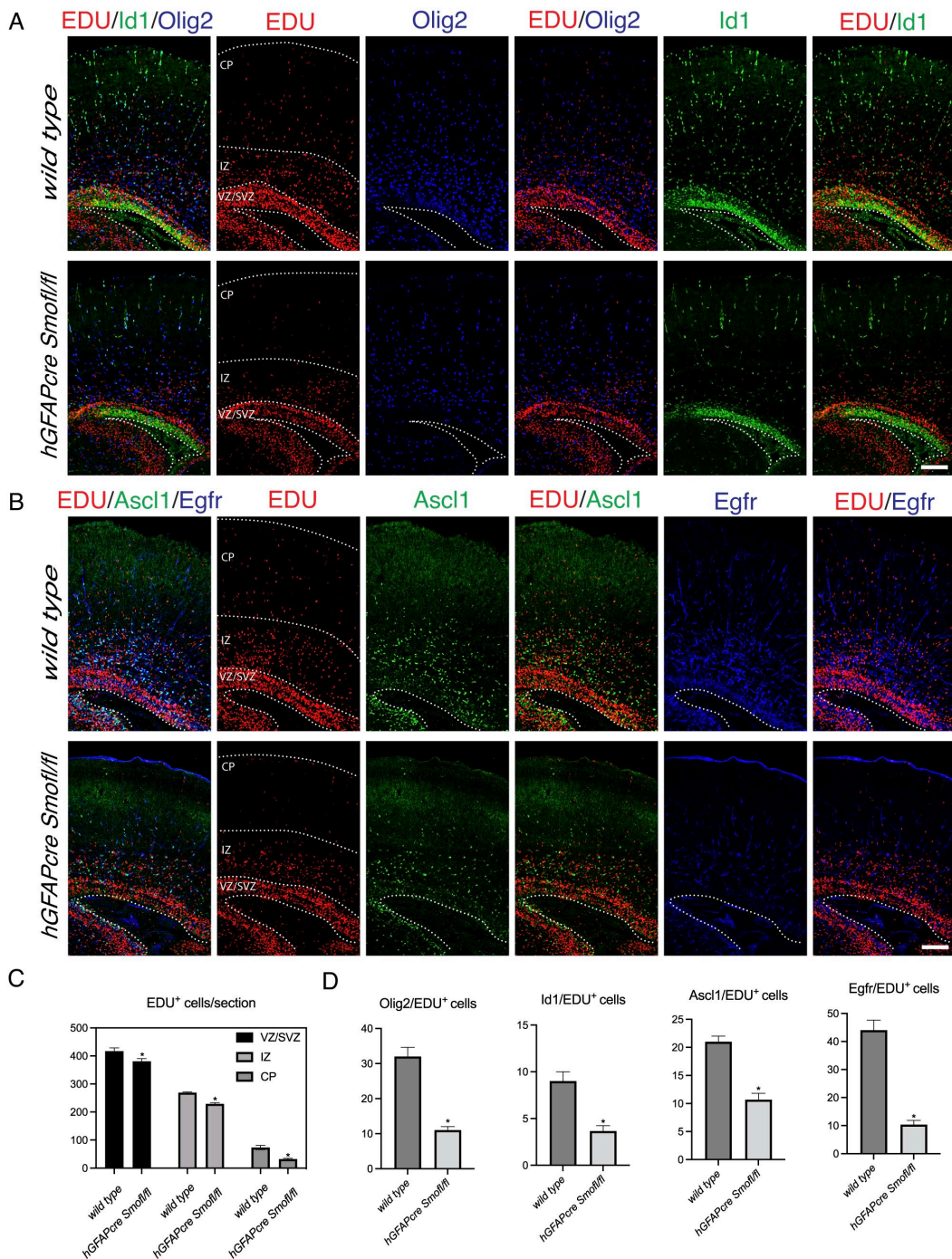


Figure 12. Less MIPCs were generated at late embryonic stage in *Smo cko* mouse brain.

(A) Immunostaining showing expressions of EdU, Olig2 and Id1 in the wildtype control and *hGFAP-Cre; Smo^{F/F}* (*Smo cko*) mice at P0. CP,

cortical plate; IZ, intermediate zone; VZ/SVZ, ventricular zone/subventricular zone. EdU were injected at E16.

(B) Immunostaining showing expressions of EdU, Ascl1 and Egfr in the wildtype control and *hGFAP-Cre; Smo^{F/F} (Smo cko)* mice at P0.

(C) Quantification of EdU positive cells per section (10x images taken by Zeiss 880 confocal microscope) in wildtype control and *hGFAP-Cre; Smo^{F/F} (Smo cko)* mice at P0.

(D) Quantification of EdU/Olig2⁺, EDU/Id1⁺, EDU/Ascl1⁺, EDU/Egfr⁺ cells per section (10x images taken by Zeiss 880 confocal microscope) in wildtype control and *hGFAP-Cre; Smo^{F/F} (Smo cko)* mice at P0.

Data in (C) were represented as means + SEM (n = 3 per genotype). *, P < 0.05; unpaired Student's t test. Scale bars: 100 μm in (A, B).

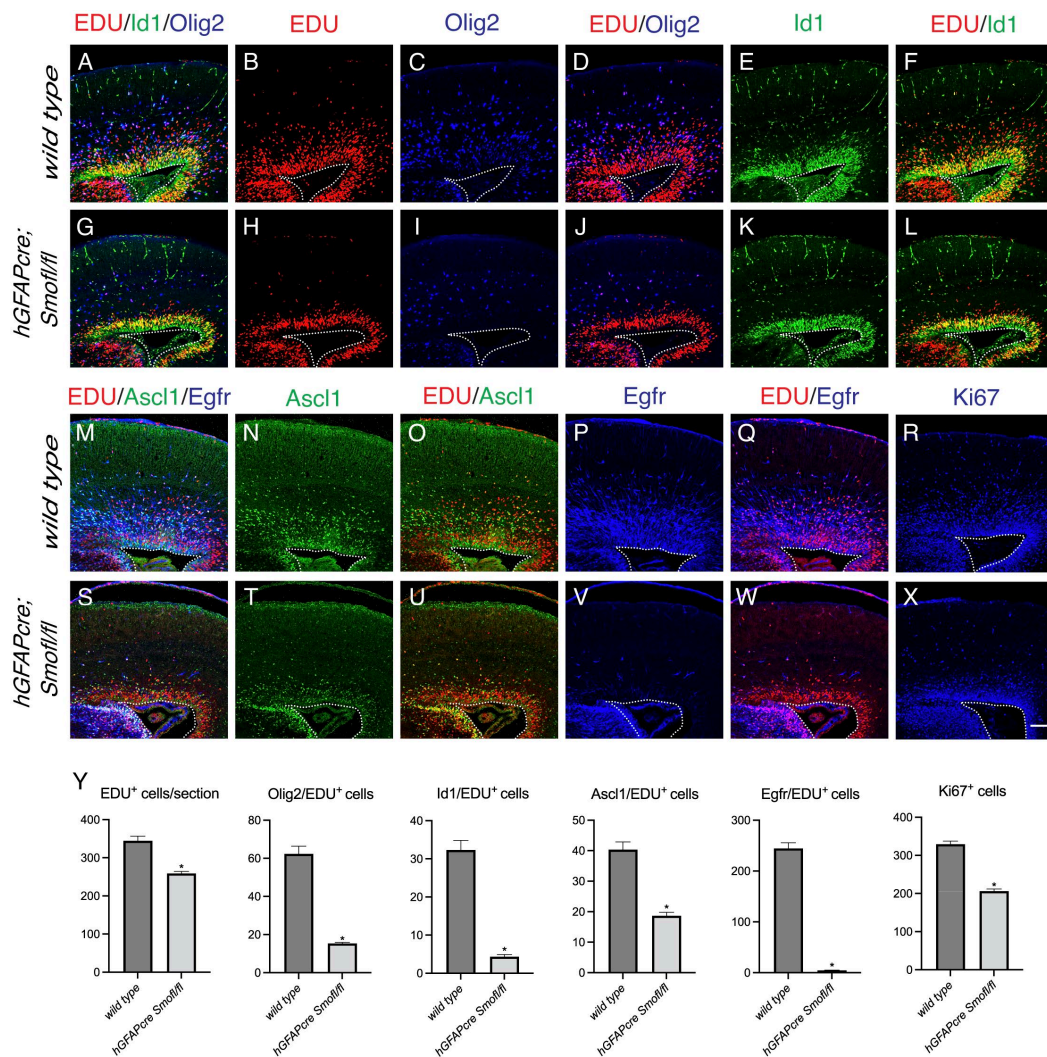


Figure 13. Less MIPCs were proliferating at late embryonic stage in *Smo cko* mouse brain.

(A - L) Immunostaining showing expressions of EdU, Olig2 and Id1 in the wildtype control and *hGFAP-Cre; Smo^{F/F}* (*Smo cko*) mice at E17.5. EdU were injected 2h before collection.

(M - Q) Immunostaining showing expressions of EdU, Ascl1 and Egfr in the wildtype control and *hGFAP-Cre; Smo^{F/F}* (*Smo cko*) mice at E17.5.

(R) Immunostaining showing expressions of Ki67 in the wildtype control and *hGFAP-Cre; Smo^{F/F}* (*Smo cko*) mice at E17.5.

(Y) Quantification of the EdU⁺, EdU/Olig2⁺, EdU/Id1⁺, EdU/Ascl1⁺, EDU/Egfr+ positive cells per section (10x images taken by Zeiss 880)

confocal microscope) in wildtype control and *hGFAP-Cre; Smo^{F/F}* (*Smo cko*) mice at E17.5.

Data in (Y) were represented as means + SEM (n = 3 per genotype). *, P < 0.05; unpaired Student's t test. Scale bars: 100 μ m in (X).

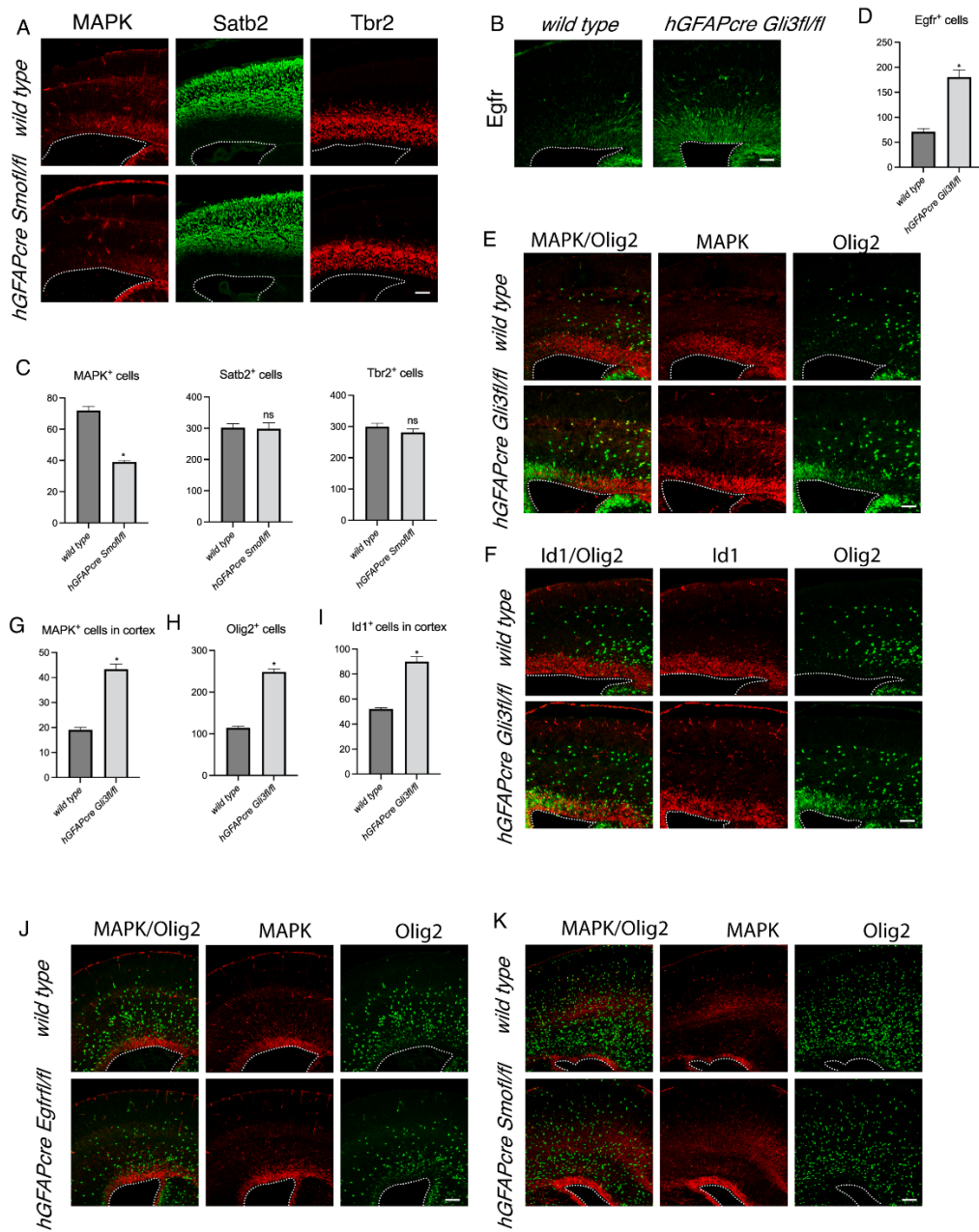


Figure14. Shh signaling is both necessary and sufficient for the expression of Egfr which activate the mitogen activated protein kinase (MAPK) pathway and generate cortical glia.

(A) Immunostaining showing expressions of Phospho-MAPK, Satb2 and Tbr2 in the wildtype control and *hGFAP-Cre; Smo^{F/F}* (*Smo cko*) mice at E15.

- (B) Immunostaining showing expressions of Egfr in the wildtype control and *hGFAP-Cre; Gli3^{F/F} (Gli3 cko)* mice at E16.
- (C) Quantification of Phospho-MAPK⁺, Satb2⁺ and Tbr2⁺ cells per section (10x images taken by Zeiss 880 confocal microscope) in wildtype control and *hGFAP-Cre; Smo^{F/F} (Smo cko)* mice at E15.
- (D) Quantification of Egfr⁺ cells per section (10x images taken by Zeiss 880 confocal microscope) in wildtype control and *hGFAP-Cre; Gli3^{F/F} (Gli3 cko)* mice at E16.
- (E) Immunostaining showing expressions of Phospho-MAPK and Olig2 in the wildtype control and *hGFAP-Cre; Gli3^{F/F} (Gli3 cko)* mice at E16.
- (F) Immunostaining showing expressions of Olig2 and Id1 in the wildtype control and *hGFAP-Cre; Gli3^{F/F} (Gli3 cko)* mice at E16.
- (G - I) Quantification of cortical Phospho-MAPK⁺, Olig2⁺, cortical Id1⁺ cells per section (10x images taken by Zeiss 880 confocal microscope) in wildtype control and *hGFAP-Cre; Gli3^{F/F} (Gli3 cko)* mice at E16.
- (J) Immunostaining showing expressions of Phospho-MAPK, Olig2 in the wildtype control and *Emx1-Cre; Egfr^{F/F}* mice at E17.5.
- (K) Immunostaining showing expressions of Phospho-MAPK, Olig2 in the wildtype control and *hGFAP-Cre; Smo^{F/F} (Smo cko)* mice at P0.
- Data in (C, D, G - I) were represented as means + SEM (n = 3 per genotype). *, P < 0.05; unpaired Student's t test. Scale bars: 100 μm in (A, B, E, F, J, K).

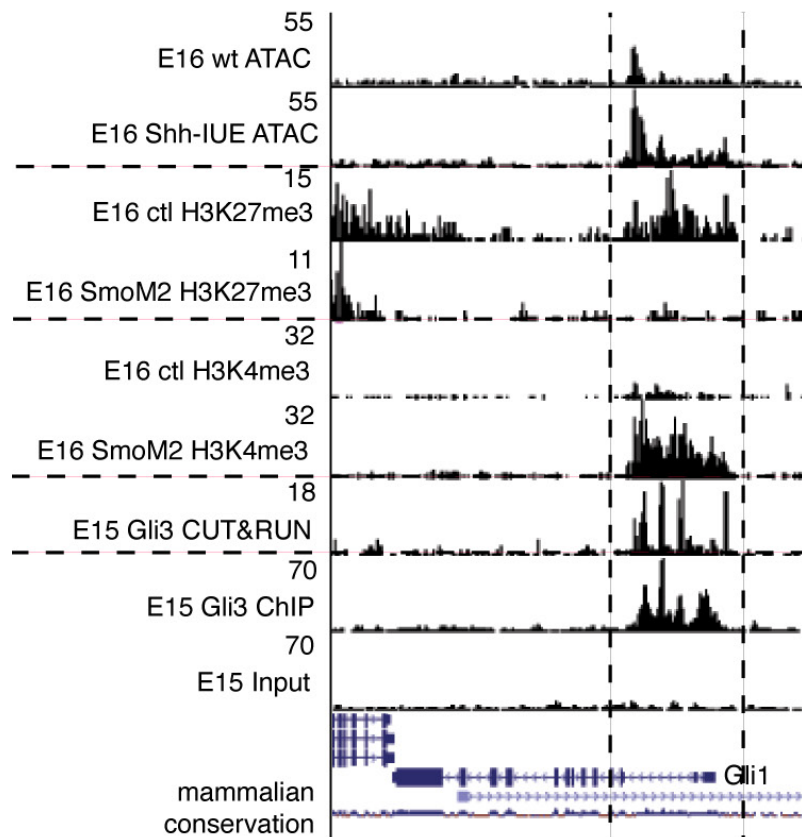


Figure 15. Establishing ChIP-seq, CUT&RUN, and ATAC-seq methods.

ATAC-seq were performed by using E16 wt cortices and cells that were electroporated with *Shh* plasmids. ChIP-seq and CUT&RUN were performed on E16 wt cortices and *SmoM2* cortices by using a Gli3 antibody, H3K27me3 antibody, H3K4me3 antibody. The results were highly consistent both within and between the ChIP-seq and CUT&RUN experiments, indicated by the specific binding to promoters and enhancers of *Shh* target genes such as *Gli1*.

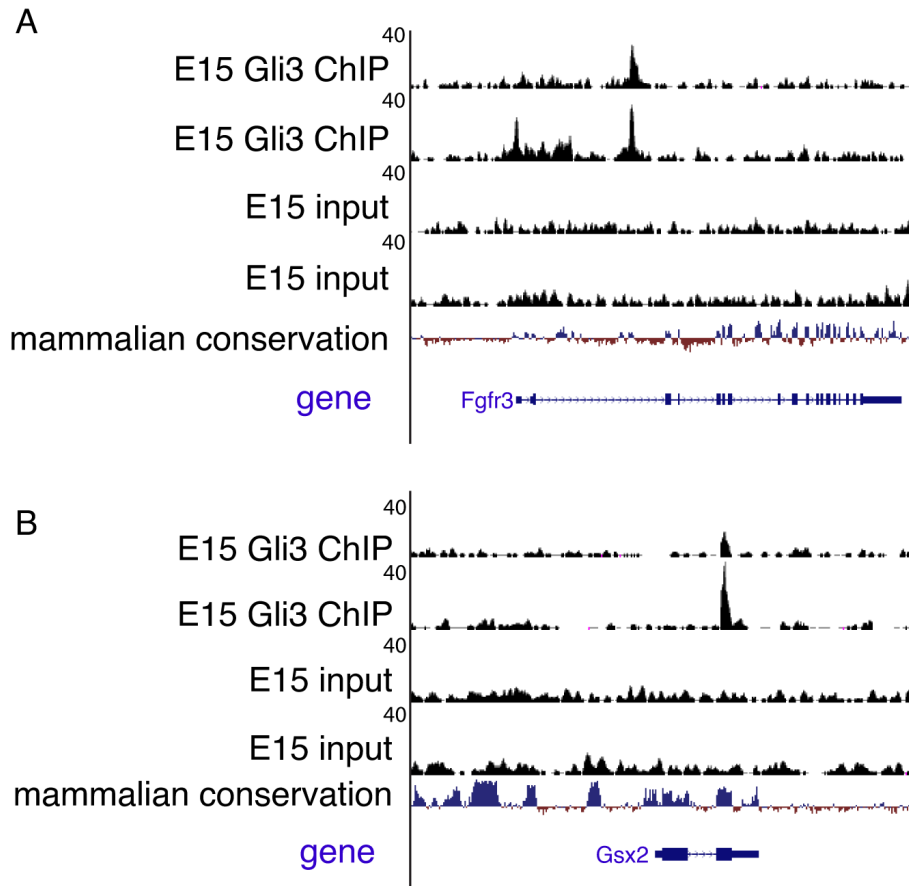


Figure 16. Gli3 ChIP-seq revealed peaks at *Fgfr3* and *Gsx2* genes.

(A) Gli3 binds to *Fgfr3* gene. 2 biological replicates were shown.

(B) Gli3 binds to *Gsx2* gene.

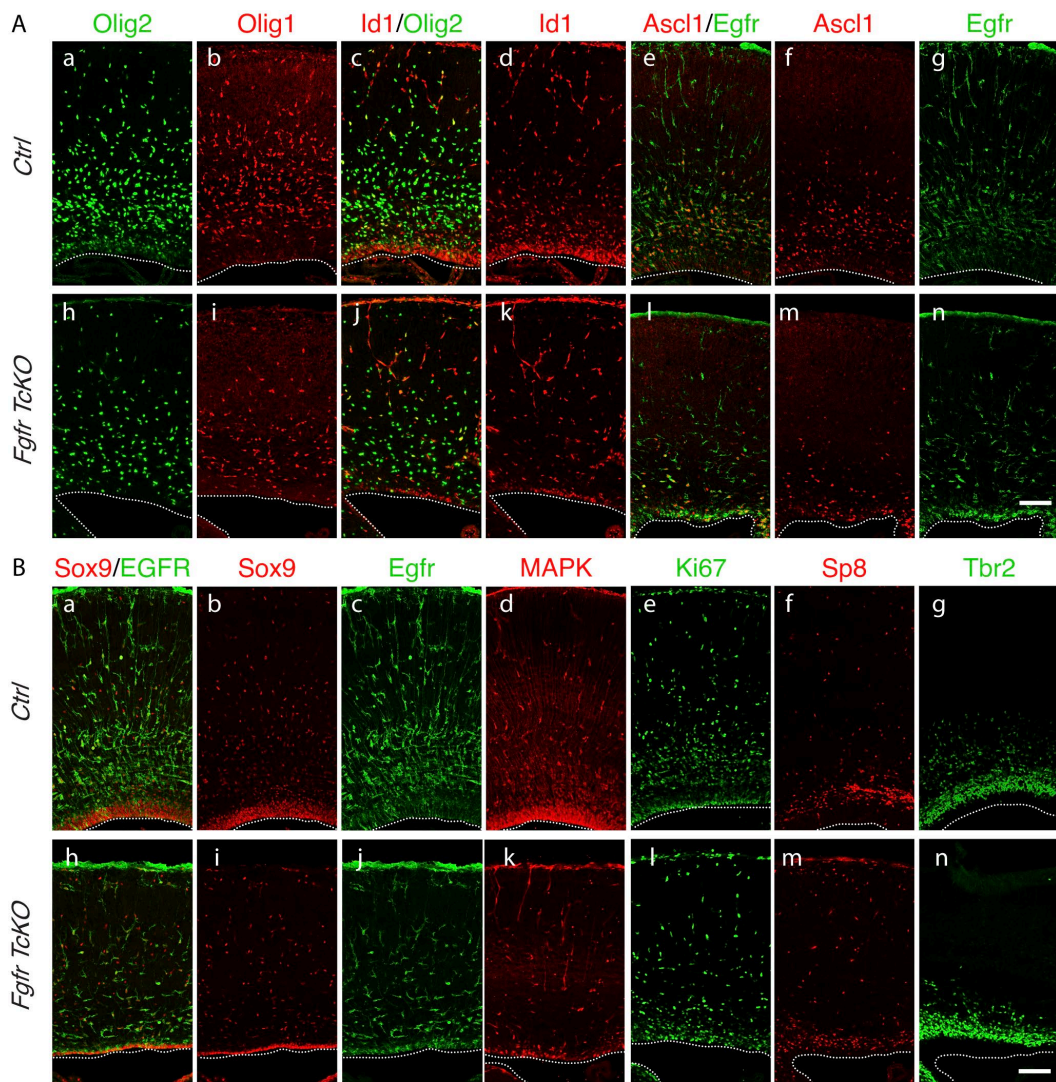


Figure 17. Less proliferation in *hGFAPcre; Fgfr1^{F/F}; Fgfr2^{F/F}; Fgfr3^{F/F} (Fgfr Tcko)* mouse brain at E18.5.

(A) Immunostaining showing expressions of Olig2, Olig1, Id1, Ascl1, Egfr in the E18.5 control and *hGFAPcre; Fgfr1^{F/F}; Fgfr2^{F/F}; Fgfr3^{F/F} (Fgfr Tcko)* brain.

(B) Immunostaining showing expressions of Sox9, Phospho-MAPK, Ki67 and Egfr in the in the E18.5 control and *hGFAPcre; Fgfr1^{F/F}; Fgfr2^{F/F}; Fgfr3^{F/F} (Fgfr Tcko)*.

Scale bars: 100 μ m in (A-n, B-n).

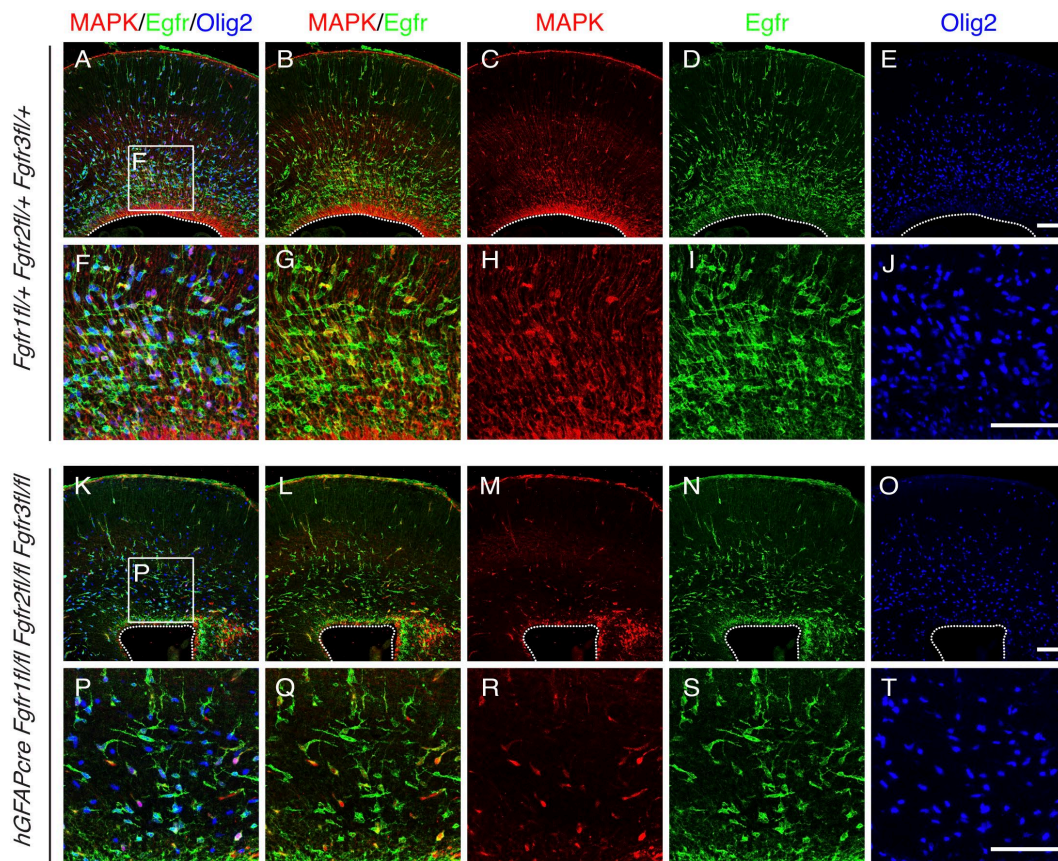


Figure 18. Most of the remaining Phospho-MAPK⁺ cells in *hGFAPcre*; *Fgfr1^{F/F}*; *Fgfr2^{F/F}*; *Fgfr3^{F/F}* (*Fgfr Tcko*) are *Egfr⁺* cells.

(A - E, K - O) Immunostaining showing expressions of Phospho-MAPK, Egfr, Olig2 in the E18.5 control and *hGFAPcre*; *Fgfr1^{F/F}*; *Fgfr2^{F/F}*; *Fgfr3^{F/F}* (*Fgfr Tcko*) brain.

(F - J, P - T) zoom in images of Phospho-MAPK, Egfr, Olig2 in the E18.5 control and *hGFAPcre*; *Fgfr1^{F/F}*; *Fgfr2^{F/F}*; *Fgfr3^{F/F}* (*Fgfr Tcko*) brain at VZ/SVZ.

Scale bars: 100 μ m in (E, J, O, T).

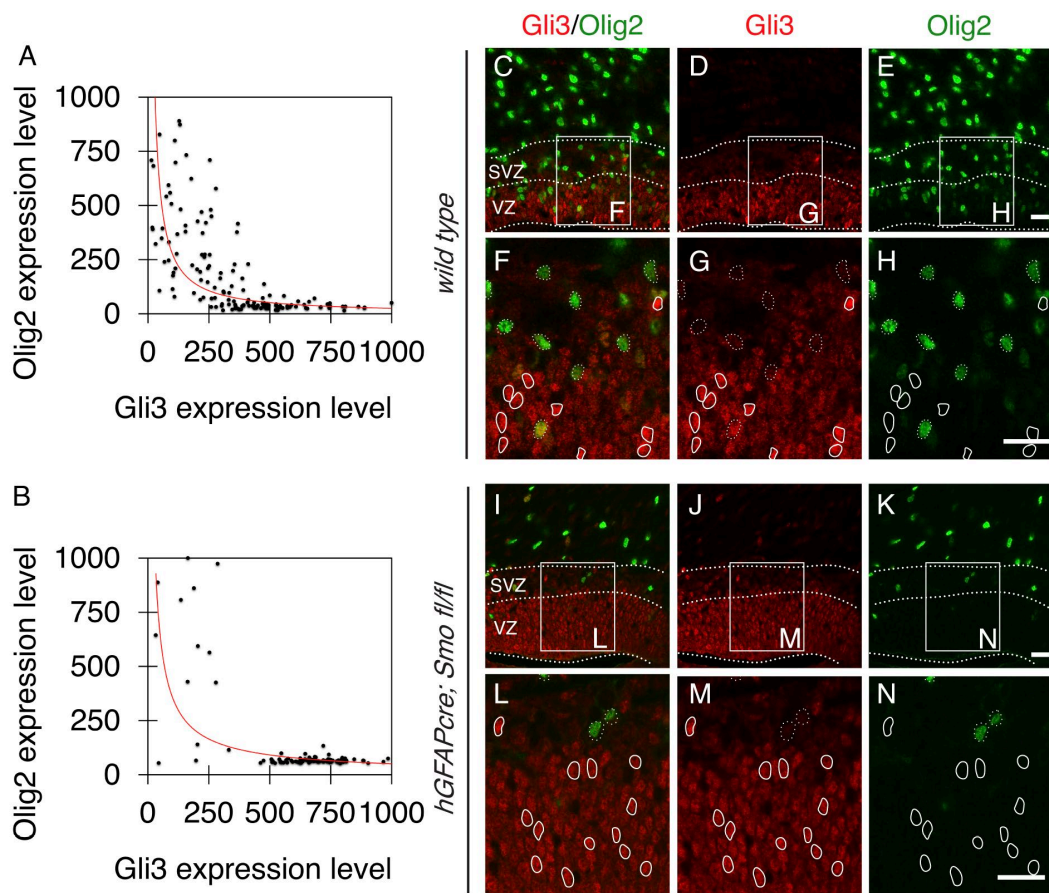


Figure 19. Anti-correlation between Gli3 and Olig2 in VZ/SVZ.

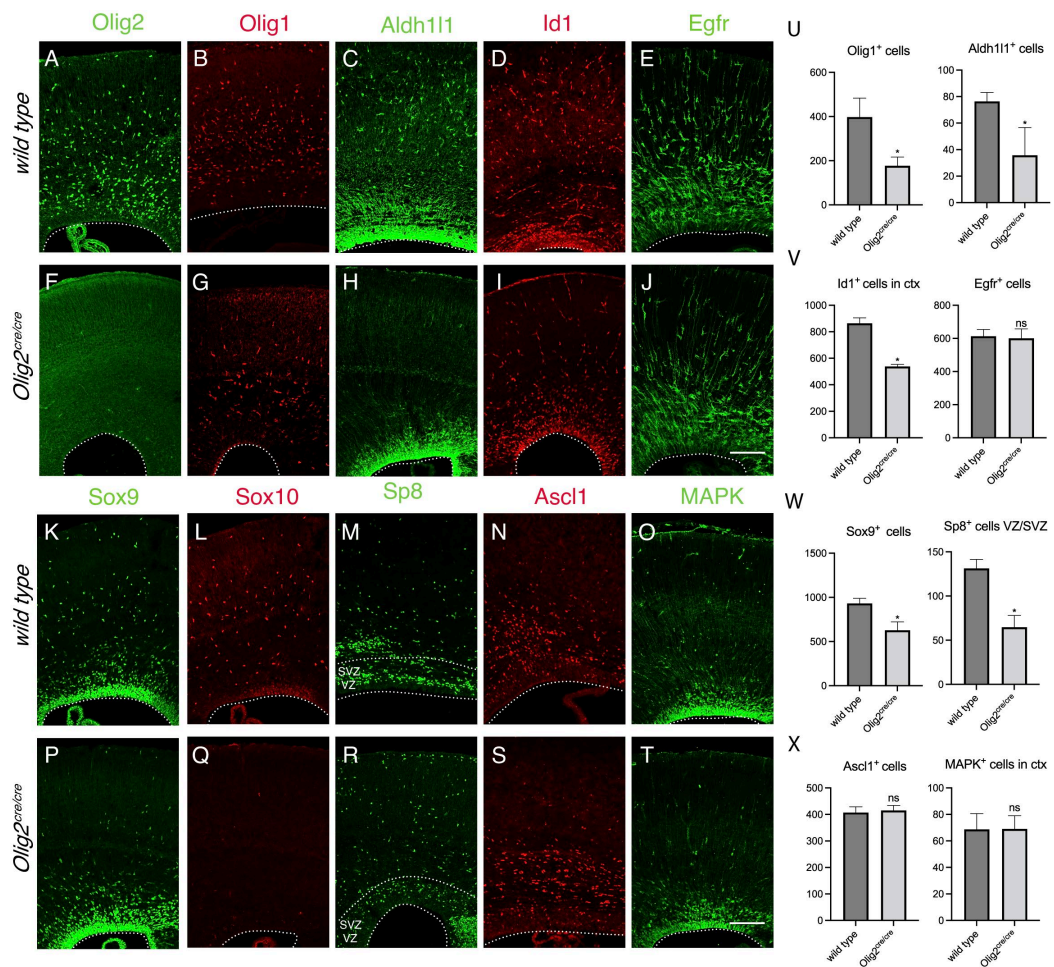
(A) Quantification of the Gli3, and Olig2 protein expression level in wild-type mouse brain in VZ/SVZ at P0. The brains were sectioned at 12um and Olig2/Gli3 immunostaining was performed on the section. 40X images were taken by using ZEISS 880 confocal microscope. The individual cells in the VZ/SVZ were selected based on DAPI staining. The sum of the values of the pixels in the selection was calculated by ImageJ as the integrated density. The average cell fluorescence value was calculated by dividing the integrated density by the area of selection. We selected 100-150 cells in the VZ/SVZ to calculate the average cell fluorescence value in each channel. The data were visualized by normalizing the max average cell fluorescence value to 1000 in each channel to show the differential expression level of the Gli3 and Olig2 proteins. Each dot represents a cell. The cell with a 1000 value is the brightest cell in the image.

(B) Quantification of the Gli3, and Olig2 protein expression level in *hGFAP-Cre; Smo^{F/F} (Smo cko)* mouse brain in VZ/SVZ at P0.

(C - E, I - K) Immunostaining showing expressions of Gli3 and Olig2 in the wildtype control and *hGFAP-Cre; Smo^{F/F} (Smo cko)* mice at P0.

(F - H, I - N) Zoom in images to show the immunostaining signal of Gli3 and Olig2 in VZ/SVZ in the wildtype control and *hGFAP-Cre; Smo^{F/F} (Smo cko)* mice. Representative cells with high expression of Gli3 in the nucleus were shown in solid line circle and representative cells with high expression of Olig2 in the nucleus were shown in dashed line circle.

Scale bars: 20µm in (E, H, K, N).



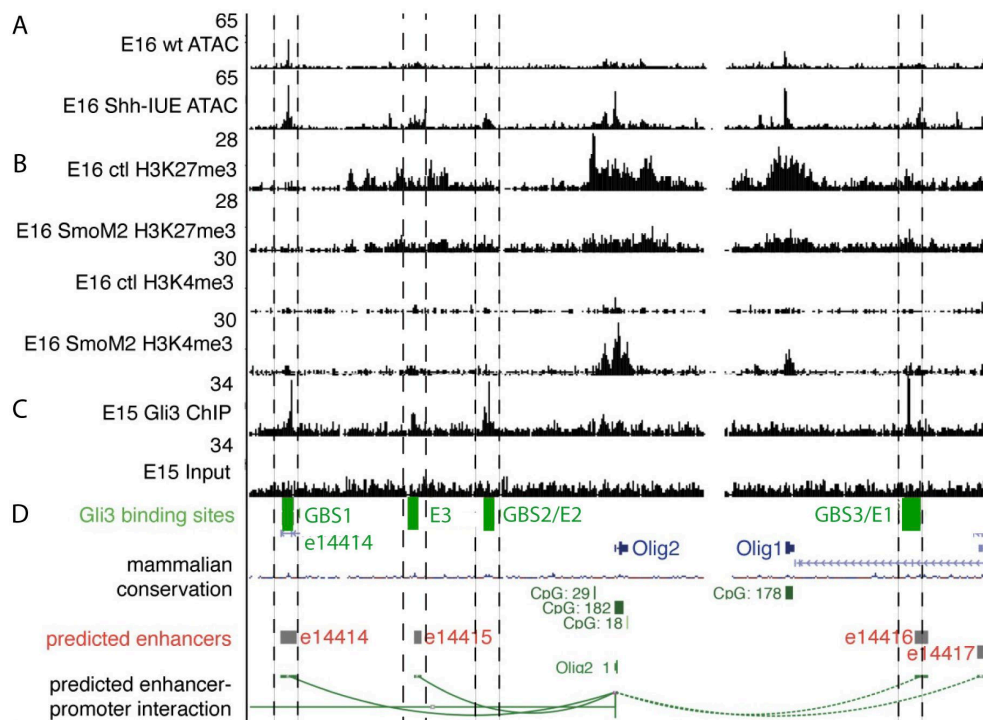


Figure 21. Gli3 binds to the predicted enhancers of Olig1/2 loci.

(A) ATAC-seq showed increased accessibility in E16 Shh-IUE cortices compare with wildtype cortices.

(B) CUT&RUN revealed increased H3K4me3 and H3K27ME3 modifications at Olig1/2 promoters locus in E16 *SmoM2* cortices and wildtype cortices.

(C) Gli3 binding sites (GBSs) identified by ChIP-seq shown in green. Enhancers predicted by ENCODE shown in red. Gli3 ChIP-seq revealed 4 Gli3 binding sites labelled by GBS1/e14414, E3, GBS2/E2, and GBS3/E1. Wavy green lines represent predicted interactions between enhancers and the Olig2 promoter. GBS1 is part of enhancer e14414. E3 is part of enhancer e14415. GBS3 is close to enhancer e14416.

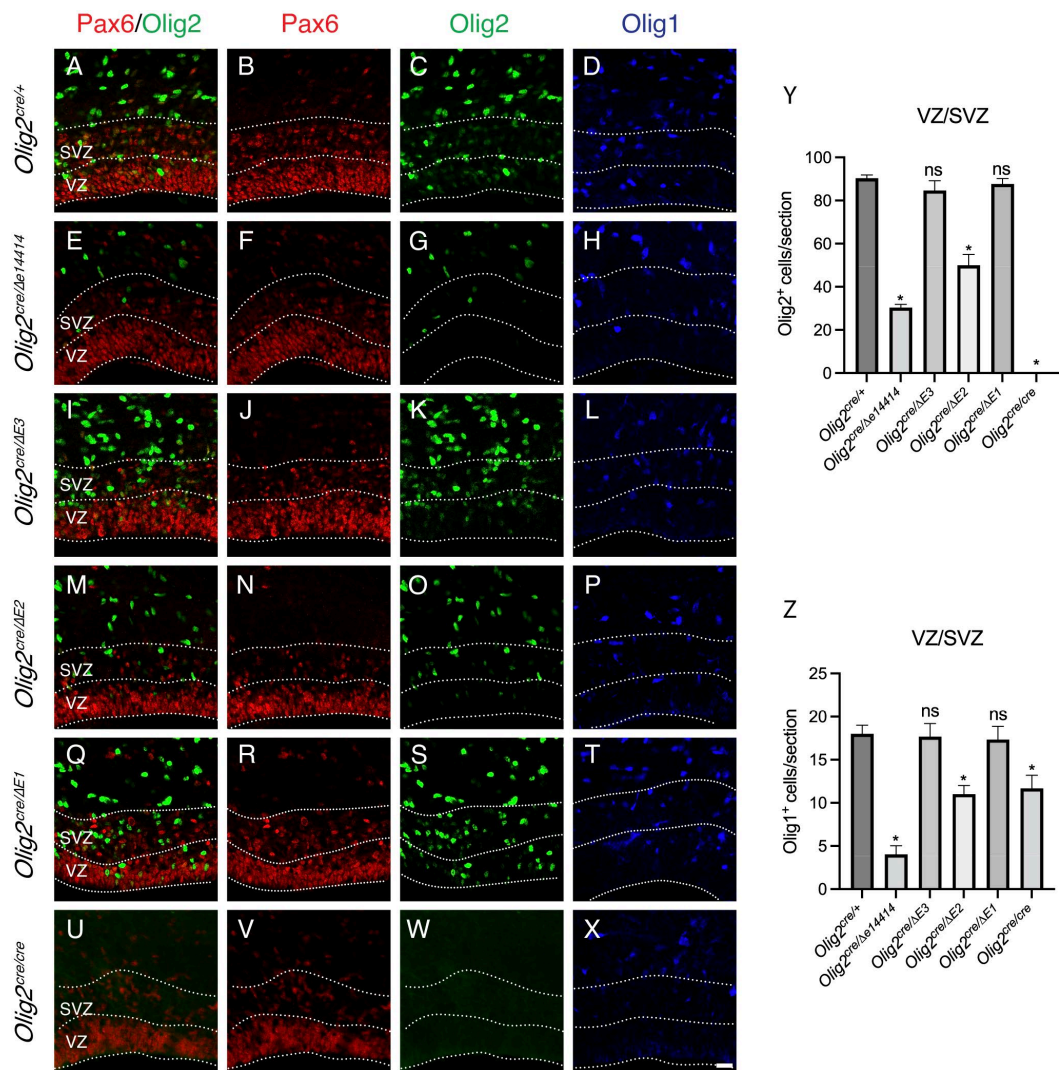


Figure 22. Enhancer e14414 and E2 regulates Olig2 and Olig1 expression in cortical VZ/SVZ.

(A - X) Immunostaining showing expressions of Pax6, Olig2, Olig1 in *Olig2^{cre/+}*, *Olig2^{cre/ Δe14414}*, *Olig2^{cre/ ΔE3}*, *Olig2^{cre/ ΔE2}*, *Olig2^{cre/ ΔE1}*, and *Olig2^{cre/ cre}* mice in cortical VZ/SVZ. Pax6 expression was used to show the VZ and SVZ.

(Y, Z) Quantification Olig2⁺, Olig1⁺ cells per 350um wide section(10x images taken by Zeiss 880 confocal microscope) in different genotypes. Representative 40X images were shown in (A - X).

Data in (Y, Z) were represented as means + SEM (n = 3 per genotype). *, P < 0.05; unpaired Student's t test. Scale bar: 20um in (X).

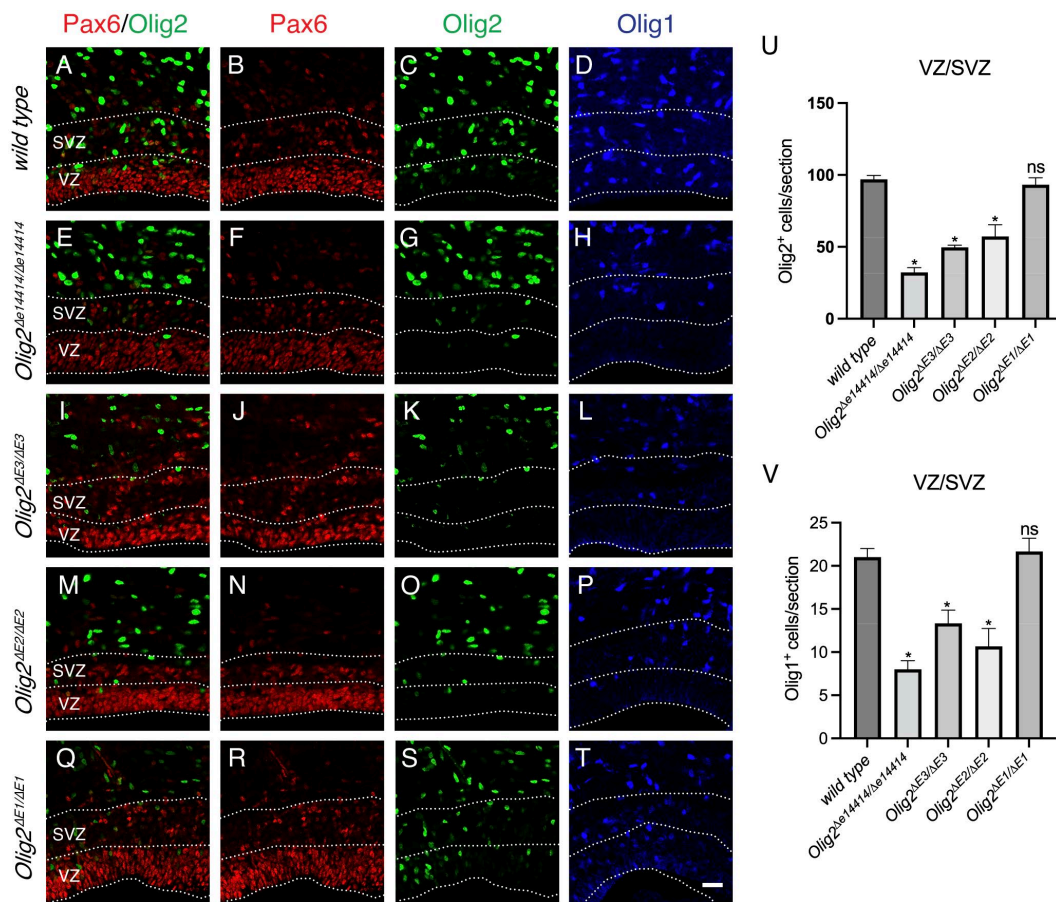


Figure 23. Olig2 and Olig1 expression in cortical VZ/SVZ requires enhancer e14414, E3 and E2 at P0

(A - T) Immunostaining showing expressions of Pax6, Olig2, Olig1 in wildtype, *Olig2^{Δe14414/ Δe14414}*, *Olig2^{ΔE3/ ΔE3}*, *Olig2^{ΔE2/ ΔE2}*, *Olig2^{ΔE1/ ΔE1}* mice in cortical VZ/SVZ. Pax6 expression was used to show the VZ and SVZ.

(U, V) Quantification Olig2⁺, Olig1⁺ cells per 350um wide section (10x images taken by Zeiss 880 confocal microscope) in different genotypes. Representative 40X images were shown in (A - T).

Data in (U, V) were represented as means + SEM (n = 3 per genotype). *, P < 0.05; unpaired Student's t test. Scale bar: 20um in (T).

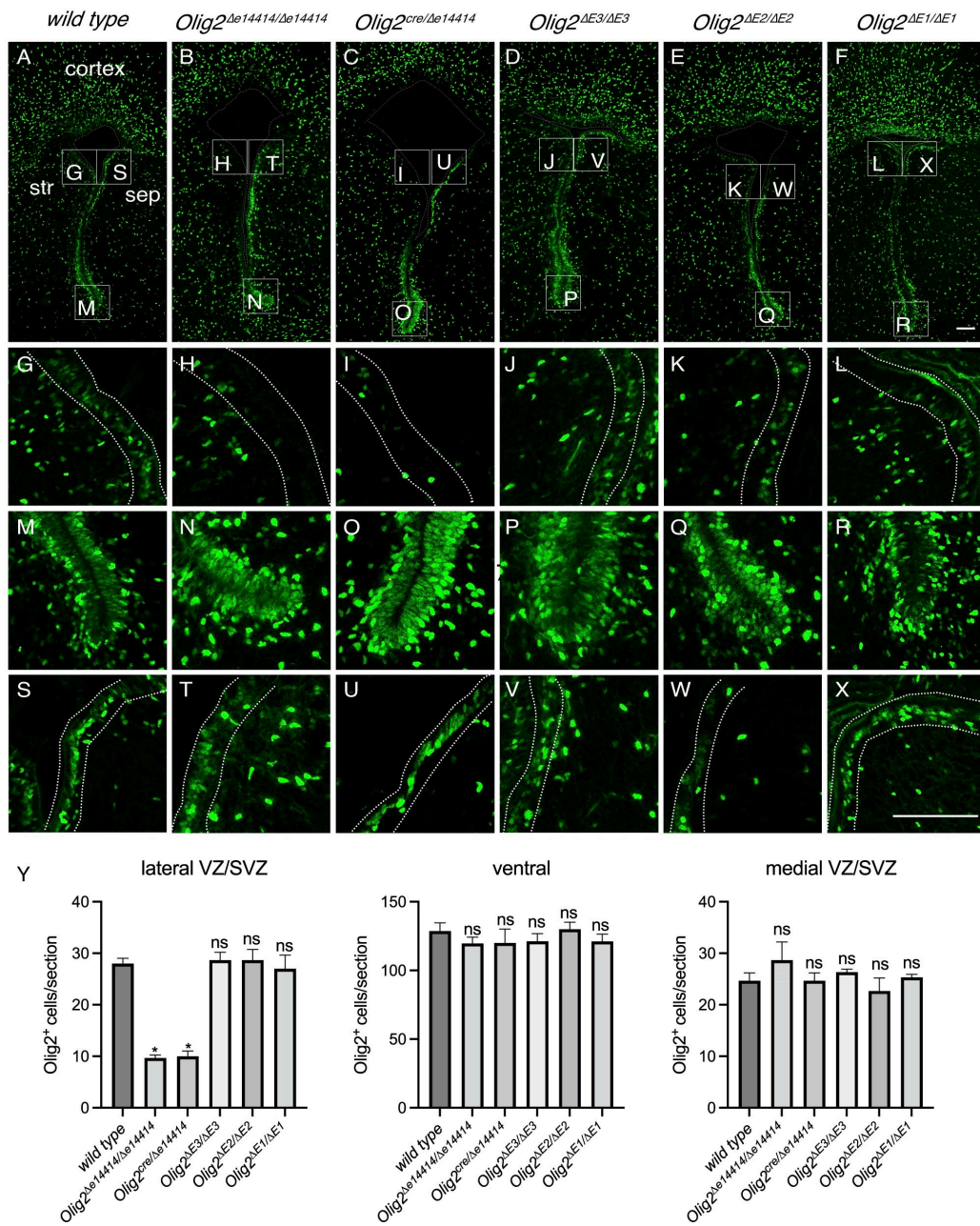


Figure 24. Enhancer e14414 regulates Olig2 expression in lateral VZ/SVZ.

(A - F) Immunostaining showing expressions of Olig2 in wildtype and *Olig2^{Δe14414/Δe14414}*, *Olig2^{cre/Δe14414}*, *Olig2^{ΔE3/ΔE3}*, *Olig2^{ΔE2/ΔE2}*, *Olig2^{ΔE1/ΔE1}* mice along the lateral ventricle.

(G - L) Enlarged image showing expressions of Olig2 in lateral VZ/SVZ.

(M - R) Enlarged image showing expressions of Olig2 in ventral VZ/SVZ.

(S - X) Enlarged image showing expressions of Olig2 in medial VZ/SVZ.

(Y) Quantifications of Olig2⁺ cells in lateral, ventral brain and medial VZ/SVZ.

Scale bar: 100um in (F, X).

Data in (Y) were represented as means + SEM (n = 3 per genotype). *, P < 0.05; unpaired Student's t test.

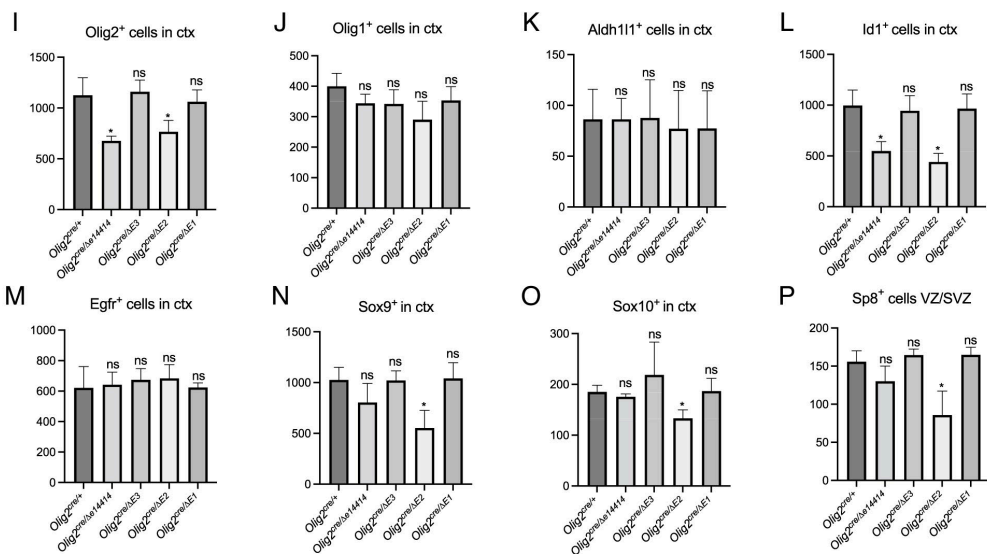
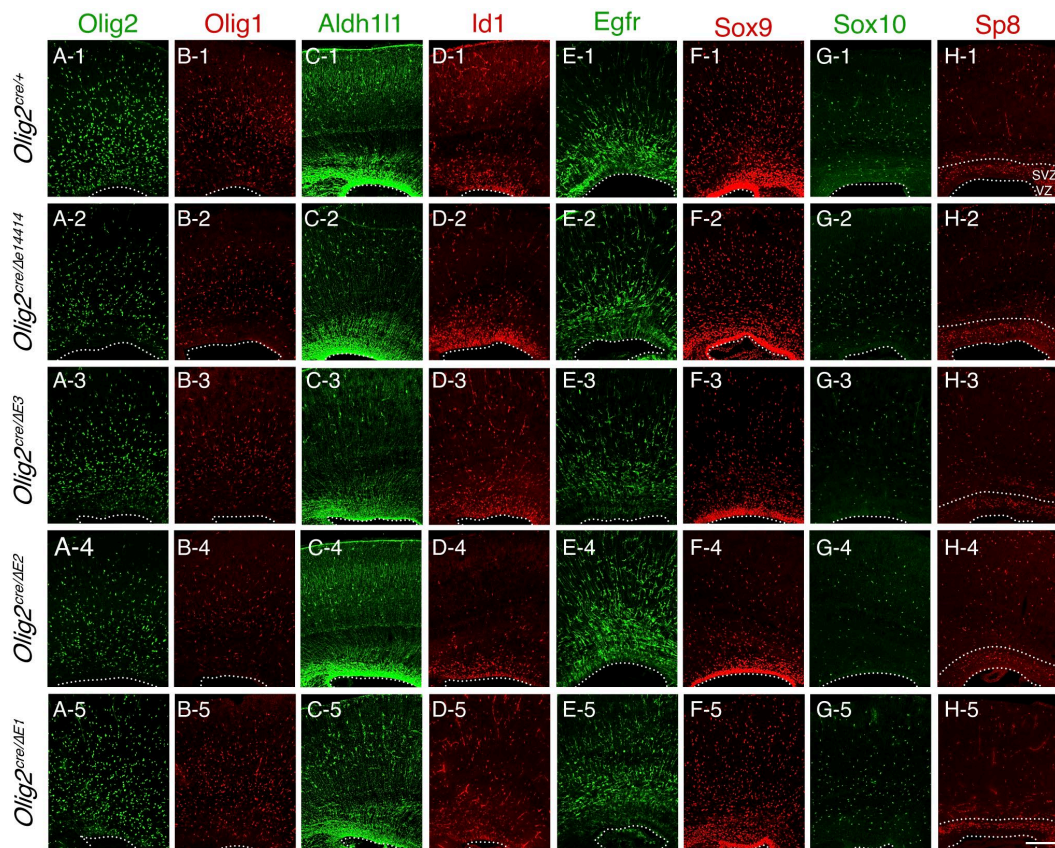


Figure 25. e14414 and E2 regulate gliogenesis in the dorsal cortex and E2 is involved in OB interneuron development.

(A - H) Immunostaining showing expressions of Olig2, Olig1, Aldh111, Id1, Egfr, Sox9, Sox10, Sp8 in *Olig2*^{cre/+} and *Olig2*^{cre/Δe14414}, *Olig2*^{cre/ΔE3}, *Olig2*^{cre/ΔE2}, *Olig2*^{cre/ΔE1}, *Olig2*^{cre/cre} mice in cortical VZ/SVZ.

(I - P) Quantification Olig2⁺, Olig1⁺, Aldh1l1⁺, Id1⁺, Egfr⁺, Sox9⁺, Sox10⁺, Sp8⁺ cells per section (10x image taken by Zeiss 880 confocal microscope) in different genotypes.

Quantifications of Olig2⁺ cells in lateral, ventral brain and medial VZ/SVZ. Data in (I - P) were represented as means + SEM (n = 3 per genotype). *, P < 0.05; unpaired Student's t test. Scale bar: 100um in (H - 5).

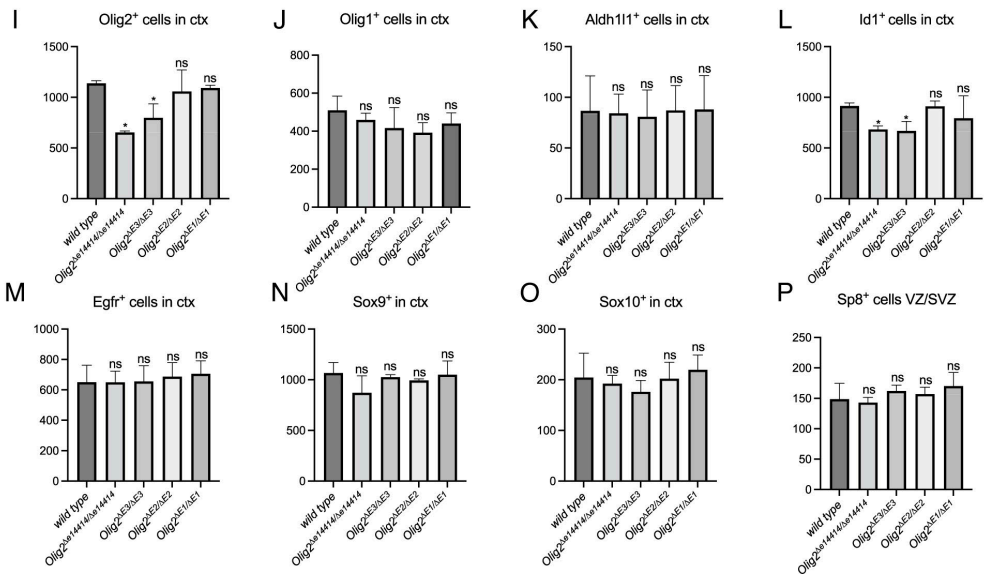
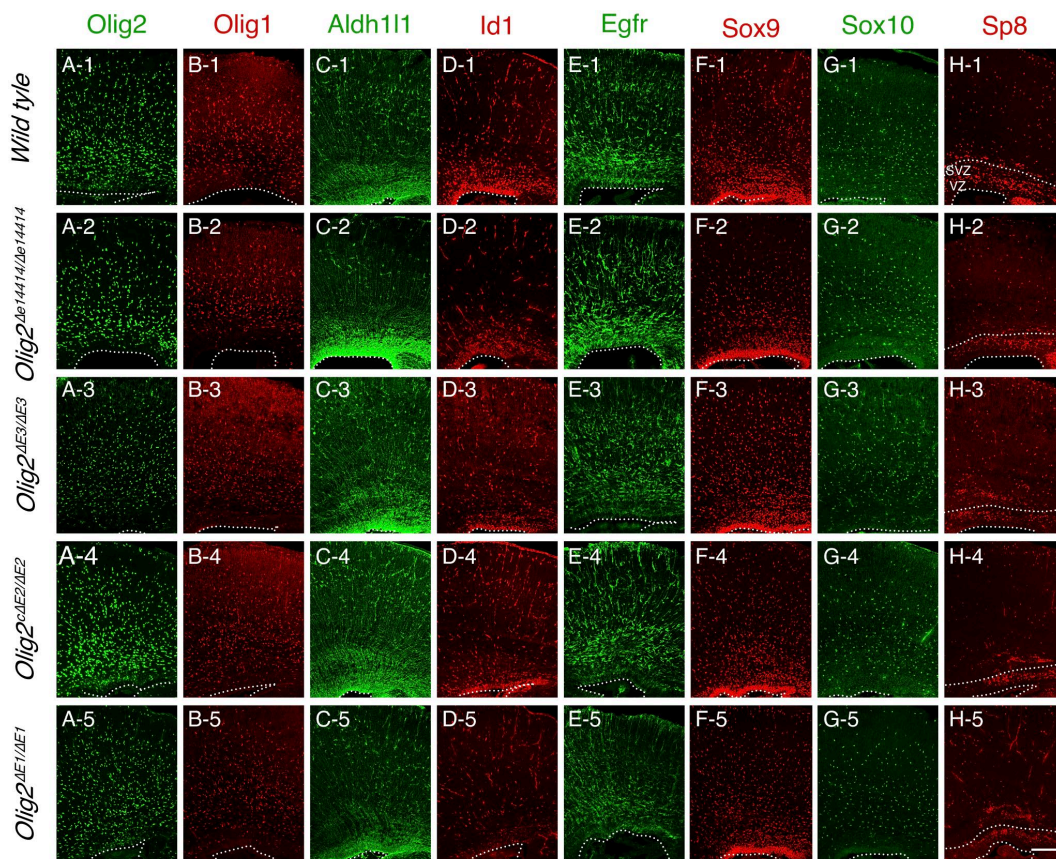


Figure 26. Olig2⁺ and Id1⁺ cells are decreased in Enhancer e14414 knockout and E3 knockout.

(A - H) Immunostaining showing expressions of Olig2, Olig1, Aldh111, Id1, Egfr, Sox9, Sox10, Sp8 in wildtype, *Olig2^{Δe14414/Δe14414}*, *Olig2^{ΔE3/ΔE3}*, *Olig2^{ΔE2/ΔE2}*, *Olig2^{ΔE1/ΔE1}* mice in dorsal cortex.

(I-P) Quantification Olig2⁺, Olig1⁺, Aldh1l1⁺, Id1⁺, Egfr⁺, Sox9⁺, Sox10⁺, Sp8⁺ cells per section (10x images taken by Zeiss 880 confocal microscope) in different genotypes.

Data in (I - P) were represented as means + SEM (n = 3 per genotype). *, P < 0.05; unpaired Student's t test. Scale bar: 100um in (H - 5).

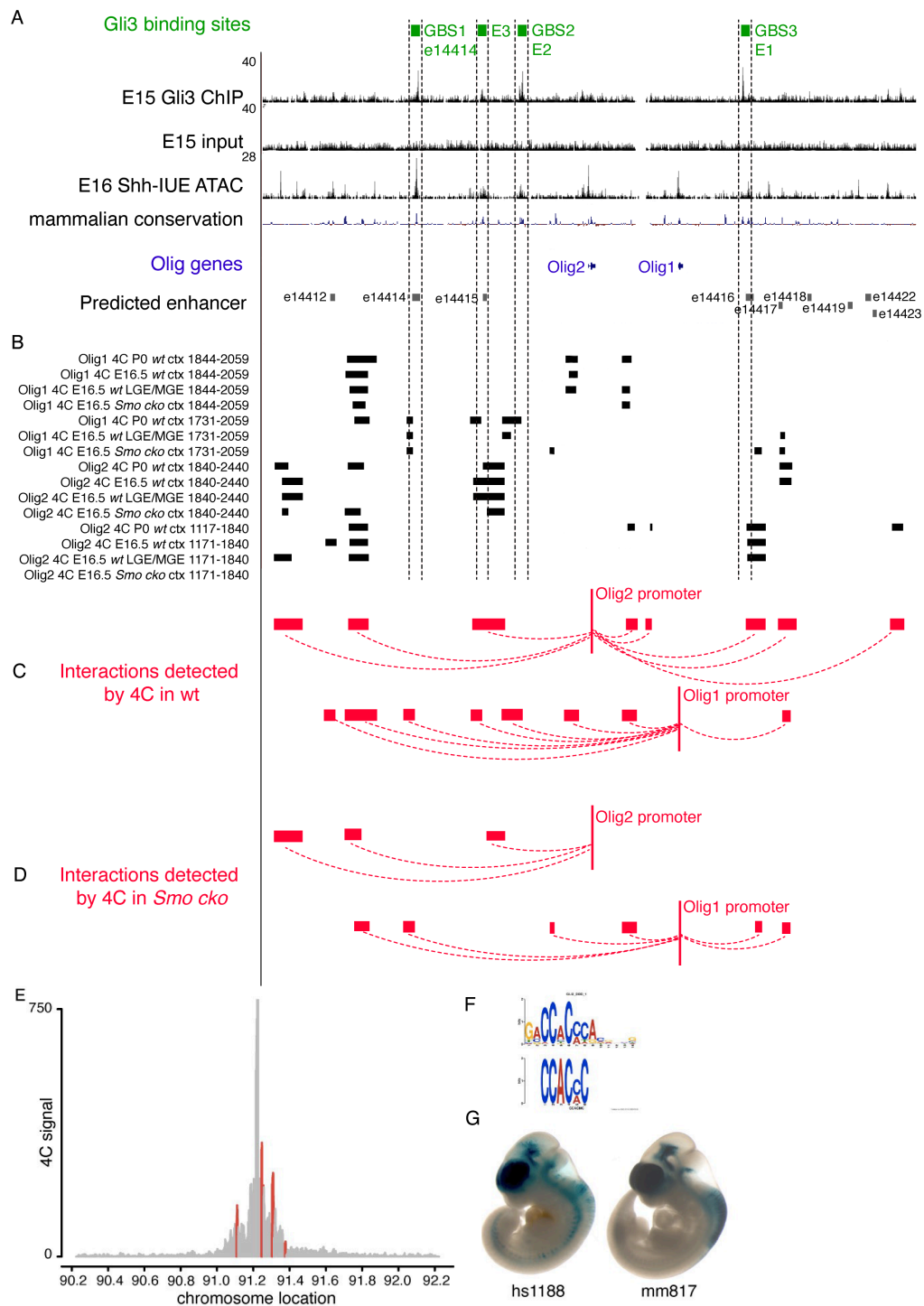


Figure 27. 4C-Seq data revealed physical interactions between Olig2/Olig1 promoters and Gli3 binding sites.

(A) Gli3 binding sites identified by ChIP-seq shown in green. Enhancers predicted by ENCODE shown in grey. Gli3 ChIP-seq revealed 4 Gli3

binding sites labelled by GBS1/e14414, E3, GBS2/E2, and GBS3/E1. These GBSs are conserved through species. Olig2/Olig1 genes are shown in blue. GBS1 is part of enhancer e14414. E3 is part of enhancer e14415. GBS3 is close to enhancer e14416.

(B) 4C-Seq were performed using P0/E16 cortices and LGE/MGE tissues in wildtype and *Smo cko* brain. Two sets of primers (1844-2059 and 1731-2059) were designed by using Olig1 promoter as the viewpoint. Another Two sets of primers (1840-2440 and 1171-1840) were designed by using Olig2 promoter as a viewpoint. Captured sequences from 4C-Seq were shown in black from each trail.

(C) Interactions detected by 4C-Seq by using wildtype tissues were summarized.

(D) Interactions detected by 4C-Seq by using *Smo cko* tissues were summarized.

(E) An example 4C experiment using Olig2 promoter as the viewpoint.

(F) The top panel shows the most significantly enriched motif identified from our Gli3 ChIP-seq IDR peaks, the bottom panel shows Gli2 binding motif.

(G) The hs1188 (left) and mm817 enhancers (right) are active in the cerebral cortex of E11.5 mouse embryos (Data from vista enhancer browser).

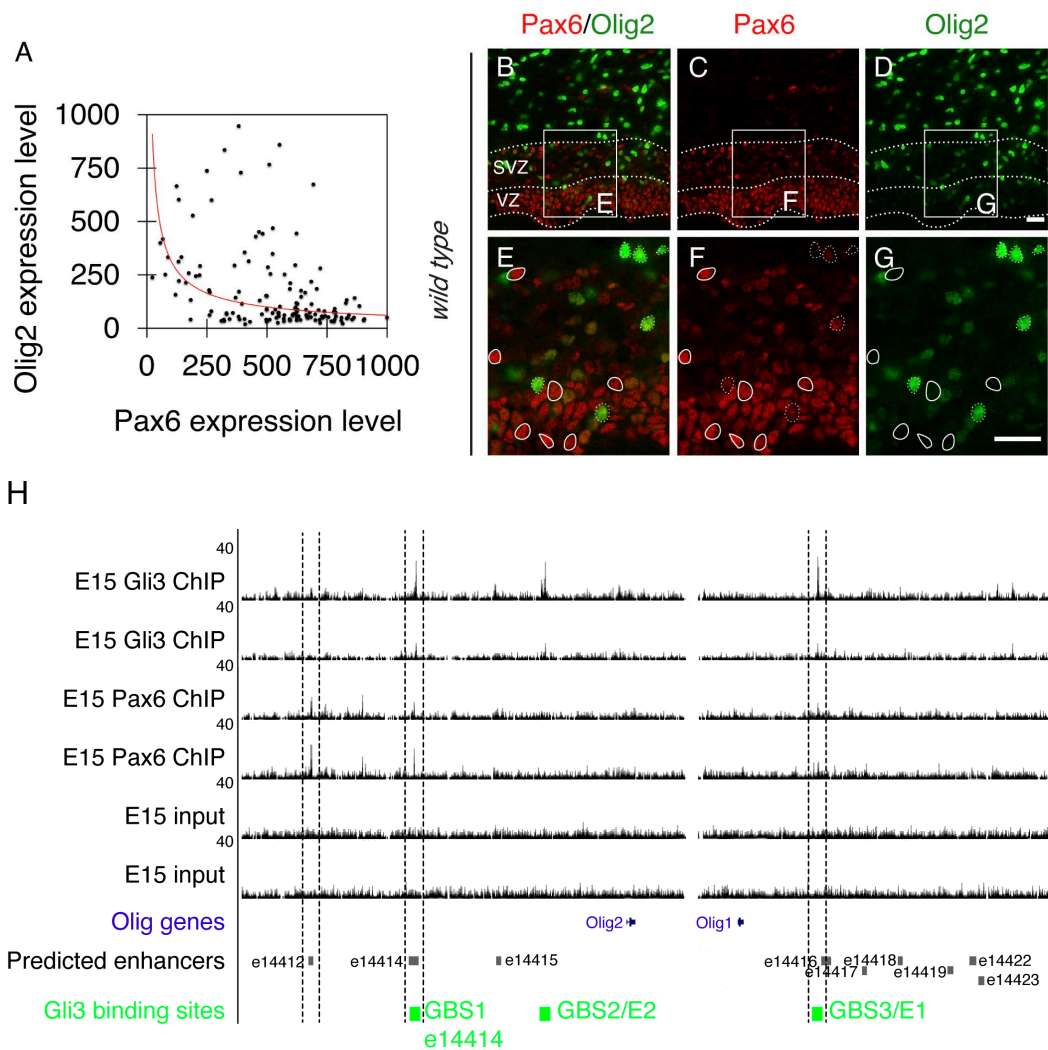


Figure 28. Anti-correlation of Pax6 and Olig2 in VZ/SVZ

(A) Quantification of the Pax6 and Olig2 protein expression level in wild-type mouse brain in VZ/SVZ at P0. The brains were sectioned at 12um and Olig2/PAX6 immunostaining was performed on the section. 40X images were taken by using ZEISS 880 confocal microscope. The individual cells in the VZ/SVZ were selected based on DAPI staining. The sum of the values of the pixels in the selection was calculated by ImageJ as the integrated density. The average cell fluorescence value was calculated by dividing the integrated density by the area of selection. We selected 100-150 cells in the VZ/SVZ to calculate the average cell fluorescence value in each channel. The data were visualized by

normalizing the max average cell fluorescence value to 1000 in each channel to show the differential expression level of the Pax6 and Olig2 proteins. Each dot represents a cell. The cell with a 1000 value is the brightest cell in the image.

(B - D) Immunostaining showing expressions of Pax6 and Olig2 in the wildtype mouse brain at P0.

(E - G) Zoom in images showing the immunostaining signal of Pax6 and Olig2 in VZ/SVZ in the wildtype brain. Representative cells with high expression of Pax6 in the nucleus were shown in solid line circle and representative cells with high expression of Olig2 in the nucleus were shown in dashed line circle.

(H) Two replicates of Pax6 ChIP-seq and two replicates of Gli3 ChIP-seq data were shown. Enhancers predicted by ENCODE shown in grey. Pax6 binds to the e14412, e14414/GBS1 and GBS3/E1.

Scale bars: 20 μ m in (E, H, K, N).

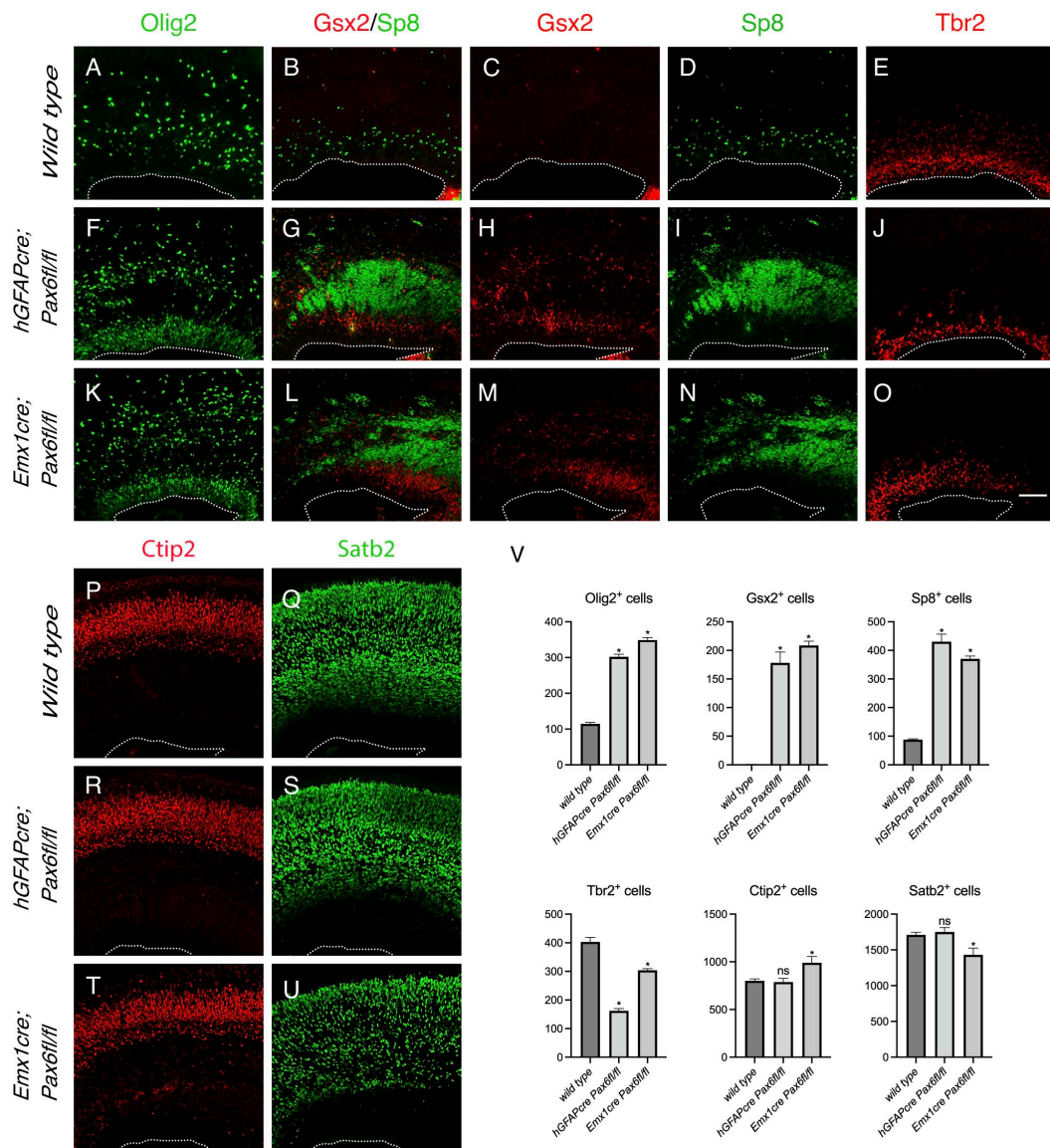
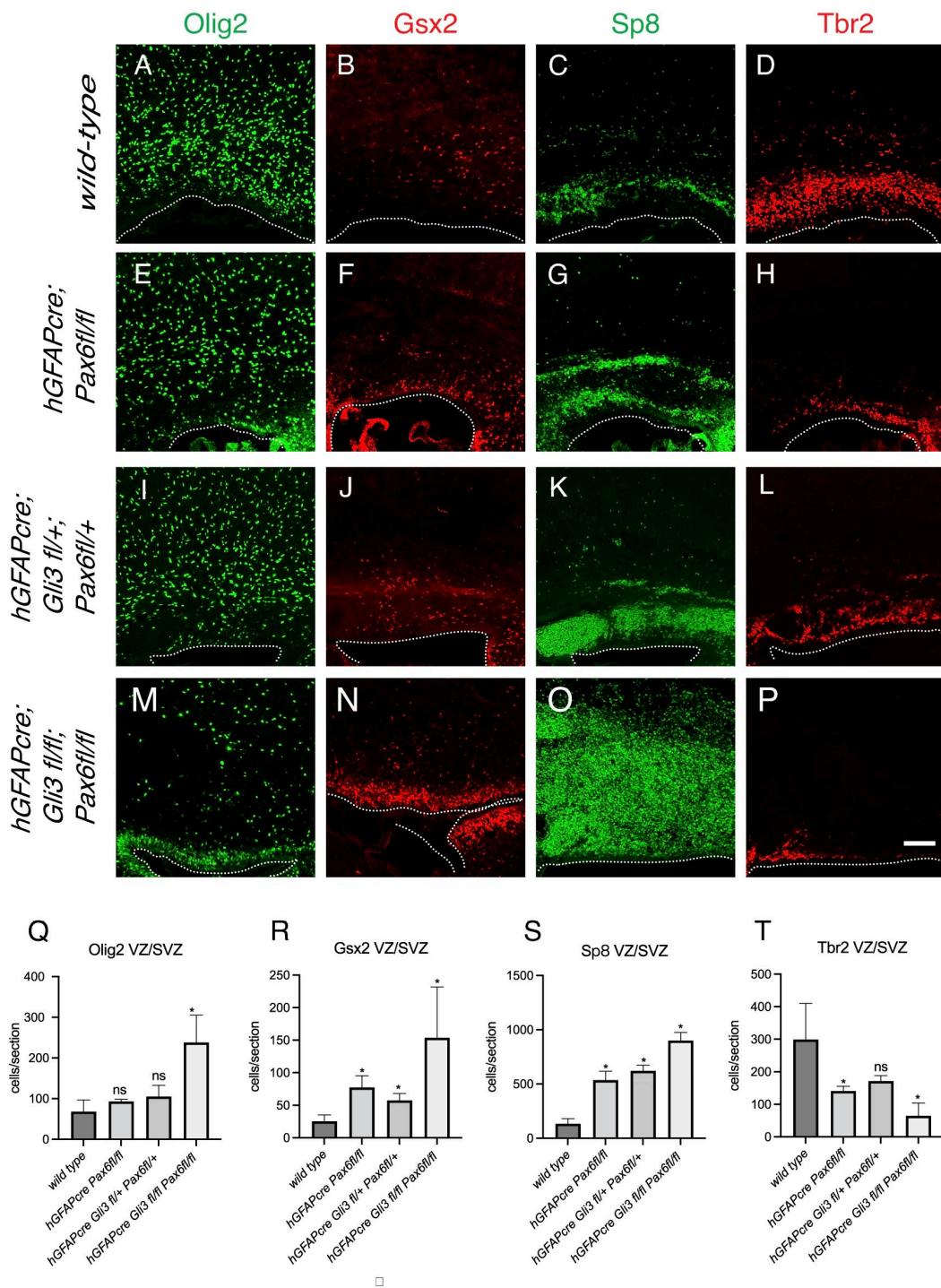


Figure 29. Pax6 represses OB lineage.

(A - U) Immunostaining showing expressions of Olig2, Gsx2, Sp8, Tbr2, Ctip2 and Satb2 in E16 wildtype, *hGFAPcre Pax6^{F/F}* and *Emx1-cre Pax6^{F/F}* mouse brain.

(V) Quantification of Olig2⁺, Gsx2⁺, Sp8⁺, Tbr2⁺, Ctip2⁺ and Satb2⁺ cells per 350μm wide section (10x images taken by Zeiss 880 confocal microscope) in different genotypes are shown.

Data in (V) were represented as means ± SEM (n = 3 per genotype). *, P < 0.05; unpaired Student's t test. Scale bar: 100μm in (O).



(Q - T) Quantification of Olig2⁺, Gsx2⁺, Sp8⁺ and Tbr2⁺ cells per 300um wide section(10x images taken by Zeiss 880 confocal microscope) in different genotypes are shown.

Data in (Q - T) were represented as means + SEM (n = 3 per genotype).

*, P < 0.05; unpaired Student's t test. Scale bar: 100um in (P).

Materials and Methods

Animals

Experiments were performed according to protocols approved by the Institutional Animal Care and Use Committee at University of California at Santa Cruz. Experiments performed at Fudan University were in accordance with institutional guidelines.

The day of the vaginal plug detection was designated as E0.5. The day of birth was designated as P0. The genders of the embryonic and early postnatal mice were not determined.

Immunohistochemistry

4% paraformaldehyde was delivered to mice via trans-cardiac perfusion. Brains were post-fixed in 4% paraformaldehyde, 0.1% saponin, and PBS for 24 hours at 4°C, followed by cryoprotection in 30% sucrose in PBS. Brains were sectioned via cryostat at 12um or 20um.

Immunohistochemistry was performed using standard protocols. Briefly, brain sections were permeabilized with 0.03% Triton X-100 in PBS for 10 min. Slides were then immersed in citrate acid buffer (10mM citric acid monohydrate, 0.05% Tween-20, pH 6.0), brought to a steamer for 25min at RT. Slides were cool down to RT after steaming and then incubated in a blocking buffer (5% Horse serum, 0.03% Triton X-100 in PBS) for 30 minutes. Blocking buffer was removed, and the sections were

incubated with primary antibodies (diluted in the blocking buffer) for 24 hours at 4°C.

The following primary antibodies were used in this study: OLIG2 (Mouse, Millipore 3319819), OLIG1(Rabbit, Abcam, ab124908), GLI3 (Goat, R&D Systems AF3690), SOX9 (Rabbit, Abcam ab185230), SOX10 (R&D System AF2864), PDGFR α (Rat, BD Pharmingen 558774), SP8 (Goat, SCBT Sc-104661), GSX2 (Rabbit, Millipore ABN162), ALDH1L1(Rabbit, Abcam ab87117), EGFR(Goat, R&D Systems AF1280), MAPK(Rabbit, Cell Signaling), ID1 (Rabbit, Biocheck, Inc BCH-1/#37-2), ID3 (Rabbit, Biocheck, Inc BCH-4/#17-3), KI67(Mouse, BD Pharmingen, #556003), ASCL1(Rabbit, Cosmo Bio, SK-T01-003), GFP (Chicken, Aves Labs GFP-879484), Activated caspase 3 (Rabbit, Cell Signaling Technology #9661), SATB2 (Rabbit, Abcam ab34735), and GAPDH (Covance, MMS-580S). H3k27me3 (Rabbit, Cell Signaling), H3k4me3 (Rabbit, Cell Signaling).

The sections were washed in PBS, and incubated with secondary antibodies conjugated to Alexa 488, Alexa 546, Alexa555, or Alexa 647 for 1.5 hour at room temperature. Secondary antibodies were from Jackson ImmunoResearch and Invitrogen. Finally, the sections were counterstained with DAPI for 5 mins before being mounted in Fluoromount-G.

***In situ* hybridization**

All in situ RNA hybridization assays were performed using digoxigenin riboprobes on 20 mm cryostat sections as previously described (Guo et al., 2019)(Zhang et al., 2016).

Gene	Forward Primer 5' → 3'	Reverse Primer 5' → 3'
<i>Smo</i>	ACATGCCCAAGTGTGAGAATGACC	GCTCTTGATGGAGAACAGAGTCAT
<i>Ptch1</i>	AAGCCCATCGACATTAGTCAGT	ATAAGAGGACAGGCAGCAGAAC
<i>Gli1</i>	TGGAGAACCTTAGGCTGGATCAGC	GGATCAGGATAGGAGACCTGCTGG
<i>Gad1</i>	ATGGCATCTTCCACTCCTTCG	TTACAGATCCTGACCCAACCTCTC
<i>Sp9</i>	ACCTGAATCGTGATTCCCAGCAG	TGCTATGGCTTTTGCAACCCAC
<i>Tshz1</i>	GAGAAGGTCACGGGCAAGGTCAGC	GAGGCGAGGACACAGCATCTGCCA
<i>Prokr2</i>	ATGGGACCCCAGAACAGA	ATGGGACCCCAGAACAGA

Amplified DNA fragments were ligated into pGEM-T Easy (Promega) plasmids, transformed into competent *E. coli* cells, and plated overnight on LB+Agar+Ampicillin plates. Colonies were picked, grown overnight in 3 mL LB+Ampicillin, and purified via miniprep kits (Sigma-Aldrich). Purified plasmids were sequenced to ensure sequence fidelity, and to determine insert orientation. Plasmids were then linearized with restriction enzymes from New England Biotech, and in vitro transcription reactions were performed with either T7 (NEB) or Sp6 (Promega) RNA polymerases, depending on insert orientation, in the presence of DIG-labeled nucleotides (Sigma-Aldrich).

Tissue was prepared as previously described by (Guo et al., 2013), and treated with DIG-labeled probes overnight at 65° C. Slides were developed with NBT/BCIP stock solution (Sigma-Aldrich).

EdU labeling

Timed pregnant mice were injected with a single dose of EdU (40mg/kg body weight; Thermo Fisher Scientific, E10187) at E16.5 or E17.5. Brains were collected at E17.5 or P0. EdU was detected via a click-chemistry reaction containing the following reagents per 1 ml of reaction: 950ul 100mM Tris PH 7.4, 40ul 100 mM CuSO₄, 10ul 200 mg/mL sodium ascorbate, and 1ul Azide 555.

CUT&RUN-seq

The E16 wt and *hGFAP-Cre; Rosa26^{SmoM2/+}* cortices (n = 3 each group) were dissected, and cells were isolated with the Accumax(Sigma-Aldrich A7089) following the manufacturer's instructions. CUT&RUN were performed according to the published protocol (Skene and Henikoff, 2017). H3K27ac H3K4me3 and H3K27me3 were used in this study. 100million cells were used for each sample. DNA libraries were constructed using NEBNext Ultra II DNA Library Prep Kit for Illumina (NEB #E7645, E7103) with index primers (NEB, E7645-S). The libraries were sequenced via NextSeq 75 cycles High (PE37) platform with 1% PhiX control. Pippen size selection was used to remove the primer dimers (140bp).

ATAC-seq

The E16 cortices from *Rosa26^{SmoM2/+}* (control) brains, *hGFAP-Cre; Rosa26^{SmoM2/+}* and *ShhN-IUE (pCAG-ShhN-Ires-GFP)* were electroporated

into the wild-type cortex at E13.5) (n = 3 each group) were carefully dissected under a fluorescent stereoscope, and incubated in 4 ml of papain solution (final con. 12 U/mL, diluted in DMEM/F-12, Gibco 11330032) for 20 min at 37 °C. The cortical tissues were gently triturated, filtered through a 40 um cell strainer, and washed with HBSS to obtain the single cell suspension. The libraries were prepared by Nextera DNA Library Prep Kit (Illumina, catalog # FC-121-1030). The primary protocol is based on the published protocol (Buenrostro et al., 2015), with the following modification: We found that column purification of the libraries does not remove primer-dimers (78 bp), and our libraries often contained large fragments 1,000-10,000 bp in length. Therefore, we use magnetic bead purification rather than column purification of the libraries. The platform was Illumina HiSeq4000, 100PE.

RNA-seq

The P0 cortices from *Rosa26^{SmoM2/+}* (control) brains, *hGFAP-Cre; Rosa26^{SmoM2/+}* and *ShhN-IUE (pCAG-ShhN-Ires-GFP)* were electroporated into the wild-type cortex at E13.5) (n = 3 each group) were dissected, and total RNA was isolated with the Direct-zol RNA Miniprep kit (Zymo, catalog #R2050) following the manufacturer's instructions. The gene expression level was reported with fragments per kilobase of exon model per million mapped reads (FPKM) (Trapnell et al., 2012). Genes with a p value < 0.05 would be called as differentially expressed.

scRNA-Seq library preparation

pCAG-ShhN-Ires-GFP plasmids were electroporated into the cortical VZ of wild-type mice at E13.5. Three days after ShhN-IUE (E16.5), embryos were quickly taken, and the brains were immediately removed and submerged in fresh ice-cold HBSS (GIBCO 14175-095).

E16.5 wild type and ShhN-IUE cortices were carefully dissected under a fluorescent stereoscope and incubated in 4 ml of papain solution (final con. 12 U/mL, diluted in DMEM/F-12, Gibco 11330032) for 20 min at 37 °C. The cortical tissues were gently triturated, filtered through a 40-um cell strainer, and washed with HBSS to obtain the single cell suspension.

scRNA-Seq analysis

High quality sequences (Clean reads) were obtained by removing low quality sequences and joints. Clean reads were then processed with Cell Ranger software to obtain quantitative information of gene expression and cell population classification. The cell statistical results are shown in the following table.

Group	ShhN - IUE	Wild - type
Estimated Number of Cells	8538	7834
Mean Reads Per Cell	50946	55069
Total Genes Detected	18151	18001

Median Genes Per Cell	2422	2368
Fraction Reads in Cells	90.90%	84.80%
Median UMI Counts Per Cell	6726	6230

Clustering was performed as previously described. Normalized counts matrices were log2 transformed, and variable genes were calculated using default Seurat parameters. Data were scaled in the space of these variable, and batch was regressed out. Principal component analysis was performed using FastPCA, and significant PCs were identified using the formula outlined in Shekhar et al. In the space of these significant PCs, the k=10 nearest neighbors were identified as per the RANN R package. The distances between these neighbors were weighted by their Jaccard distance, and louvain clustering was performed using the igraph R package. If any clusters contained only 1 cell, the process was repeated with k=11 and up until no clusters contained only 1 cell. Cluster markers and tSNE (t-Distributed Stochastic Neighbor Embedding) plots were generated with Seurat package default parameters. Differentially expressed genes for each cluster were shown in Figures S6 and S7. Cell lineages trajectory was analyzed using Monocle 2, a computational method based on a machine learning technique called reversed graph embedding to construct the single-cell trajectories (Trapnell et al. 2014). Monocle uses the algorithm to extract the sequence of gene expression changes each cell must go through in biological processes, therefore, to predict lineage trajectories and bifurcations by ordering the pseudo-timeline. The pseudo-timeline is a

developmental tree, that a cell at the beginning of the biological process starts at the root and progresses along the trunk and choose different path to finally arrive the leaf. A cell's pseudo time value is the distance that it would have to travel to get back to the root. The lineage trajectory reconstructed by monocle is referred to as predicted developmental trajectory. The cluster of RGC serves as the root point. To analyze the events of lineage switch for cortical progenitors, we extracted the progenitor cells (including clusters of RGC, OB-IPC, OPC, and tri-IPC) from the Shh-IUE sample. We pooled all the subpopulations for the following analysis. We first imported the Seurat object containing cleaned, standardized, and clustered dataset to the monocle 2. Then, the most dispersed genes to use for pseudo-time ordering were calculated using the 'estimate dispersions' function. R package DDRTree was used to reduce dimensions with selected dispersed genes. In the meantime, the effects of numbers of UMI, donor, and library preparation batch were corrected. Finally, visualization function 'plot_cell_trajectory' was used to plot the minimum spanning tree on cells.

Quantification and statistical analysis

RNA-Seq data, scRNA-Seq data and analysis are provided in the above methods sections. Statistical tests were performed using GraphPad Prism software, Microsoft Excel and R language. No statistical methods were used to estimate sample size. Number of cells are shown as mean \pm SEM and statistical significance was determined using two-tailed Student's

t tests. Significance was set as * for $p < 0.05$, ** for $p < 0.01$, and *** $p < 0.001$.

Data and code availability

Bulk RNA-seq data and scRNA-Seq data have been deposited at the National Center for Biotechnology Information BioProjects Gene Expression Omnibus and are accessible through GEO: GSE140817.

In utero electroporation

In utero electroporation (IUE) of wild-type or *Gsx2^{Flpo/+};IS* embryos was performed at E13.5 or E14.5. Plasmids *pCAG-Cre* (Addgene #13775), *pCAG-GFP* (Addgene #11150), *pCAG-ShhN-Ires-GFP*, or *pCAG-GFP* (final concentration of 1-2 mg/ml, 0.5ml each embryo) were mixed with 0.05% Fast Green (Sigma), and injected into the lateral ventricle of embryos using a beveled pulled glass micropipette. Five electrical pulses (duration: 50 ms) were applied at 31V for E13.5 embryos and 35V for E14.5 embryos across the uterine wall with a 950 ms interval between pulses. Electroporation was performed using a pair of 7 mm platinum electrodes (BTX, Tweezertrode 45-0488, Harvard Apparatus) connected to an electroporator (BTX, ECM830). Embryos were analyzed at different time points.

Image acquisition and analysis

Images for quantitative analyses were acquired with a Zeiss 880 confocal microscope. Cell counting was performed on single z-slices. The unpaired t test was used to determine statistical significance. Analyses were done using GraphPad Prism 8.0, Microsoft Excel and R language.

The numbers of GFP⁺ or/and tdT⁺ cells in the OB, and GFP⁺ oligodendrocytes and astrocytes in the cortex (0.40 mm² area for the OB and 1.10 mm² area for the cortex) were quantified in 3-4 randomly chosen 30 mm sections for P21 *Gsx2^{Fipo/+}; IS; pCAG-Cre* IUE@E14.5 mice. The numbers of S100b⁺, GFP⁺ S100b⁺, OLIG2⁺ and GFP⁺ OLIG2⁺ cells in the cortex (0.67mm² area) were quantified in 4 randomly chosen 30 mm sections for P21 *Emx1-Cre; Gsx2^{Fipo/+}; IS* mice. The numbers of GFP⁺ oligodendrocytes and astrocytes in the cortex (1.78 mm² area) were quantified in 4 randomly chosen 30 mm sections for P21 *Emx1-Cre; Gsx2^{Fipo/+}; IS* mice, and the percentages of the oligodendrocytes and astrocytes among all GFP⁺ cells in the cortex were calculated. *Gsx2⁺* and *Eomes⁺* cells in the entire cortex were quantified in 2 randomly chosen 10 mm sections at rostral, intermediate, and caudal telencephalic levels, respectively, from wild-type mice. The numbers of *Gsx2⁺* cells and *Sp8⁺* cells in the P2 cortices were counted in 3 randomly chosen 12 mm sections for each group of mice. Two or three brains for each genotype at each stage were used.

10X images taken by Zeiss 880 confocal microscope were used for quantifying the numbers of *Gsx2⁺*, *Sp8⁺*, *Eomes⁺*, *Olig2⁺*, *EdU⁺*, *Ascl1⁺*, *Egfr⁺*, *Aldh1l1⁺*, *Id1⁺*, *Id3⁺*, *Sox10⁺*, *Sox9⁺* cells in the cortical VZ/SVZ and

CTX in the P0 and P3 brains. The control brain and mutant brains were sectioned on the same slide and imaged at the same time under the same condition. The numbers of cells in a 300 mm width or 1000px width were counted. Three matched sections from each brain, and three brains for each genotype at each stage were used.

ChIP-seq

E15 wt cortices cortices(n = 3 each group) were dissected, fixed for 10 min with 1% formaldehyde and neutralized with glycine. Chip-seq were performed according to the published protocol (Johnson et al., 2007). The cells were lysed, and the chromatin was sheared into 100~300-bp fragments. Immunoprecipitation reactions were performed using the Gli3 and Pax6 antibody. Sequencing libraries were generated from the ChIP-ed DNA and input DNA for control using Ovation Ultralow System V2 kit according to the manufacturer's protocol. Sequencing was performed on Hiseq4000, 100PE platform.

4C-Seq

E16 and P0 wt Cortices, LGE/CGE tissues(n = 3 for each sample) were dissected and used for 4C-Seq according to published protocol (Krijger et al., 2020). Olig2 and Olig1 promoter were used as viewpoints. Primers were designed by using Primer3. The following restriction enzymes(RE) and primers were used in this study. 4C libraries were

generated with dual index NEB primers (E7780-S). The pooled library has low complexity and needs about 20% PhiX spike in control. The platform is NextSeq 150 cycles MID output (PE75). The following pipeline were used to analyze the data <https://github.com/deLaatLab/pipe4C>(Krijger et al., 2020).

Gene	Olig2
1st RE	Csp6I
2nd RE	DpnII
Fragment	1840-2440
seq primer	TATTGTCAGTGTAGCGTCAG
reading primer	TACACGACGCTCTTCCGATCTTATTGTCAGTGTAGCGTCAG
outward primer	CTCCAAAGTGGCTAGGATT
non-reading primer	ACTGGAGTTCAGACGTGTGCTCTTCCGATCTCTCCAAAGTGGCTAGGATT
Gene	Olig2
1st RE	DpnII
2nd RE	Csp6I
Fragment	1840-2440
seq primer	TATTGTCAGTGTAGCGTCAG
reading primer	TACACGACGCTCTTCCGATCTTATTGTCAGTGTAGCGTCAG
outward primer	CTCCAAAGTGGCTAGGATT
non-reading primer	ACTGGAGTTCAGACGTGTGCTCTTCCGATCTCTCCAAAGTGGCTAGGATT
Gene	Olig2
1st RE	DpnII
2nd RE	Csp6I
Fragment	1117-1840
seq primer	CACACACATACAAAGCTGAG
reading primer	TACACGACGCTCTTCCGATCTCACACACATACAAAGCTGAG
outward primer	CGGACGAGTTTGAGATT
non-reading primer	ACTGGAGTTCAGACGTGTGCTCTTCCGATCTCGGACGAGTTTGAGATT
Gene	Olig1
1st RE	DpnII
2nd RE	Csp6I
Fragment	1844-2059
seq primer	TGCCTTGTAATAATGTGATC
reading primer	TACACGACGCTCTTCCGATCTTGCCTTGTAATAATGTGATC
outward primer	GATAACCCTCTGGAAC
non-reading primer	ACTGGAGTTCAGACGTGTGCTCTTCCGATCTGATAACCCTCTGGAAC
Gene	Olig1
1st RE	NlaIII
2nd RE	Csp6I
Fragment	1731-2059
seq primer	GGTTGGCTGTTATAAAAATGC
reading primer	TACACGACGCTCTTCCGATCTGGTTGGCTGTTATAAAAATGC
outward primer	GATAACCCTCTGGAAC
non-reading primer	ACTGGAGTTCAGACGTGTGCTCTTCCGATCTGATAACCCTCTGGAAC

Bibliography

Balordi, F., and Fishell, G. (2007). Hedgehog Signaling in the Subventricular Zone Is Required for Both the Maintenance of Stem Cells and the Migration of Newborn Neurons. *J. Neurosci.* 27, 5936–5947. <https://doi.org/10.1523/JNEUROSCI.1040-07.2007>.

Bayraktar, O.A., Fuentealba, L.C., Alvarez-Buylla, A., and Rowitch, D.H. (2015). Astrocyte Development and Heterogeneity. *Cold Spring Harb. Perspect. Biol.* 7, a020362. <https://doi.org/10.1101/cshperspect.a020362>.

Beattie, R., Postiglione, M.P., Burnett, L.E., Laukoter, S., Streicher, C., Pauler, F.M., Xiao, G., Klezovitch, O., Vasioukhin, V., Ghashghaei, T.H., et al. (2017). Mosaic Analysis with Double Markers Reveals Distinct Sequential Functions of Lgl1 in Neural Stem Cells. *Neuron* 94, 517-533.e3. <https://doi.org/10.1016/j.neuron.2017.04.012>.

Blaess, S., Stephen, D., and Joyner, A.L. (2008). Gli3 coordinates three-dimensional patterning and growth of the tectum and cerebellum by integrating Shh and Fgf8 signaling. *Development* 135, 2093–2103. <https://doi.org/10.1242/dev.015990>.

Blondel, V.D., Guillaume, J.-L., Lambiotte, R., and Lefebvre, E. (2008). Fast unfolding of communities in large networks. *J. Stat. Mech. Theory Exp.* 2008, P10008. <https://doi.org/10.1088/1742-5468/2008/10/P10008>.

Bowling, S., Sritharan, D., Osorio, F.G., Nguyen, M., Cheung, P., Rodriguez-Fraticelli, A., Patel, S., Yuan, W.-C., Fujiwara, Y., Li, B.E., et al. (2020). An Engineered CRISPR-Cas9 Mouse Line for Simultaneous Readout of Lineage Histories and Gene Expression Profiles in Single Cells. *Cell* 181, 1410-1422.e27. <https://doi.org/10.1016/j.cell.2020.04.048>.

Brewer, J.R., Mazot, P., and Soriano, P. (2016). Genetic insights into the mechanisms of Fgf signaling. *Genes Dev.* 30, 751–771. <https://doi.org/10.1101/gad.277137.115>.

Buchholz, F., Angrand, P.-O., and Stewart, A.F. (1998). Improved properties of FLP recombinase evolved by cycling mutagenesis. *Nat. Biotechnol.* 16, 657–662. <https://doi.org/10.1038/nbt0798-657>.

Buenrostro, J.D., Wu, B., Chang, H.Y., and Greenleaf, W.J. (2015). ATAC-seq: A Method for Assaying Chromatin Accessibility Genome-Wide. *Curr. Protoc. Mol. Biol.* 109. <https://doi.org/10.1002/0471142727.mb2129s109>.

Bulfone, A., Martinez, S., Marigo, V., Campanella, M., Basile, A., Quaderi, N., Gattuso, C., Rubenstein, J.L.R., and Ballabio, A. (1999). Expression pattern of the Tbr2 (Eomesodermin) gene during mouse and chick brain development. *Mech. Dev.* 84, 133–138. [https://doi.org/10.1016/S0925-4773\(99\)00053-2](https://doi.org/10.1016/S0925-4773(99)00053-2).

Cai, J., Chen, Y., Cai, W.-H., Hurlock, E.C., Wu, H., Kernie, S.G., Parada, L.F., and Lu, Q.R. (2007). A crucial role for Olig2 in white matter astrocyte

development. *Development* *134*, 1887–1899.
<https://doi.org/10.1242/dev.02847>.

Cai, Y., Zhang, Y., Shen, Q., Rubenstein, J.L.R., and Yang, Z. (2013). A Subpopulation of Individual Neural Progenitors in the Mammalian Dorsal Pallium Generates Both Projection Neurons and Interneurons In Vitro. *Stem Cells* *31*, 1193–1201. <https://doi.org/10.1002/stem.1363>.

Carballo, G.B., Honorato, J.R., de Lopes, G.P.F., and Spohr, T.C.L. de S. e (2018). A highlight on Sonic hedgehog pathway. *Cell Commun. Signal.* *16*, 11. <https://doi.org/10.1186/s12964-018-0220-7>.

Chapman, H., Waclaw, R.R., Pei, Z., Nakafuku, M., and Campbell, K. (2013). The homeobox gene *Gsx2* controls the timing of oligodendroglial fate specification in mouse lateral ganglionic eminence progenitors. *Development* *140*, 2289–2298. <https://doi.org/10.1242/dev.091090>.

Chapman, H., Riesenberg, A., Ehrman, L.A., Kohli, V., Nardini, D., Nakafuku, M., Campbell, K., and Waclaw, R.R. (2018). *Gsx* transcription factors control neuronal versus glial specification in ventricular zone progenitors of the mouse lateral ganglionic eminence. *Dev. Biol.* *442*, 115–126. <https://doi.org/10.1016/j.ydbio.2018.07.005>.

Corrales, J.D., Blaess, S., Mahoney, E.M., and Joyner, A.L. (2006). The level of sonic hedgehog signaling regulates the complexity of cerebellar foliation. *Development* *133*, 1811–1821. <https://doi.org/10.1242/dev.02351>.

Desmaris, E., Keruzore, M., Saulnier, A., Ratié, L., Assimacopoulos, S., De Clercq, S., Nan, X., Roychoudhury, K., Qin, S., Kricha, S., et al. (2018). DMRT5, DMRT3, and EMX2 Cooperatively Repress *Gsx2* at the Pallium–Subpallium Boundary to Maintain Cortical Identity in Dorsal Telencephalic Progenitors. *J. Neurosci.* **38**, 9105–9121. <https://doi.org/10.1523/JNEUROSCI.0375-18.2018>.

Diez del Corral, R., and Morales, A.V. (2017). The Multiple Roles of FGF Signaling in the Developing Spinal Cord. *Front. Cell Dev. Biol.* **5**, 58. <https://doi.org/10.3389/fcell.2017.00058>.

Dinh Duong, T.A., Hoshiba, Y., Saito, K., Kawasaki, K., Ichikawa, Y., Matsumoto, N., Shinmyo, Y., and Kawasaki, H. (2019). FGF Signaling Directs the Cell Fate Switch from Neurons to Astrocytes in the Developing Mouse Cerebral Cortex. *J. Neurosci.* **39**, 6081–6094. <https://doi.org/10.1523/JNEUROSCI.2195-18.2019>.

Doe, C.Q. (2017). Temporal Patterning in the *Drosophila* CNS. **24**. .

Dulken, B.W., Leeman, D.S., Boutet, S.C., Hebestreit, K., and Brunet, A. (2017). Single-Cell Transcriptomic Analysis Defines Heterogeneity and Transcriptional Dynamics in the Adult Neural Stem Cell Lineage. *Cell Rep.* **18**, 777–790. <https://doi.org/10.1016/j.celrep.2016.12.060>.

Elbaz, B., and Popko, B. (2019). Molecular Control of Oligodendrocyte Development. *Trends Neurosci.* **42**, 263–277. <https://doi.org/10.1016/j.tins.2019.01.002>.

Englund, C. (2005). Pax6, Tbr2, and Tbr1 Are Expressed Sequentially by Radial Glia, Intermediate Progenitor Cells, and Postmitotic Neurons in Developing Neocortex. *J. Neurosci.* 25, 247–251. <https://doi.org/10.1523/JNEUROSCI.2899-04.2005>.

Fernandes-Silva, H., Correia-Pinto, J., and Moura, R. (2017). Canonical Sonic Hedgehog Signaling in Early Lung Development. *J. Dev. Biol.* 5, 3. <https://doi.org/10.3390/jdb5010003>.

Fuccillo, M., Rutlin, M., and Fishell, G. (2006). Removal of Pax6 Partially Rescues the Loss of Ventral Structures in Shh Null Mice. *Cereb. Cortex* 16, i96–i102. <https://doi.org/10.1093/cercor/bhk023>.

Fuentealba, L.C., Rompani, S.B., Parraguez, J.I., Obernier, K., Romero, R., Cepko, C.L., and Alvarez-Buylla, A. (2015). Embryonic Origin of Postnatal Neural Stem Cells. *Cell* 161, 1644–1655. <https://doi.org/10.1016/j.cell.2015.05.041>.

Gao, P., Postiglione, M.P., Krieger, T.G., Hernandez, L., Wang, C., Han, Z., Streicher, C., Papusheva, E., Insolera, R., Chugh, K., et al. (2014). Deterministic Progenitor Behavior and Unitary Production of Neurons in the Neocortex. *Cell* 159, 775–788. <https://doi.org/10.1016/j.cell.2014.10.027>.

Gorski, J.A., Talley, T., Qiu, M., Puelles, L., Rubenstein, J.L.R., and Jones, K.R. (2002). Cortical Excitatory Neurons and Glia, But Not GABAergic Neurons, Are Produced in the Emx1-Expressing Lineage. *J. Neurosci.* 22, 6309–6314. <https://doi.org/10.1523/JNEUROSCI.22-15-06309.2002>.

Guo, C., Eckler, M.J., McKenna, W.L., McKinsey, G.L., Rubenstein, J.L.R., and Chen, B. (2013). *Fezf2* Expression Identifies a Multipotent Progenitor for Neocortical Projection Neurons, Astrocytes, and Oligodendrocytes. *Neuron* 80, 1167–1174. <https://doi.org/10.1016/j.neuron.2013.09.037>.

Guo, T., Liu, G., Du, H., Wen, Y., Wei, S., Li, Z., Tao, G., Shang, Z., Song, X., Zhang, Z., et al. (2019). *Dlx1/2* are Central and Essential Components in the Transcriptional Code for Generating Olfactory Bulb Interneurons. *Cereb. Cortex* <https://doi.org/10.1093/cercor/bhz018>.

Hasenpusch-Theil, K., and Theil, T. (2021). The Multifaceted Roles of Primary Cilia in the Development of the Cerebral Cortex. *Front. Cell Dev. Biol.* 9, 630161. <https://doi.org/10.3389/fcell.2021.630161>.

Hasenpusch-Theil, K., West, S., Kelman, A., Kozic, Z., Horrocks, S., McMahon, A.P., Price, D.J., Mason, J.O., and Theil, T. (2018). *Gli3* controls the onset of cortical neurogenesis by regulating the radial glial cell cycle through *Cdk6* expression. *Development* 145, dev163147. <https://doi.org/10.1242/dev.163147>.

He, M., Tucciarone, J., Lee, S., Nigro, M.J., Kim, Y., Levine, J.M., Kelly, S.M., Krugikov, I., Wu, P., Chen, Y., et al. (2016). Strategies and Tools for Combinatorial Targeting of GABAergic Neurons in Mouse Cerebral Cortex. *Neuron* 92, 555. <https://doi.org/10.1016/j.neuron.2016.10.009>.

Hébert, J.M., and Fishell, G. (2008). The genetics of early telencephalon patterning: some assembly required. *Nat. Rev. Neurosci.* 9, 678–685. <https://doi.org/10.1038/nrn2463>.

Hevner, R.F. (2019). Intermediate progenitors and Tbr2 in cortical development. *J. Anat.* 235, 616–625. <https://doi.org/10.1111/joa.12939>.

Hu, J.S., Vogt, D., Sandberg, M., and Rubenstein, J.L. (2017). Cortical interneuron development: a tale of time and space. *Development* 144, 3867–3878. <https://doi.org/10.1242/dev.132852>.

Hui, C., and Angers, S. (2011). Gli Proteins in Development and Disease. *Annu. Rev. Cell Dev. Biol.* 27, 513–537. <https://doi.org/10.1146/annurev-cellbio-092910-154048>.

Jang, E.S., and Goldman, J.E. (2011). Pax6 Expression Is Sufficient to Induce a Neurogenic Fate in Glial Progenitors of the Neonatal Subventricular Zone. *PLoS ONE* 6, e20894. <https://doi.org/10.1371/journal.pone.0020894>.

Jeong, J., Mao, J., Tenzen, T., Kottmann, A.H., and McMahon, A.P. (2004). Hedgehog signaling in the neural crest cells regulates the patterning and growth of facial primordia. *Genes Dev.* 18, 937–951. <https://doi.org/10.1101/gad.1190304>.

Johnson, D.S., Mortazavi, A., Myers, R.M., and Wold, B. (2007). Genome-wide mapping of in vivo protein-DNA interactions. *Science* 316, 1497–1502. <https://doi.org/10.1126/science.1141319>.

Kessarlis, N., Fogarty, M., Iannarelli, P., Grist, M., Wegner, M., and Richardson, W.D. (2006). Competing waves of oligodendrocytes in the forebrain and postnatal elimination of an embryonic lineage. *Nat. Neurosci.* 9, 173–179. <https://doi.org/10.1038/nn1620>.

Kohwi, M., and Doe, C.Q. (2013). Temporal fate specification and neural progenitor competence during development. *Nat. Rev. Neurosci.* 14, 823–838. <https://doi.org/10.1038/nrn3618>.

Kohwi, M., Petryniak, M.A., Long, J.E., Ekker, M., Obata, K., Yanagawa, Y., Rubenstein, J.L.R., and Alvarez-Buylla, A. (2007). A Subpopulation of Olfactory Bulb GABAergic Interneurons Is Derived from Emx1- and Dlx5/6-Expressing Progenitors. *J. Neurosci.* 27, 6878–6891. <https://doi.org/10.1523/JNEUROSCI.0254-07.2007>.

Komada, M., Iguchi, T., Takeda, T., Ishibashi, M., and Sato, M. (2013). Smoothed controls cyclinD2 expression and regulates the generation of intermediate progenitors in the developing cortex. *Neurosci. Lett.* 547, 87–91. <https://doi.org/10.1016/j.neulet.2013.05.006>.

Korsensky, L., and Ron, D. (2016). Regulation of FGF signaling: Recent insights from studying positive and negative modulators. *Semin. Cell Dev. Biol.* 53, 101–114. <https://doi.org/10.1016/j.semcdb.2016.01.023>.

Kowalczyk, T., Pontious, A., Englund, C., Daza, R.A.M., Bedogni, F., Hodge, R., Attardo, A., Bell, C., Huttner, W.B., and Hevner, R.F. (2009). Intermediate Neuronal Progenitors (Basal Progenitors) Produce Pyramidal–Projection Neurons for All Layers of Cerebral Cortex. *Cereb. Cortex* *19*, 2439–2450. <https://doi.org/10.1093/cercor/bhn260>.

Kriegstein, A., and Alvarez-Buylla, A. (2009). The Glial Nature of Embryonic and Adult Neural Stem Cells. *Annu. Rev. Neurosci.* *32*, 149–184. <https://doi.org/10.1146/annurev.neuro.051508.135600>.

Krijger, P.H.L., Geeven, G., Bianchi, V., Hilvering, C.R.E., and de Laat, W. (2020). 4C-seq from beginning to end: A detailed protocol for sample preparation and data analysis. *Methods* *170*, 17–32. <https://doi.org/10.1016/j.ymeth.2019.07.014>.

Kroll, T.T., and O’Leary, D.D.M. (2005). Ventralized dorsal telencephalic progenitors in Pax6 mutant mice generate GABA interneurons of a lateral ganglionic eminence fate. *Proc. Natl. Acad. Sci.* *102*, 7374–7379. <https://doi.org/10.1073/pnas.0500819102>.

Kuspert, M., Hammer, A., Bosl, M.R., and Wegner, M. (2011). Olig2 regulates Sox10 expression in oligodendrocyte precursors through an evolutionary conserved distal enhancer. *Nucleic Acids Res.* *39*, 1280–1293. <https://doi.org/10.1093/nar/gkq951>.

Kwan, K.Y., Šestan, N., and Anton, E.S. (2012). Transcriptional co-regulation of neuronal migration and laminar identity in the neocortex. *Development* 139, 1535–1546. <https://doi.org/10.1242/dev.069963>.

Leone, D.P., Srinivasan, K., Chen, B., Alcamo, E., and McConnell, S.K. (2008). The determination of projection neuron identity in the developing cerebral cortex. *Curr. Opin. Neurobiol.* 18, 28–35. <https://doi.org/10.1016/j.conb.2008.05.006>.

Levine, M. (2010). Transcriptional Enhancers in Animal Development and Evolution. *Curr. Biol.* 20, R754–R763. <https://doi.org/10.1016/j.cub.2010.06.070>.

Li, J., Wang, C., Zhang, Z., Wen, Y., An, L., Liang, Q., Xu, Z., Wei, S., Li, W., Guo, T., et al. (2018). Transcription Factors Sp8 and Sp9 Coordinately Regulate Olfactory Bulb Interneuron Development. *Cereb. Cortex* 28, 3278–3294. <https://doi.org/10.1093/cercor/bhx199>.

Li, X., Newbern, J.M., Wu, Y., Morgan-Smith, M., Zhong, J., Charron, J., and Snider, W.D. (2012). MEK Is a Key Regulator of Gliogenesis in the Developing Brain. *Neuron* 75, 1035–1050. <https://doi.org/10.1016/j.neuron.2012.08.031>.

Li, X., Liu, G., Yang, L., Li, Z., Zhang, Z., Xu, Z., Cai, Y., Du, H., Su, Z., Wang, Z., et al. (2021). Decoding Cortical Glial Cell Development. *Neurosci. Bull.* <https://doi.org/10.1007/s12264-021-00640-9>.

Lim, L., Mi, D., Llorca, A., and Marín, O. (2018). Development and Functional Diversification of Cortical Interneurons. *Neuron* 100, 294–313. <https://doi.org/10.1016/j.neuron.2018.10.009>.

Lindtner, S., Catta-Preta, R., Tian, H., Su-Feher, L., Price, J.D., Dickel, D.E., Greiner, V., Silberberg, S.N., McKinsey, G.L., McManus, M.T., et al. (2019). Genomic Resolution of DLX-Orchestrated Transcriptional Circuits Driving Development of Forebrain GABAergic Neurons. *Cell Rep.* 28, 2048-2063.e8. <https://doi.org/10.1016/j.celrep.2019.07.022>.

Liu, W., Zhou, H., Liu, L., Zhao, C., Deng, Y., Chen, L., Wu, L., Mandrycky, N., McNabb, C.T., Peng, Y., et al. (2015). Disruption of neurogenesis and cortical development in transgenic mice misexpressing Olig2, a gene in the Down syndrome critical region. *Neurobiol. Dis.* 77, 106–116. <https://doi.org/10.1016/j.nbd.2015.02.021>.

Long, J.E., Garel, S., Alvarez-Dolado, M., Yoshikawa, K., Osumi, N., Alvarez-Buylla, A., and Rubenstein, J.L.R. (2007). Dlx-Dependent and -Independent Regulation of Olfactory Bulb Interneuron Differentiation. *J. Neurosci.* 27, 3230–3243. <https://doi.org/10.1523/JNEUROSCI.5265-06.2007>.

Lv, X., Ren, S.-Q., Zhang, X.-J., Shen, Z., Ghosh, T., Xianyu, A., Gao, P., Li, Z., Lin, S., Yu, Y., et al. (2019). TBR2 coordinates neurogenesis expansion and precise microcircuit organization via Protocadherin 19 in the

mammalian cortex. *Nat. Commun.* *10*, 3946.
<https://doi.org/10.1038/s41467-019-11854-x>.

Ma, T., Zhang, Q., Cai, Y., You, Y., Rubenstein, J.L.R., and Yang, Z. (2012). A Subpopulation of Dorsal Lateral/Caudal Ganglionic Eminence-Derived Neocortical Interneurons Expresses the Transcription Factor Sp8. *Cereb. Cortex* *22*, 2120–2130. <https://doi.org/10.1093/cercor/bhr296>.

Macosko, E.Z., Basu, A., Satija, R., Nemesh, J., Shekhar, K., Goldman, M., Tirosh, I., Bialas, A.R., Kamitaki, N., Martersteck, E.M., et al. (2015). Highly Parallel Genome-wide Expression Profiling of Individual Cells Using Nanoliter Droplets. *Cell* *161*, 1202–1214.
<https://doi.org/10.1016/j.cell.2015.05.002>.

Majd, N., and Penas-Prado, M. (2019). Updates on Management of Adult Medulloblastoma. *Curr. Treat. Options Oncol.* *20*, 64.
<https://doi.org/10.1007/s11864-019-0663-0>.

Marshall, C.A.G. (2005). Olig2 Directs Astrocyte and Oligodendrocyte Formation in Postnatal Subventricular Zone Cells. *J. Neurosci.* *25*, 7289–7298. <https://doi.org/10.1523/JNEUROSCI.1924-05.2005>.

Martínez-Cerdeño, V., Cunningham, C.L., Camacho, J., Antczak, J.L., Prakash, A.N., Cziep, M.E., Walker, A.I., and Noctor, S.C. (2012). Comparative Analysis of the Subventricular Zone in Rat, Ferret and Macaque: Evidence for an Outer Subventricular Zone in Rodents. *PLoS ONE* *7*, e30178. <https://doi.org/10.1371/journal.pone.0030178>.

Merkle, F.T., Mirzadeh, Z., and Alvarez-Buylla, A. (2007). Mosaic Organization of Neural Stem Cells in the Adult Brain. *Science* 317, 381–384. <https://doi.org/10.1126/science.1144914>.

Mihalas, A.B., Elsen, G.E., Bedogni, F., Daza, R.A.M., Ramos-Laguna, K.A., Arnold, S.J., and Hevner, R.F. (2016). Intermediate Progenitor Cohorts Differentially Generate Cortical Layers and Require Tbr2 for Timely Acquisition of Neuronal Subtype Identity. *Cell Rep.* 16, 92–105. <https://doi.org/10.1016/j.celrep.2016.05.072>.

Miyares, R.L., and Lee, T. (2019). Temporal control of Drosophila central nervous system development. *Curr. Opin. Neurobiol.* 56, 24–32. <https://doi.org/10.1016/j.conb.2018.10.016>.

Nasrabad, S.E., Rizvi, B., Goldman, J.E., and Brickman, A.M. (2018). White matter changes in Alzheimer's disease: a focus on myelin and oligodendrocytes. *Acta Neuropathol. Commun.* 6, 22. <https://doi.org/10.1186/s40478-018-0515-3>.

Noctor, S.C., Martínez-Cerdeño, V., Ivic, L., and Kriegstein, A.R. (2004). Cortical neurons arise in symmetric and asymmetric division zones and migrate through specific phases. *Nat. Neurosci.* 7, 136–144. <https://doi.org/10.1038/nn1172>.

Obernier, K., and Alvarez-Buylla, A. (2019). Neural stem cells: origin, heterogeneity and regulation in the adult mammalian brain. *Development* 146, dev156059. <https://doi.org/10.1242/dev.156059>.

Ohkubo, Y., Chiang, C., and Rubenstein, J.L.R. (2002). Coordinate regulation and synergistic actions of BMP4, SHH and FGF8 in the rostral prosencephalon regulate morphogenesis of the telencephalic and optic vesicles. *Neuroscience* 111, 1–17. [https://doi.org/10.1016/S0306-4522\(01\)00616-9](https://doi.org/10.1016/S0306-4522(01)00616-9).

Ono, K., Takebayashi, H., Ikeda, K., Furusho, M., Nishizawa, T., Watanabe, K., and Ikenaka, K. (2008). Regional- and temporal-dependent changes in the differentiation of Olig2 progenitors in the forebrain, and the impact on astrocyte development in the dorsal pallium. *Dev. Biol.* 320, 456–468. <https://doi.org/10.1016/j.ydbio.2008.06.001>.

Ono, K., Takebayashi, H., and Ikenaka, K. (2009). Olig2 transcription factor in the developing and injured forebrain; cell lineage and glial development. *Mol. Cells* 27, 397–401. <https://doi.org/10.1007/s10059-009-0067-2>.

Ortega, J.A., Radonjić, N.V., and Zecevic, N. (2013). Sonic hedgehog promotes generation and maintenance of human forebrain Olig2 progenitors. *Front. Cell. Neurosci.* 7. <https://doi.org/10.3389/fncel.2013.00254>.

Osterwalder, M., Barozzi, I., Tissières, V., Fukuda-Yuzawa, Y., Mannion, B.J., Afzal, S.Y., Lee, E.A., Zhu, Y., Plajzer-Frick, I., Pickle, C.S., et al. (2018). Enhancer redundancy provides phenotypic robustness in mammalian development. *Nature* 554, 239–243. <https://doi.org/10.1038/nature25461>.

Petrova, R., Garcia, A.D.R., and Joyner, A.L. (2013). Titration of GLI3 Repressor Activity by Sonic Hedgehog Signaling Is Critical for Maintaining Multiple Adult Neural Stem Cell and Astrocyte Functions. *J. Neurosci.* **33**, 17490–17505. <https://doi.org/10.1523/JNEUROSCI.2042-13.2013>.

Potter, G.B., Petryniak, M.A., Shevchenko, E., McKinsey, G.L., Ekker, M., and Rubenstein, J.L.R. (2009). Generation of Cre-transgenic mice using Dlx1/Dlx2 enhancers and their characterization in GABAergic interneurons. *Mol. Cell. Neurosci.* **40**, 167–186. <https://doi.org/10.1016/j.mcn.2008.10.003>.

Qiu, X., Mao, Q., Tang, Y., Wang, L., Chawla, R., Pliner, H.A., and Trapnell, C. (2017a). Reversed graph embedding resolves complex single-cell trajectories. *Nat. Methods* **14**, 979–982. <https://doi.org/10.1038/nmeth.4402>.

Qiu, X., Hill, A., Packer, J., Lin, D., Ma, Y.-A., and Trapnell, C. (2017b). Single-cell mRNA quantification and differential analysis with Census. *Nat. Methods* **14**, 309–315. <https://doi.org/10.1038/nmeth.4150>.

Raff, M.C., Miller, R.H., and Noble, M. (1983). A glial progenitor cell that develops in vitro into an astrocyte or an oligodendrocyte depending on culture medium. *Nature* **303**, 390–396. <https://doi.org/10.1038/303390a0>.

Rallu, M., Machold, R., Gaiano, N., Corbin, J.G., McMahon, A.P., and Fishell, G. (2002). Dorsoventral patterning is established in the telencephalon of mutants lacking both Gli3 and Hedgehog signaling. *Development* **129**, 4963–4974. <https://doi.org/10.1242/dev.129.21.4963>.

Rash, B.G., and Grove, E.A. (2007). Patterning the Dorsal Telencephalon: A Role for Sonic Hedgehog? *J. Neurosci.* 27, 11595–11603. <https://doi.org/10.1523/JNEUROSCI.3204-07.2007>.

Rimkus, T., Carpenter, R., Qasem, S., Chan, M., and Lo, H.-W. (2016). Targeting the Sonic Hedgehog Signaling Pathway: Review of Smoothed and GLI Inhibitors. *Cancers* 8, 22. <https://doi.org/10.3390/cancers8020022>.

Shikata, Y., Okada, T., Hashimoto, M., Ellis, T., Matsumaru, D., Shiroishi, T., Ogawa, M., Wainwright, B., and Motoyama, J. (2011). Ptch1-mediated dosage-dependent action of Shh signaling regulates neural progenitor development at late gestational stages. *Dev. Biol.* 349, 147–159. <https://doi.org/10.1016/j.ydbio.2010.10.014>.

Skene, P.J., and Henikoff, S. (2017). CUT&RUN: Targeted *in situ* genome-wide profiling with high efficiency for low cell numbers (*Genomics*).

Sousa, V.H., and Fishell, G. (2010). Sonic hedgehog functions through dynamic changes in temporal competence in the developing forebrain. *Curr. Opin. Genet. Dev.* 20, 391–399. <https://doi.org/10.1016/j.gde.2010.04.008>.

Stenman, J., Toresson, H., and Campbell, K. (2003). Identification of Two Distinct Progenitor Populations in the Lateral Ganglionic Eminence: Implications for Striatal and Olfactory Bulb Neurogenesis. *J. Neurosci.* 23, 167–174. <https://doi.org/10.1523/JNEUROSCI.23-01-00167.2003>.

Takebayashi, H., Nabeshima, Y., Yoshida, S., Chisaka, O., Ikenaka, K., and Nabeshima, Y. (2002a). The Basic Helix-Loop-Helix Factor Olig2 Is Essential for the Development of Motoneuron and Oligodendrocyte Lineages. *Curr. Biol.* 12, 1157–1163. [https://doi.org/10.1016/S0960-9822\(02\)00926-0](https://doi.org/10.1016/S0960-9822(02)00926-0).

Takebayashi, H., Nabeshima, Y., Yoshida, S., Chisaka, O., Ikenaka, K., and Nabeshima, Y. (2002b). The Basic Helix-Loop-Helix Factor Olig2 Is Essential for the Development of Motoneuron and Oligodendrocyte Lineages. *Curr. Biol.* 12, 1157–1163. [https://doi.org/10.1016/S0960-9822\(02\)00926-0](https://doi.org/10.1016/S0960-9822(02)00926-0).

Theil, T., Alvarez-Bolado, G., Walter, A., and Rüter, U. (1999). Gli3 is required for Emx gene expression during dorsal telencephalon development. *Dev. Camb. Engl.* 126, 3561–3571. <https://doi.org/10.1242/dev.126.16.3561>.

Tole, S., Ragsdale, C.W., and Grove, E.A. (2000). Dorsoventral Patterning of the Telencephalon Is Disrupted in the Mouse Mutant extra-toes. *Dev. Biol.* 217, 254–265. <https://doi.org/10.1006/dbio.1999.9509>.

Tong, C.K., Fuentealba, L.C., Shah, J.K., Lindquist, R.A., Ihrie, R.A., Guinto, C.D., Rodas-Rodriguez, J.L., and Alvarez-Buylla, A. (2015). A Dorsal SHH-Dependent Domain in the V-SVZ Produces Large Numbers of Oligodendroglial Lineage Cells in the Postnatal Brain. *Stem Cell Rep.* 5, 461–470. <https://doi.org/10.1016/j.stemcr.2015.08.013>.

Toresson, H., and Campbell, K. Gsh1 function in the Gsh2^{-/-} telencephalon. 12. .

Traiffort, E., Zakaria, M., Laouarem, Y., and Ferent, J. (2016). Hedgehog: A Key Signaling in the Development of the Oligodendrocyte Lineage. *J. Dev. Biol.* 4, 28. <https://doi.org/10.3390/jdb4030028>.

Trapnell, C., Roberts, A., Goff, L., Pertea, G., Kim, D., Kelley, D.R., Pimentel, H., Salzberg, S.L., Rinn, J.L., and Pachter, L. (2012). Differential gene and transcript expression analysis of RNA-seq experiments with TopHat and Cufflinks. *Nat. Protoc.* 7, 562–578. <https://doi.org/10.1038/nprot.2012.016>.

Vaillant, C., and Monard, D. (2009). SHH Pathway and Cerebellar Development. *The Cerebellum* 8, 291–301. <https://doi.org/10.1007/s12311-009-0094-8>.

Vasistha, N.A., García-Moreno, F., Arora, S., Cheung, A.F.P., Arnold, S.J., Robertson, E.J., and Molnár, Z. (2015). Cortical and Clonal Contribution of Tbr2 Expressing Progenitors in the Developing Mouse Brain. *Cereb. Cortex* 25, 3290–3302. <https://doi.org/10.1093/cercor/bhu125>.

Ventura, R.E., and Goldman, J.E. (2007). Dorsal Radial Glia Generate Olfactory Bulb Interneurons in the Postnatal Murine Brain. *J. Neurosci.* 27, 4297–4302. <https://doi.org/10.1523/JNEUROSCI.0399-07.2007>.

Visel, A., Minovitsky, S., Dubchak, I., and Pennacchio, L.A. (2007). VISTA Enhancer Browser--a database of tissue-specific human enhancers. *Nucleic Acids Res.* 35, D88–D92. <https://doi.org/10.1093/nar/gkl822>.

Waclaw, R.R., Wang, B., Pei, Z., Ehrman, L.A., and Campbell, K. (2009). Distinct Temporal Requirements for the Homeobox Gene *Gsx2* in Specifying Striatal and Olfactory Bulb Neuronal Fates. *Neuron* 63, 451–465. <https://doi.org/10.1016/j.neuron.2009.07.015>.

Wang, L.-C., and Almazan, G. (2016). Role of Sonic Hedgehog Signaling in Oligodendrocyte Differentiation. *Neurochem. Res.* 41, 3289–3299. <https://doi.org/10.1007/s11064-016-2061-3>.

Wang, B., Long, J.E., Flandin, P., Pla, R., Waclaw, R.R., Campbell, K., and Rubenstein, J.L.R. (2013a). Loss of *Gsx1* and *Gsx2* function rescues distinct phenotypes in *Dlx1/2* mutants. *J. Comp. Neurol.* 521, 1561–1584. <https://doi.org/10.1002/cne.23242>.

Wang, H., Kane, A.W., Lee, C., and Ahn, S. (2014). Gli3 Repressor Controls Cell Fates and Cell Adhesion for Proper Establishment of Neurogenic Niche. *Cell Rep.* 8, 1093–1104. <https://doi.org/10.1016/j.celrep.2014.07.006>.

Wang, S., Sun, H., Ma, J., Zang, C., Wang, C., Wang, J., Tang, Q., Meyer, C.A., Zhang, Y., and Liu, X.S. (2013b). Target analysis by integration of transcriptome and ChIP-seq data with BETA. *Nat. Protoc.* 8, 2502–2515. <https://doi.org/10.1038/nprot.2013.150>.

Wen, Y., Zhang, Z., Li, Z., Liu, G., Tao, G., Song, X., Xu, Z., Shang, Z., Guo, T., Su, Z., et al. (2019). The PROK2/PROKR2 signaling pathway is required for the migration of most olfactory bulb interneurons. *J. Comp. Neurol.* 527, 2931–2947. <https://doi.org/10.1002/cne.24719>.

Weng, Q., Wang, J., Wang, J., He, D., Cheng, Z., Zhang, F., Verma, R., Xu, L., Dong, X., Liao, Y., et al. (2019). Single-Cell Transcriptomics Uncovers Glial Progenitor Diversity and Cell Fate Determinants during Development and Gliomagenesis. *Cell Stem Cell* 24, 707-723.e8. <https://doi.org/10.1016/j.stem.2019.03.006>.

Winkler, C.C., and Franco, S.J. (2019). Loss of Shh signaling in the neocortex reveals heterogeneous cell recovery responses from distinct oligodendrocyte populations. *Dev. Biol.* 452, 55–65. <https://doi.org/10.1016/j.ydbio.2019.04.016>.

Winkler, C.C., Yabut, O.R., Fregoso, S.P., Gomez, H.G., Dwyer, B.E., Pleasure, S.J., and Franco, S.J. (2018). The Dorsal Wave of Neocortical Oligodendrogenesis Begins Embryonically and Requires Multiple Sources of Sonic Hedgehog. *J. Neurosci.* 38, 5237–5250. <https://doi.org/10.1523/JNEUROSCI.3392-17.2018>.

Yabut, O.R., Fernandez, G., Huynh, T., Yoon, K., and Pleasure, S.J. (2015). Suppressor of Fused Is Critical for Maintenance of Neuronal Progenitor Identity during Corticogenesis. *Cell Rep.* 12, 2021–2034. <https://doi.org/10.1016/j.celrep.2015.08.031>.

Young, K.M., Fogarty, M., Kessar, N., and Richardson, W.D. (2007). Subventricular Zone Stem Cells Are Heterogeneous with Respect to Their Embryonic Origins and Neurogenic Fates in the Adult Olfactory Bulb. *J. Neurosci.* 27, 8286–8296. <https://doi.org/10.1523/JNEUROSCI.0476-07.2007>.

Zeidán-Chuliá, F., de Oliveira, B.-H.N., Casanova, M.F., Casanova, E.L., Noda, M., Salmina, A.B., and Verkhratsky, A. (2016). Up-Regulation of Oligodendrocyte Lineage Markers in the Cerebellum of Autistic Patients: Evidence from Network Analysis of Gene Expression. *Mol. Neurobiol.* 53, 4019–4025. <https://doi.org/10.1007/s12035-015-9351-7>.

Zhang, Q., Zhang, Y., Wang, C., Xu, Z., Liang, Q., An, L., Li, J., Liu, Z., You, Y., He, M., et al. (2016). The Zinc Finger Transcription Factor Sp9 Is Required for the Development of Striatopallidal Projection Neurons. *Cell Rep.* 16, 1431–1444. <https://doi.org/10.1016/j.celrep.2016.06.090>.

Zhang, Y., Liu, G., Guo, T., Liang, X.G., Du, H., Yang, L., Bhaduri, A., Li, X., Xu, Z., Zhang, Z., et al. (2020). Cortical Neural Stem Cell Lineage Progression Is Regulated by Extrinsic Signaling Molecule Sonic Hedgehog. *Cell Rep.* 30, 4490-4504.e4. <https://doi.org/10.1016/j.celrep.2020.03.027>.

Zhuo, L., Sun, B., Zhang, C.-L., Fine, A., Chiu, S.-Y., and Messing, A. (1997). Live Astrocytes Visualized by Green Fluorescent Protein in Transgenic Mice. *Dev. Biol.* 187, 36–42. <https://doi.org/10.1006/dbio.1997.8601>.

Zhuo, L., Theis, M., Alvarez-Maya, I., Brenner, M., Willecke, K., and Messing, A. (2001). hGFAP-cre transgenic mice for manipulation of glial and neuronal function in vivo. *Genesis* 31, 85–94. <https://doi.org/10.1002/gene.10008>.